No. 613 **September 2019**

An isogeometric mortar method for the coupling of multiple NURBS domains with optimal convergence rates

W. Dornisch, J. Stöckler

ISSN: 2190-1767

An isogeometric mortar method for the coupling of multiple NURBS domains with optimal convergence rates

W. Dornisch[a], J. Stöckler[b,*]

[a] *Fachgebiet Statik und Dynamik, Brandenburgische Technische Universität Cottbus-Senftenberg, Konrad-Wachsmann-Allee 2, 03046 Cottbus, Germany*
[b] *Fakultät für Mathematik, Technische Universität Dortmund, Vogelpothsweg 87, 44221 Dortmund, Germany*

Abstract

We investigate the mortar finite element method for second order elliptic boundary value problems on domains which are decomposed into patches Ω_k with tensor-product NURBS parameterizations. We follow the methodology of IsoGeometric Analysis (IGA) and choose discrete spaces $X_{h,k}$ on each patch Ω_k as tensor-product NURBS spaces of the same or higher degree as given by the parameterization. Our work is an extension of [12] and highlights several aspects which did not receive full attention before. In particular, by choosing appropriate spaces of polynomial splines as Lagrange multipliers, we obtain a uniform infsup-inequality. Moreover, we provide a new additional condition on the discrete spaces $X_{h,k}$ which is required for obtaining optimal convergence rates of the mortar method. Our numerical examples demonstrate that the optimal rate is lost if this condition is neglected.

Keywords: Isogeometric analysis, Optimal convergence, Mortar method, Coupling of non-conforming meshes, modified Lagrange multiplier space, infsup-stability
2010 MSC: 65N30, 65N55, 41A15

*Corresponding author
Email address: joachim.stoeckler@math.tu-dortmund.de (J. Stöckler)

1. Introduction

Our main focus is on the theoretical foundation of an IsoGeometric Analysis (IGA) approach to mixed finite element methods using non-uniform rational B-splines (NURBS) for the finite element discretization. We investigate the mortar finite element method on domains

$$\overline{\Omega} = \bigcup_{k=1}^{K} \overline{\Omega_k} \subset \mathbb{R}^2$$

which are decomposed into patches Ω_k with tensor-product NURBS parameterizations

$$\mathbf{F}_k : [0,1]^2 \to \overline{\Omega_k}.$$

For the original mortar method we refer to [6, 7, 24]. A comprehensive description of the finite-element discretization using the methodology of IsoGeometric Analysis (IGA) is given in [12]. Prior uses of the mortar method in IGA have also been documented in [2, 15, 16, 17]. Its centerpieces are discrete spaces $X_{h,k} \subset H^1(\Omega_k)$, which are pushforward of tensor-product NURBS spaces on the parameter domain $[0,1]^2$ and which have the same or higher degree given by the parameterization $\mathbf{F}_k$. Furthermore, discrete spaces $M_{h,l}$ of Lagrange multipliers are defined for the representation of weak continuity conditions across the interfaces γ_l. In [12] the pushforward of polynomial spline spaces of the same or lower degree are proposed.

Our work is an extension of [12] and highlights several aspects which did not receive full attention before.

1. In our numerical experiments based on the method in [12], using parameterizations by quartic NURBS with multiple interior knots and quartic splines as Lagrange multipliers, we observed that the optimal approximation rate claimed in Theorem 5.5 of [12] is not obtained. In Section 7 we show that a simple additional condition on the discrete spaces $X_{h,k}$ is sufficient in order to obtain the optimal approximation rate, see Assumption 4 and Proposition 7.11. We give a short explanation here. Let the interface γ_l be a boundary line of the patch Ω_k and $u|_{\Omega_k} \in H^{p_k+1}(\Omega_k)$ for some integer p_k. In the non-parametric setting of [6, 7, 24], several arguments in the proof for the optimal approximation order employ trace theorems of the form

$$u|_{\gamma_l} \in H^{p_k+1/2}(\gamma_l), \qquad \left.\frac{\partial u}{\partial \nu_l}\right|_{\gamma_l} \in H^{p_k-1/2}(\gamma_l).$$

   Here, ν_l denotes the outer normal of Ω_k on γ_l. The trace theorem is valid in this form, if γ_l is supposed to be smooth (in fact, it is a straight line in [6, 7, 24]). However, in the IGA setting γ_l is a NURBS curve of degree p_k with interior knots, and its smoothness at these knots can degrade as much as continuity being the only remaining assumption. The method of "bent Sobolev spaces" was introduced in [3, 4] in order to remedy this defect. We add some missing pieces which are essential for an application of these results to the IGA mortar method. First, a careful analysis of the traces $u|_{\gamma_l}$ and $\nabla u|\gamma_l$ with respect to non-smooth

curves γ_l is performed using results from [19]. Secondly, a result of super-approximation is given in Theorem 7.6 in order to obtain non-integer approximation orders

$$\inf_{v \in W_{h,l}} \|u - v\|_{L_2(\gamma_l)} \leq C h_k^{p_k+1/2} \, \|u\|_{H^{p_k+1}(\Omega_k)},$$

where $W_{h,l}$ is the trace space on γ_l of the discretization subspace $X_{h,k}$. Finally, and most importantly, in spite of the fact that the pullback of $M_{h,l}^1$ on the parameter domain contains all polynomials of degree $p_k - 1$, the optimal rate

$$\inf_{\mu \in M_{h,l}^1} \left\| \frac{\partial u}{\partial \nu_l} - \mu \right\|_{L_2(\gamma_l)} \leq C h_k^{p_k-1/2} \, \|u\|_{H^{p_k+1}(\Omega_k)}$$

is not always obtained. This leads to a defect of the overall approximation order of the discrete solution which is induced by a defect of the consistency error. We provide a simple extra condition on the discretization (see Assumption 4) and prove in Proposition 7.11, that the optimal rate is obtained under this assumption.

2. The formulation of the mortar method as a saddle point problem involves Lagrange multiplier spaces $M_{h,l}$ for the representation of weak continuity conditions across the interfaces γ_l of the domain decomposition. In order to achieve the optimal approximation order of the mortar method, a good choice for $M_{h,l}$ is the pushforward of the polynomial spline space of the same degree as $X_{h,k}$, if γ_l is an edge of the patch Ω_k, and with suitable modifications at both endpoints of γ_l, see [12, Section 4.3]. It is only a conjecture in [12] that this choice justifies a uniform infsup-condition. In Section 4.2 we define a spline space $M_{h,l}^1$ of the same degree with another type of endpoint modifications, for which we provide the analytical proof of the infsup-inequality in Section 6. As a side-effect of the new definition of the space of Lagrange multipliers, we show in Section 8 that the sparsity of the mass matrix is increased slightly.

3. In the geometrically conforming case, $\overline{\gamma_{kl}} = \partial\Omega_k \cap \partial\Omega_l$ is either empty, a vertex or a full edge of both patches. In engineering applications of CAD-tools, the decomposition of Ω can often be geometrically non-conforming and includes T-intersections of the patch boundaries. The setting in [2, 12, 15, 17, 16] allows certain types of T-intersections, but excludes configurations of staircase type, where $\overline{\gamma_{kl}}$ is neither an edge of Ω_k nor of Ω_l. We provide an adaptation of the discrete spaces $X_{h,k}$ and allow full flexibility of designing the multi-patch layout of the geometry.

In order to keep the overhead of notations small, we present our analytical results about the infsup-condition and the a-priori error estimates for a simple class of second order elliptic problems. We proceed to more elaborate models in elasticity in our numerical experiments in Section 9. The scope of applications of the IGA mortar method has recently been extended to a class of contact problems in [1, 20, 22], and the infsup-condition and the a-priori error estimates by [12] provided the theoretical foundation. We believe that our results in Sections 6 and 7 will be valuable ingredients for further developments in this direction.

We begin with the elliptic problem

$$-\mathrm{div}(\alpha\nabla u) + \beta u = f \quad \text{in} \quad \Omega$$

on a Lipschitz domain $\Omega \subset \mathbb{R}^2$ with boundary conditions

$$u|_{\Gamma_D} = 0, \qquad \alpha \left.\frac{\partial u}{\partial \nu}\right|_{\Gamma_N} = g,$$

where Γ_D has positive measure and $\Gamma_N = \partial\Omega \setminus \Gamma_D$. For its weak formulation we define $H^1_{0,D}(\Omega) = \{v \in H^1(\Omega) : v|_{\Gamma_D} = 0\}$ and the bilinear form

$$a(u,v) = \int_\Omega (\alpha\nabla u \cdot \nabla v + \beta uv)\, dx, \qquad u, v \in H^1_{0,D}(\Omega). \tag{1}$$

We assume that α is a uniformly positive definite matrix with entries $\alpha_{i,j} \in L^\infty(\Omega)$ and $\beta \in L^\infty(\Omega)$ is nonnegative. Then the bilinear form a is coercive. In the weak formulation, we look for $u \in H^1_{0,D}(\Omega)$ such that

$$a(u,v) = \int_\Omega fv\, dx + \int_{\Gamma_N} gv\, ds \quad \text{for all} \quad v \in H^1_{0,D}(\Omega). \tag{2}$$

We often use Sobolev spaces $H^s(\Omega)$ with smoothness order $s \geq 0$ which is not always an integer. The norm and semi-norm are denoted as usual by $\|v\|_{s,\Omega}$ and $|v|_{s,\Omega}$.

We end the introduction by a short outline of our work. We repeat from [12] the geometric description and the general setting of the weak formulation as a saddle point problem in Sections 2 and 3. Section 4 gives the definitions of the discrete spaces $X_{h,k}$ and the new spaces M^1_h of Lagrange multipliers. Sections 5 and 6 deal with the L^2-stability of the mortar projection and the uniform infsup-inequality. Section 7 provides a detailed analysis of the approximation order of the discrete solution. In Section 8 we give some information about the implementation, with special emphasis on the mass matrix, and Section 9 provides several numerical results for the Poisson problem and for elasticity problems.

2. NURBS description of the geometry

The geometrical setting is formulated as in [12]. In order to fix the notations, we repeat some of the material in the referenced article.

Let $\Omega_1, \ldots, \Omega_K \subset \mathbb{R}^2$ define a nonoverlapping decomposition of the domain Ω by curvilinear quadrilaterals (patches), i.e.

$$\overline{\Omega} = \bigcup_{k=1}^{K} \overline{\Omega}_k, \qquad \Omega_k \cap \Omega_l = \emptyset \text{ for } k \neq l.$$

The decomposition may be geometrically non-conforming, as we allow T-intersections at the boundaries of the patches. A sketch of such decomposition is given in Fig. 1.

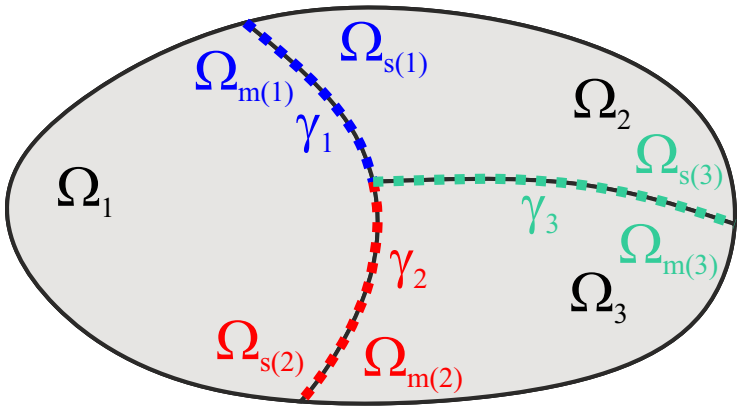

Figure 1: Decomposition of domains

Each patch Ω_k is parameterized by a homeomorphism $\mathbf{F}_k : \hat{\Omega} = [0,1]^2 \to \overline{\Omega_k}$ which is bi-Lipschitz. Throughout this article, $\mathbf{F}_k$ is a bivariate NURBS parameterization

$$\mathbf{F}_k(\xi_1,\xi_2) = \sum_{\mathbf{i}\in\mathbf{I}_k} \mathbf{C}_{k,\mathbf{i}} \hat{N}_{k,\mathbf{i}}(\xi_1,\xi_2), \qquad (\xi_1,\xi_2) \in \hat{\Omega} = [0,1]^2, \tag{3}$$

where $(\hat{N}_{k,\mathbf{i}})_{\mathbf{i}\in\mathbf{I}_k}$ is the family of NURBS basis functions of degree p_k with respect to the bivariate knot sequence

$$\Xi_k = \Xi_k^{(1)} \times \Xi_k^{(2)} \subset \hat{\Omega}$$

and with positive weights $\{\omega_{k,\mathbf{i}},\ \mathbf{i} \in \mathbf{I}_k\}$. More specifically, $\hat{N}_{k,\mathbf{i}}$ is defined by

$$\hat{N}_{k,\mathbf{i}}(\xi_1,\xi_2) = \frac{\omega_{k,\mathbf{i}} \hat{B}_{k,\mathbf{i}}^{p_k}(\xi_1,\xi_2)}{\hat{w}_k(\xi_1,\xi_2)}, \qquad \hat{w}_k(\xi_1,\xi_2) = \sum_{\mathbf{i}\in\mathbf{I}_k} \omega_{k,\mathbf{i}} \hat{B}_{k,\mathbf{i}}^{p_k}(\xi_1,\xi_2), \tag{4}$$

where $(\hat{B}_{k,\mathbf{i}}^{p_k})_{\mathbf{i}\in\mathbf{I}_k}$ is the basis of tensor-product B-splines of polynomial degree p_k in both coordinate directions. We assume throughout this article that all knot sequences are open; i.e., the first and last knot have multiplicity $p_k + 1$.

For $1 \le j,k \le K$, $k \ne j$, we define the interface γ_{jk} as the interior of the intersection $\overline{\gamma}_{jk} = \partial\Omega_j \cap \partial\Omega_k$. We consider only those pairs (j,k) with non-empty γ_{jk} and renumber the interfaces as γ_l, $l = 1,\dots,L$. For each interface γ_l, we choose one of the adjacent patches as master cell $\Omega_{m(l)}$ and the other one as slave cell $\Omega_{s(l)}$, so that $\overline{\gamma}_l = \partial\Omega_{m(l)} \cap \partial\Omega_{s(l)}$. This assignment allows an arbitrary choice for each interface, i.e. Ω_k can be a master cell for one of its boundary lines and a slave cell for another boundary line. We define $\hat{\gamma}_l = \mathbf{F}_{s(l)}^{-1}(\gamma_l)$ and use the notation $F_l := \mathbf{F}_{s(l)}|_{\hat{\gamma}_l}$ for the parameterization of the interface.

Remark 2.1. In a geometrically conforming case, every interface γ_l is a full edge of $\Omega_{s(l)}$ and $\Omega_{m(l)}$. Its pre-image under $\mathbf{F}_{s(l)}$ is a boundary line

$$\hat{\gamma}_l = (0,1)\times\{0\},\ (0,1)\times\{1\},\ \ \{0\}\times(0,1),\ \ \text{or}\ \ \{1\}\times(0,1), \tag{5}$$

of $\hat{\Omega}$. Without causing confusion, we drop the irrelevant dimension and use $\hat{\gamma}_l = (0,1)$.

For a geometrically non-conforming decomposition we allow T-intersections of the interfaces and consider the following two scenarios in parallel.

NC1 The interface γ_l is a full edge of the slave patch $\Omega_{s(l)}$. As before, $\hat{\gamma}_l$ is as in (5) and we use the abbreviated form $\hat{\gamma}_l = (0,1)$. This restriction on the choice of the master/slave correspondence was used in [12]. It limits the applicability of the mortar method since staircase patch topologies cannot be treated.

NC2 There is no geometrical restriction on the choice of the master/slave correspondence. Then we introduce a C^0-line as an extension of the ending interface of a T-intersection into the adjacent patch Ω_k. This is done by inserting a knot ζ of multiplicity p_k (or increasing the multiplicity of an existent knot to p_k) into the relevant knot sequence $\Xi_k^{(1)}$ or $\Xi_k^{(2)}$. It does not change the patch geometry, but affects the initial parameterization $\mathbf{F}_k$ by using a larger set of NURBS basis functions. The immediate effect on the discrete space $X_{h,k}$ is equivalent to splitting the patch Ω_k along the line $\mathbf{F}_k(\zeta,t)$ (or $\mathbf{F}_k(t,\zeta)$), $t \in [0,1]$, and connecting the control points by shared degrees of freedom. By doing so, we get a setting where only geometrical conforming cases are present. Full flexibility in the choice of the master/slave correspondence is obtained and all forms of multi-patch layouts can be computed. This extension leads to the additional element lines visible in Figures 10 and 25. It is important to note that the required refinement does not propagate to further patches. After this initial modification has been done for all T-intersections, each interface $\gamma_l = F_l(\hat{\gamma}_l)$ is a parameterized NURBS curve with an open knot sequence $\Theta_l \subset \overline{\hat{\gamma}_l} = [\xi_{l,1}, \xi_{l,2}] \subset [0,1]$, and $\xi_{l,1}, \xi_{l,2}$ are the parameter values of the endpoints of γ_l.

To unify our notations, we let $\xi_{l,1} = 0$ and $\xi_{l,2} = 1$ in the geometrically conforming case and NC1; then $\hat{\gamma}_l = (\xi_{l,1}, \xi_{l,2})$ is valid for all cases.

The trace on γ_l of the NURBS basis functions of the slave cell $\Omega_{s(l)}$ are univariate NURBS basis functions of degree $q_l := p_{s(l)}$ on the interval $[\xi_{l,1}, \xi_{l,2}]$. In the geometrically conforming case or for NC1, the correspoinding knot sequence Θ_l is one of the four sets

$$\Xi_{s(l)}^{(1)} \times \{0\},\ \Xi_{s(l)}^{(1)} \times \{1\},\ \ \{0\} \times \Xi_{s(l)}^{(2)},\ \ \{1\} \times \Xi_{s(l)}^{(2)}.$$

Again, we suppress the obsolete dimension and use Θ_l as an open knot sequence on $[0,1]$,

$$\Theta_l = \{0 = \theta_{l,1} = \cdots = \theta_{l,q_l+1} < \theta_{l,q_l+2} \le \cdots \le \theta_{l,n_l} < \theta_{l,n_l+1} = \cdots = \theta_{l,n_l+q_l+1} = 1\}.$$

The parameter n_l denotes the dimension of the initial NURBS space for the parameterization $F_l : (0,1) \to \gamma_l$. With the corresponding subset of weigths $w_{l,i} = \omega_{s(l),\mathbf{i}}$, $1 \le i \le n_l$, along this interface, the univariate NURBS basis functions on $\hat{\gamma}_l$ are

$$\hat{N}_{l,i}(\xi) = \frac{w_{l,i}\hat{B}_{l,i}^{q_l}(\xi)}{\hat{w}_l(\xi)}, \qquad \hat{w}_l(\xi) = \sum_{j=1}^{n_l} w_{l,j}\hat{B}_{l,j}^{q_l}(\xi), \qquad \xi \in [0,1]. \tag{6}$$

Here we denote by $\hat{B}_{l,i}^{q_l}$ the univariate B-splines of degree q_l with knot sequence Θ_l. For the nonconforming geometry NC2, the open knot sequence Θ_l has endpoints $\theta_{l,1} = \xi_{l,1}$ and $\theta_{l,n_l+q_l+1} = \xi_{l,2}$ of multiplicity $q_l + 1$. Only a subset of the NURBS basis functions of the patch $\Omega_{s(l)}$ have nonzero trace on γ_l in this case.

The same consideration leads to the univariate NURBS basis functions $\hat{N}_{l,j}^m$ of degree $p_{m(l)}$ with respect to the master cell $\Omega_{m(l)}$. The extra superscript m is used here in order to point out the role of the master cell.

The standard inner product on γ_l is given by

$$\int_{\gamma_l} uv\, ds = \int_{\hat{\gamma}_l} (u \circ F_l)(\xi)\, (v \circ F_l)(\xi)\, \tau_l(\xi)\, d\xi, \qquad u, v \in L^2(\gamma_l),$$

where $\tau_l = |F_l'|$ is the length of the tangent vector of γ_l. For later use, we also define the weighted inner product

$$\langle u, v \rangle_{\rho_l} := \int_{\gamma_l} \rho_l uv\, ds$$

with a positive weight function ρ_l with $0 < c \leq \rho_l \leq C$. We will often choose $\rho_l = \frac{\hat{w}_l^2}{\tau_l} \circ F_l^{-1}$, and then obtain

$$\langle u, v \rangle_{\rho_l} = \int_{\hat{\gamma}_l} \hat{w}_l^2(\xi)\, (u \circ F_l)(\xi)\, (v \circ F_l)(\xi)\, d\xi. \tag{7}$$

The inner products are defined for pairs $u, v \in L^2(\gamma_l)$, or for $u \in H^{1/2}(\gamma_l)$ and $v \in (H^{1/2}(\gamma_l))'$. The induced norm is equivalent to the standard L^2-norm on γ_l.

We make the following assumption on the parameterization which is essential for our method.

Assumption 1. The geometry is waterproof; i.e. the mapping $\mathbf{F}_{m(l)}^{-1} \circ \mathbf{F}_{s(l)} : \hat{\gamma}_l \to (0, 1)$ for "switching the sides" at an interface γ_l is well-defined.

Remark 2.2. The methods proposed in this paper can also be used for non-waterproof geometries, whereby from the mathematical point of view a variational crime is committed. This results in an additional error which does not vanish in the fine limit. However, as shown in [12], the mortar method is robust with respect to these kinds of non-matching interfaces and sufficient accuracy for engineering applications is obtained.

3. Weak formulation of the saddle point problem

The natural function space used in mixed finite element methods for the Dirichlet problem is the direct product

$$X = \{v \in L^2(\Omega) : v_k = v|_{\Omega_k} \in H^1(\Omega_k),\ v_k|_{\Gamma_D \cap \partial\Omega_k} = 0\}$$

endowed with the norm

$$\|v\|_X = \left(\sum_{k=1}^{K} \|v_k\|_{1,\Omega_k}^2 \right)^{1/2}.$$

The bilinear form a in (1) is canonically extended to $X \times X$ by

$$a(u,v) = \sum_{k=1}^{K} \int_{\Omega_k} (\alpha \nabla u \cdot \nabla v + \beta uv)\, dx.$$

The continuity and coercivity of this extension of a are obvious.

Clearly, X is not a subspace of $H^1_{0,D}(\Omega)$. For the formulation of weak continuity conditions on every interface γ_l, we define the space of Lagrange multipliers

$$M = \left\{ \psi = (\psi_l) \in \prod_{l=1}^{L} (H^{1/2}(\gamma_l))' : \ \exists q \in H_0(\mathrm{div}, \Omega) \text{ such that } \psi_l = q \cdot \nu_l \right\},$$

where ν_l denotes the outer normal of $\Omega_{s(l)}$ along γ_l. With the notation $[v]_l = (v_{s(l)} - v_{m(l)})|_{\gamma_l}$ for the jump of $v \in X$ across γ_l, and with the weighted inner product (7), we define the bilinear form

$$b_\rho : X \times M \to \mathbb{R}, \qquad b_\rho(v,\psi) = \sum_{l=1}^{L} \langle [v]_l, \psi_l \rangle_{\rho_l}, \tag{8}$$

with weight functions $\rho_l = \frac{\hat{w}_l^2}{\tau_l} \circ F_l^{-1}$. Based on the fact that

$$V = \{ v \in X : b_\rho(v,\psi) = 0 \text{ for all } \psi \in M \} = H^1_{0,D}(\Omega),$$

the weak solution of (2) is obtained from the solution of the following saddle point problem: *Find* $(u,\lambda) \in X \times M$ *such that*

$$\begin{array}{lcll} a(u,v) + b_\rho(v,\lambda) & = & \int_\Omega f v\, dx + \int_{\Gamma_N} g v\, ds, & v \in X, \\ b_\rho(u,\mu) & = & 0, & \mu \in M. \end{array} \tag{9}$$

This problem has a unique solution $(u,\lambda) \in X \times M$, whose first component $u \in V$ satisfies (2). The second component $\lambda \in M$ represents the (weighted) normal flux. Due to the presence of the weight ρ_l in (9), its component $\lambda_l \in (H^{1/2}(\gamma_l))'$ is

$$\lambda_l = \frac{\alpha}{\rho_l} \frac{\partial u}{\partial \nu_l}. \tag{10}$$

The usual stability analysis provides the upper bound

$$\|u\|_{1,\Omega} + \|\lambda\|_M \le C(\|f\|_{L^2(\Omega)} + \|g\|_{L^2(\Gamma_N)}).$$

The reason why we use a weighted inner product instead of the standard inner product of $L^2(\gamma_l)$ will become clear when we consider the numerical computation of the mass matrix in 8.

4. Discretization of the saddle point problem using NURBS and B-splines

The discretization of the saddle point problem is obtained by choosing a suitable pair of finite-dimensional spaces $X_h \subset X$ and $M_h \subset M$, where the subscript h represents a vector $h = (h_k)_{k=1,\dots,K}$ for the spatial resolutions on the patches Ω_k. The mixed method for the solution of (9) is formulated as follows: *Find* $(u_h, \lambda_h) \in X_h \times M_h$ *such that*

$$\begin{array}{lcll} a(u_h, v) + b_\rho(v, \lambda_h) & = & \int_\Omega f v \, dx + \int_{\Gamma_N} g v \, ds & \text{for all } \ v \in X_h, \\ b_\rho(u_h, \mu) & = & 0 & \text{for all } \ \mu \in M_h. \end{array} \tag{11}$$

The solution space for u_h will be denoted by

$$V_h = \{v \in X_h : b_\rho(v, \mu) = 0 \text{ for all } \mu \in M_h\}. \tag{12}$$

If the weak solution u of (2) is locally smooth, i.e. $u \in H^1_{0,D}(\Omega) \cap \prod_{k=1}^K H^{p_k+1}(\Omega_k)$, we look for error estimates of the form

$$\|u - u_h\|_X^2 + \|\lambda - \lambda_h\|_{-1/2,h}^2 \le C \sum_{k=1}^K h_k^{2p_k} |u|^2_{H^{p_k+1}(\Omega_k)}. \tag{13}$$

Here we use the mesh-dependent norm on M_h as in [11, 24]

$$\|\mu\|_{\sigma,h} = \left(\sum_{l=1}^L h_{s(l)}^{-2\sigma} \|\mu\|^2_{L^2(\gamma_l)} \right)^{1/2} \tag{14}$$

with $\sigma = -1/2$. In this article, we follow [12] for the definition of the space X_h, but we propose an alternative space M_h of Lagrange multipliers.

4.1. The space X_h defined by NURBS

The initial knot sequences $\Xi_k \subset [0,1]^2$ were used for the parameterizations $\mathbf{F}_k : [0,1]^2 \to \overline{\Omega_k}$ of the patches Ω_k. (In a geometrically non-conforming case NC2 of Remark 2.1, we assume that the knots $\xi_{l,1}, \xi_{l,2}$ are already existent with multiplicity p_k in $\Xi_k^{(1)}$ or $\Xi_k^{(2)}$, respectively.) The finite element discretization uses refined knot sequences on each patch independently. Every refined knot sequence $\Xi_{h,k} = \Xi_{h,k}^{(1)} \times \Xi_{h,k}^{(2)} \subset [0,1]^2$ defines a grid of two open knot sequences with knots $\xi_{h,k,j}^{(r)}$, $1 \le j \le n_{h,k}^{(r)} + p_k + 1$ and $r = 1, 2$. The numbers $n_{h,k}^{(r)}$, $r = 1, 2$, denote the dimension of the space of univariate NURBS with knots $\Xi_{h,k}^{(r)}$. To ensure that all NURBS basis functions are continuous in the patch Ω_k, we require that all knots in $(0,1)$ have at most multiplicity p_k, i.e.

$$h_{k,i}^{(r)} = \xi_{h,k,i+p_k}^{(r)} - \xi_{h,k,i}^{(r)} > 0, \qquad r = 1,2, \quad 2 \le i \le n_{h,k}^{(r)}.$$

The representative mesh-size h_k for Ω_k is defined as

$$h_k := \max_{r=1,2} \max_{2 \le i \le n_{h,k}^{(r)}} h_{k,i}^{(r)}. \tag{15}$$

The following terminology for knot sequences will be useful.

Definition 4.1. Let Θ_h be a family of open knot sequences with first and last knot of multiplicity $p+1$. This family is called *locally quasi-uniform of order p*, if there exist $0 < c_1 \le c_2$ such that for all h

$$c_1 \le \frac{\theta_{h,i+p} - \theta_{h,i}}{\theta_{h,i+p+1} - \theta_{h,i+1}} \le c_2, \qquad 2 \le i \le n_h - 1. \tag{16}$$

It is called *quasi-uniform of order p*, if there exist $0 < c_1 \le c_2$ such that for all h

$$c_1 \le \frac{\theta_{h,i+p} - \theta_{h,i}}{\theta_{h,j+p} - \theta_{h,j}} \le c_2, \qquad 2 \le i, j \le n_h. \tag{17}$$

A family of bivariate knot sequences $\boldsymbol{\Xi}_h = \Xi_h^{(1)} \times Xi_h^{(2)}$ is called *shape-regular*, if the ratio of the diameter and the smallest edge of every rectangle defined by the distinct knots is uniformly bounded.

The bivariate NURBS function $\hat{N}_{h,k,\mathbf{i}}$ with knots $\boldsymbol{\Xi}_{h,k} \subset [0,1]^2$ are defined as in (4), where tensor-product B-splines $\hat{B}^{p_k}_{h,k,\mathbf{i}}$ with respect to the refined knot sequence $\boldsymbol{\Xi}_{h,k}$ are inserted and the weight vector $(\omega_{h,k,\mathbf{i}})$ is obtained from the initial weights $(\omega_{k,\mathbf{i}})$ by "knot insertion"; i.e., the denominator

$$\hat{w}_k = \sum_{\mathbf{i} \in \mathbf{I}_k} \omega_{k,\mathbf{i}} \hat{B}^{p_k}_{k,\mathbf{i}} = \sum_{\mathbf{i} \in \mathbf{I}_{h,k}} \omega_{h,k,\mathbf{i}} \hat{B}^{p_k}_{h,k,\mathbf{i}}$$

remains the same before and after the refinement. The span of all $\hat{N}_{h,k,\mathbf{i}}$ is denoted by $\hat{X}_{h,k}$, its counterpart on $\Omega_k = \mathbf{F}_k([0,1]^2)$ is

$$X_{h,k} = \{\hat{v}_h \circ \mathbf{F}_k^{-1} : \hat{v}_h \in \hat{X}_{h,k}\}.$$

Finally, we let

$$X_h = \prod_{k=1}^{K} X_{h,k} \cap H^1_{0,D}(\Omega).$$

Our assumptions about the knots guarantee that $X_{h,k} \subset C(\overline{\Omega_k})$, so that $X_h \subset X$.

Remark 4.2. The parameters $h^{(r)}_{k,j}$ are also useful for inverse inequalities of functions $\hat{v} \in \hat{X}_{h,k}$. They replace the single stepsizes which are often used for piecewise linear finite elements.

For each interface γ_l, we let $\Theta_{h,l}$ be the refined knot sequence on the parameter interval $\overline{\hat{\gamma}_l} = [\xi_{l,1}, \xi_{l,2}]$; i.e., $\Theta_{h,l} = \Xi^{(1)}_{h,s(l)}$ or $\Xi^{(2)}_{h,s(l)}$ in the geometrically conforming case and in case NC1 of Remark 2.1, whereas $\Theta_{h,l}$ is only the part $\Xi^{(r)}_{h,s(l)} \cap [\xi_{l,1}, \xi_{l,2}]$ and the multiplicity of both endpoints is raised to $p_{s(l)} + 1$. We also let $q_l := p_{s(l)}$ and denote by $n_{h,l}$ the number of NURBS basis functions with knots $\Theta_{h,l}$. Following Brivadis et al. [12], we define the trace spaces

$$W_{h,l} = X_{h,s(l)}|_{\gamma_l}, \qquad W_{h,l,0} = W_{h,l} \cap H^1_0(\gamma_l)$$

and their counterparts on $\hat{\gamma}_l$ given by

$$\hat{W}_{h,l} = \operatorname{span}(\hat{N}_{h,l,j}; 1 \le j \le n_{h,l}), \qquad \hat{W}_{h,l,0} = \operatorname{span}(\hat{N}_{h,l,j}; 2 \le j \le n_{h,l} - 1).$$

Note that all linear combinations $y = \sum_{j=1}^{n_{h,l}} c_j \hat{N}_{h,l,j}$ satisfy the endpoint interpolation conditions $y(\xi_{l,1}) = c_1$ and $y(\xi_{l,2}) = c_{n_{h,l}}$.

4.2. The space M_h defined by B-splines

The definition of the space M_h of Lagrange multipliers is based on the space of polynomial splines of degree q_l,

$$\hat{S}^{q_l}(\Theta_{h,l}) = \operatorname{span}(\hat{B}^{q_l}_{h,l,j} : 1 \le j \le n_{h,l}).$$

We provide some information about B-splines which is essential in the sequel. Let us drop the indices h, l for a moment. The fundamental stability result for B-splines [13] states that there is a constant $\kappa_q > 0$ such that for arbitrary coefficients $c_j \in \mathbb{R}$ the following inequality holds:

$$\kappa_q^{-1} \sum_j |c_j|^2 \le \left\| \sum_j c_j h_j^{-1/2} \hat{B}^q_j \right\|^2_{L^2(\mathbb{R})} \le \sum_j |c_j|^2, \qquad h_j = \frac{\theta_{j+q+1} - \theta_j}{q+1}. \tag{18}$$

The constant κ_q does not depend on Θ and is called the condition number of B-splines of degree q. Another well-known result for B-splines is the recurrence relation for derivatives

$$(\hat{B}^q_j)' = \frac{q}{\theta_{j+q} - \theta_j} \hat{B}^{q-1}_j - \frac{q}{\theta_{j+q+1} - \theta_{j+1}} \hat{B}^{q-1}_{j+1}. \tag{19}$$

Combined with (18), the inverse estimate

$$\|\hat{v}'\|_{L^2(\mathbb{R})} \le 2\sqrt{q(q+1)\kappa_q} h_{\min}^{-1} \|\hat{v}\|_{L^2(\mathbb{R})} \tag{20}$$

follows easily for all $\hat{v} \in \hat{S}^q(\Theta)$, where $h_{\min} = \min_i(\theta_{i+q} - \theta_i) > 0$ is assumed.

We now return to our notations for $\hat{S}^{q_l}(\Theta_{h,l})$. The spline space with homogeneous boundary conditions is

$$\hat{S}^{q_l}_0(\Theta_{h,l}) = \hat{S}^{q_l}(\Theta_{h,l}) \cap H^1_0(\hat{\gamma}_l).$$

The orthogonal projection onto $\hat{S}^{q_l}(\Theta_{h,l})$ is denoted by

$$\hat{P}_{h,l} : L^2(\hat{\gamma}_l) \to \hat{S}^{q_l}(\Theta_{h,l}), \qquad \int_{\hat{\gamma}_l} (f - \hat{P}_{h,l} f)\, \hat{v}_l \, d\xi = 0 \quad \text{for all} \quad \hat{v}_l \in \hat{S}^{q_l}(\Theta_{h,l}). \tag{21}$$

Another important operator is the local spline projector from [21, Section 4.6]

$$\hat{\Pi}_{h,l} : L^2(\hat{\gamma}_l) \to \hat{S}^{q_l}(\Theta_{h,l}), \qquad \hat{\Pi}_{h,l}(f) = \sum_{j=1}^{n_{h,l}} \lambda_j(f) \hat{B}^{q_l}_{h,l,j}, \tag{22}$$

where the linear functionals $\lambda_j = \lambda_{h,l,j}$ only take values of f in the interval $[\theta_{h,l,j}, \theta_{h,l,j+q_l+1}]$ which is the support of $\hat{B}^{q_l}_{h,l,j}$. The corresponding operator on the physical domain is defined by

$$\Pi_{h,l} : L^2(\gamma_l) \to W_{h,l}, \qquad \Pi_{h,l} f = \left(\frac{1}{\hat{w}_l} \hat{\Pi}_{h,l}(\hat{w}_l\, (f \circ F_l)) \right) \circ F_l^{-1}. \tag{23}$$

The following approximation properties of $\hat{\Pi}_{h,l}$ are known from [21, Section 6.5] and summarized in [4, Lemma 4.3].

Proposition 4.3. *Let $\Theta_{h,l} \subset \overline{\hat{\gamma}_l}$ be an open knot sequence, $I_{h,i} = (\theta_{h,l,i}, \theta_{h,l,i+1})$ a non-empty interval and*

$$\widetilde{I}_{h,i} = (\theta_{h,l,i-q_l}, \theta_{h,l,i+q_l+1}) \tag{24}$$

the associated "support extension". There exists $C > 0$ depending only on q_l, such that

$$\|f - \hat{\Pi}_{h,l}(f)\|_{L^2(I_{h,i})} \le C|\widetilde{I}_{h,i}|^s \, |f|_{H^s(\widetilde{I}_{h,i})} \quad \text{for every } f \in H^s(\hat{\gamma}_l),\ 0 \le s \le q_l + 1. \tag{25}$$

If $\Theta_{h,l}$ is locally quasi-uniform of order q_l, there is $C > 0$ depending only on q_l and the constants c_1, c_2 in Definition 4.1, such that

$$|f - \hat{\Pi}_{h,l}(f)|_{H^1(I_{h,i})} \le C|\widetilde{I}_{h,i}|^{s-1} \, |f|_{H^s(\widetilde{I}_{h,i})} \quad \text{for every } f \in H^s(\hat{\gamma}_l),\ 1 \le s \le q_l + 1. \tag{26}$$

Remark 4.4. The second result in [4, Lemma 4.3] is for semi-norms of order $1 \le r \le s$ and for locally quasi-uniform knot sequences, which means that adjacent non-empty knot intervals have comparable lengths. The proof in [4] uses an inverse inequality for splines. The weaker assumption of local quasi-uniformity of order q_l is sufficient for the error estimate in the H^1-semi-norm.

We describe in more detail the choice of two suitable subspaces $\hat{M}^t_{h,l} \subset \hat{S}^{q_l}(\Theta_{h,l})$ of Lagrange multipliers of dimension $n_{h,l} - 2$, with upper index $t = 0$ or $t = 1$ denoting the chosen alternative. The subspaces on the physical domain are then obtained as

$$M^t_{h,l} = \left\{ (\hat{w}_l^{-1}\hat{\mu}_l) \circ F_l^{-1} : \hat{\mu}_l \in \hat{M}^t_{h,l} \right\} \subset W_{h,l}. \tag{27}$$

The definition for $t = 0$ follows Brivadis et al. [12, page 305] and describes the "p/p setting with boundary modification." The space

$$\hat{M}^0_{h,l} = \{\hat{\mu} \in \hat{S}^{q_l}(\Theta_{h,l}) : \frac{d^{q_l}}{d\xi^{q_l}}\hat{\mu}(\xi) = 0 \text{ for } \xi = 0 \text{ and } \xi = 1\} \subset \hat{S}^{q_l}(\Theta_{h,l}) \tag{28}$$

contains all splines in $\hat{S}^{q_l}(\Theta_{h,l})$ whose polynomial pieces in the first and last knot intervals $(\xi_{l,1}, \theta_{h,l,q_l+2})$, $(\theta_{h,l,n_{h,l}}, \xi_{l,2})$ have degree at most $q_l - 1$. (This is also a common choice for Lagrange multipliers in FEM discretizations.) We summarize the results in [12].

Proposition 4.5. *Let $q = q_l$ and $n = n_{h,l} \ge q_l + 2$.*

(a) The space $\hat{M}^0_{h,l}$ has dimension $n - 2$ and a basis with local support

$$\hat{\mu}^0_j = \hat{B}^q_{h,l,j} - \rho_j \hat{B}^q_{h,l,1} - \sigma_j \hat{B}^q_{h,l,n}, \qquad 2 \le j \le n - 1,$$

where

$$\rho_j = \frac{\frac{d^q}{d\xi^q}\hat{B}^q_{h,l,j}(\xi_{l,1})}{\frac{d^q}{d\xi^q}\hat{B}^q_{h,l,1}(\xi_{l,1})}, \qquad \sigma_j = \frac{\frac{d^q}{d\xi^q}\hat{B}^q_{h,l,j}(\xi_{l,2})}{\frac{d^q}{d\xi^q}\hat{B}^q_{h,l,n}(\xi_{l,2})}.$$

In particular, $\rho_j = 0$ for $j \ge q + 2$ and $\sigma_j = 0$ for $j \le n - q - 1$.

(b) $\hat{M}^0_{h,l}$ contains all polynomials of degree $q - 1$.

The authors in [12] explain that the discrete infsup-condition

$$\inf_{\hat{\mu}\in\hat{M}^0_{h,l}} \sup_{\hat{v}\in\hat{S}^{q_l}(\Theta_{h,l})} \frac{\int_{\hat{\gamma}_l} \hat{\mu}\hat{v}\, d\xi}{\|\hat{v}\|_{L^2(\hat{\gamma}_l)}\, \|\hat{\mu}\|_{L_2(\hat{\gamma}_l)}} \geq c > 0, \tag{29}$$

has not been proved yet. They provide numerical evidence for its validity.

Next we define the space $\hat{M}^1_{h,l} \subset \hat{S}^{q_l}(\Theta_{h,l})$, which is very similar to $\hat{M}^0_{h,l}$ and for which we can prove the infsup-condition analytically. Roughly speaking, we choose a space with the same dimension $n_{h,l} - 2$ containing all polynomials of degree $q_l - 1$, but with different modifications near the endpoints of $\hat{\gamma}_l$. For this purpose, we use the B-spline $\hat{B}^{2q_l}_{h,l,1}$ of double degree $2q_l$, which is defined with respect to the knot sequence $\Theta = \Theta_{h,l}$ whose first and last knot have multiplicity $q_l + 1$. Note that $\hat{B}^{2q_l}_{h,l,1}$ has vanishing function values and derivatives up to order $q_l - 1$ at both endpoints. The same is true for $\hat{B}^{2q_l}_{h,l,n_{h,l}-q_l}$. We employ the recurrence relation for derivatives of B-splines in (19) and define

$$\hat{e}_{h,l,1} = \frac{d^{q_l}}{d\xi^{q_l}}\, \hat{B}^{2q_l}_{h,l,1} = \sum_{j=1}^{q_l+1} \alpha_j \hat{B}^{q_l}_{h,l,j}, \tag{30}$$

where the coefficients $\alpha_j \neq 0$, $1 \leq j \leq q_l + 1$, can be easily computed via (19). (In fact, α_j's alternate in sign.) Likewise, near the other endpoint $\xi = 1$ and with $n = n_{h,l}$, we define

$$\hat{e}_{h,l,2} = \frac{d^{q_l}}{d\xi^{q_l}}\, \hat{B}^{2q_l}_{h,l,n-q_l} = \sum_{j=n-q_l}^{n} \beta_j \hat{B}^{q_l}_{h,l,j} \tag{31}$$

with nonzero coefficients β_j, $n - q_l \leq j \leq n$. We assume, as in Proposition 4.5, that there is at least one interior knot, so $n = n_{h,l} \geq q_l + 2$ and the functions $\hat{e}_{h,l,1}$ and $\hat{e}_{h,l,2}$ satisfy the boundary conditions

$$\frac{\hat{e}_{h,l,1}(\xi_{l,1})}{\alpha_1} = \frac{\hat{e}_{h,l,2}(\xi_{l,2})}{\beta_n} = 1, \qquad \hat{e}_{h,l,1}(\xi_{l,2}) = \hat{e}_{h,l,2}(\xi_{l,1}) = 0. \tag{32}$$

In particular, both functions are linearly independent. Their supports are

$$\operatorname{supp} \hat{e}_{h,l,1} = [\xi_{l,1}, \theta_{h,l,2q_l+2}], \qquad \operatorname{supp} \hat{e}_{h,l,2} = [\theta_{h,l,n-q_l}, \xi_{l,2}]. \tag{33}$$

The space

$$\hat{E}^1_{h,l} := \operatorname{span}(\hat{e}_{h,l,1}, \hat{e}_{h,l,2}) \tag{34}$$

of dimension 2 plays a prominent role in our construction. We define the orthogonal projection $P_{\hat{E}^1_{h,l}} : L^2(\hat{\gamma}_l) \to \hat{E}^1_{h,l}$. An orthogonal basis of $\hat{E}^1_{h,l}$ is given by the two splines $\hat{e}_{h,l,1}$ and

$$\widetilde{e}_{h,l,2} = \hat{e}_{h,l,2} - \frac{\langle \hat{e}_{h,l,2}, \hat{e}_{h,l,1} \rangle_{L^2(\hat{\gamma}_l)}}{\langle \hat{e}_{h,l,1}, \hat{e}_{h,l,1} \rangle_{L^2(\hat{\gamma}_l)}}\, \hat{e}_{h,l,1},$$

by the Gram-Schmidt orthogonalization procedure. Note that for $n = n_{h,l} \geq 3q_l + 2$, the supports of $\hat{e}_{h,l,1}$ and $\hat{e}_{h,l,2}$ do not overlap, so $\widetilde{e}_{h,l,2} = \hat{e}_{h,l,2}$.

We are now ready to define the spaces $\hat{M}^1_{h,l}$ as an alternative choice for the Lagrange multipliers.

Proposition 4.6. *Let $q = q_l$, $n = n_{h,l}$ and assume $n \geq q + 2$. Then $\hat{M}^1_{h,l}$ is the orthogonal complement of $\hat{E}^1_{h,l}$ in $\hat{S}^q(\Theta_{h,l})$; i.e.*

$$\hat{M}^1_{h,l} = (\mathrm{id} - P_{\hat{E}^1_{h,l}})(\hat{S}^q(\Theta_{h,l})).$$

(a) $\hat{M}^1_{h,l}$ has dimension $n-2$ and a basis with local support

$$\hat{\mu}^1_{h,l,j} = (\mathrm{id} - P_{\hat{E}^1_{h,l}})(\hat{B}^q_{h,l,j}) = \hat{B}^q_{h,l,j} - \rho_j \hat{e}_{h,l,1} - \sigma_j \widetilde{e}_{h,l,2},, \qquad 2 \leq j \leq n-1, \tag{35}$$

where

$$\rho_j = \frac{\langle \hat{B}^q_{h,l,j}, \hat{e}_{h,l,1} \rangle_{L^2(\hat{\gamma}_l)}}{\langle \hat{e}_{h,l,1}, \hat{e}_{h,l,1} \rangle_{L^2(\hat{\gamma}_l)}}, \qquad \sigma_j = \frac{\langle \hat{B}^q_{h,l,j}, \widetilde{e}_{h,l,2} \rangle_{L^2(\hat{\gamma}_l)}}{\langle \widetilde{e}_{h,l,2}, \widetilde{e}_{h,l,2} \rangle_{L^2(\hat{\gamma}_l)}}.$$

In particular, $\rho_j = 0$ for $j \geq 2q+2$ and $\sigma_j = 0$ for $j \leq n - 2q - 1$.

(b) $\hat{M}^1_{h,l}$ contains all polynomials of degree $q-1$.

Proof. We can drop the indices h and l without causing confusion. We already observed that $\hat{E}^1$ has dimension 2, and consequently $\hat{M}^1$ has dimension $n-2$. Moreover, by their definition, all splines $\hat{\mu}^1_j$ in (35) are orthogonal to $\hat{E}^1$, so they are elements of $\hat{M}^1$. Their linear independence is shown as follows. The identity

$$0 = \sum_{j=2}^{n-1} c_j \hat{\mu}^1_j = (\mathrm{id} - P_{\hat{E}^1}) \left(\sum_{j=2}^{n-1} c_j \hat{B}^q_j \right)$$

for some $(c_2, \ldots, c_{n-1}) \in \mathbb{R}^{n-2}$ implies that

$$y := \sum_{j=2}^{n-1} c_j \hat{B}^q_j \in \hat{E}^1 = \mathrm{span}(\hat{e}_1, \hat{e}_2).$$

This spline y has boundary values $y(\xi_{l,1}) = y(\xi_{l,2}) = 0$, because all B-splines $\hat{B}^q_j$ in the sum vanish at both endpoints of $\hat{\gamma}_l$. By (32) it follows that $y \equiv 0$, and by the linear independence of the B-splines, it follows further that all coefficients c_j, $2 \leq j \leq n-2$, must vanish. Therefore, the splines $\hat{\mu}_j$, $2 \leq j \leq n-1$, in (35) are a basis of $\hat{M}^1$. Their local support and the zero-values for the coefficients ρ_j, σ_j are simple consequences of the support properties in (33).

For part (b), it is sufficient to prove that every polynomial $\hat{g}$ of degree $q-1$ is orthogonal to both basis elements $\hat{e}^1_j$, $j = 1, 2$. Since the B-spline $\hat{B}^{2q}_1$ of double degree has vanishing function values and derivatives up to order $q-1$ at both endpoints of $\hat{\gamma}_l$, integration by parts gives

$$\int_{\hat{\gamma}_l} \hat{g}(\xi) \hat{e}_1(\xi)\, d\xi = (-1)^q \int_{\hat{\gamma}_l} \frac{d^q}{d\xi^q} \hat{g}(\xi) \hat{B}^{2q}_1(\xi)\, d\xi = 0.$$

Analogously, the orthogonality of $\hat{g}$ and $\hat{e}_2$ follows. □

Remark 4.7. The effect of choosing $\hat{E}^1_{h,l}$ as the orthogonal complement of the Lagrange multiplier space $\hat{M}^1_{h,l}$ can be further explained as follows. Consider a function $v_h \in V_h$ in the discrete solution space. By the definition of V_h in (12), the jump

$$[v_h]_l = v_{h,s(l)}|_{\gamma_l} - v_{h,m(l)}|_{\gamma_l}$$

satisfies

$$\langle [v_h]_l, \mu_l \rangle_{\rho_l} = \int_{\hat{\gamma}_l} \hat{w}_l \, ([v_h]_l \circ F_l) \, \hat{\mu}_l \, d\xi = 0$$

for all $\hat{\mu}_l \in \hat{M}^1_{h,l}$. In other words, with the orthogonal projection $\hat{P}_{h,l}$ onto $\hat{S}^{q_l}(\Theta_{h,l})$ and with $\hat{w}_l(v_{h,s(l)}|_{\gamma_l} \circ F_l) \in \hat{S}^{q_l}(\Theta_{h,l})$, we have

$$\hat{P}_{h,l} \, (\hat{w}_l \, ([v_h]_l \circ F_l)) = \hat{w}_l \, (v_{h,s(l)} \circ \, F_l) - \hat{P}_{h,l} \left(\hat{w}_l \, (v_{h,m(l)} \circ \, F_l) \right) \in \hat{E}^1_{h,l}. \tag{36}$$

Note that all functions in $\hat{E}^1_{h,l}$ have support in $[\xi_{l,1}, \theta_{h,l,2q_l+2}] \cup [\theta_{h,l,n_{h,l}-q_l}, \xi_{l,2}]$. Therefore, we have

$$v_{h,s(l)} \circ \, F_l(\xi) = \frac{1}{\hat{w}_l(\xi)} \, \hat{P}_{h,l} \left(\hat{w}_l \, (v_{h,m(l)} \circ \, F_l) \right) (\xi) \quad \text{for all} \quad \xi \in [\theta_{h,l,2q_l+2}, \theta_{h,l,n_{h,l}-q_l}].$$

In particular, if the two discretizations of γ_l as a boundary line of $\Omega_{s(l)}$ and $\Omega_{m(l)}$ coincide (the fully conforming case), then the orthogonal projection has no effect at all and we obtain

$$v_{h,s(l)} \circ \, F_l(\xi) = v_{h,m(l)} \circ \, F_l(\xi) \quad \text{for all} \quad \xi \in [\theta_{h,l,2q_l+2}, \theta_{h,l,n_{h,l}-q_l}]. \tag{37}$$

Hence, in the fully conforming case, the jump across γ_l of every function $v_h \in V_h$ is nonzero only in a small neighbourhood of the endpoints of γ_l. This property is not valid, if the Lagrange multiplier space $\hat{M}^1_{h,l}$ is replaced by $\hat{M}^0_{h,l}$ as proposed in [12], because the orthogonal complement $\hat{E}^0_{h,l}$ of $\hat{M}^0_{h,l}$ in the spline space has no local basis.

We next prove the following stability result for $\hat{e}_{h,l,1}$ and $\hat{e}_{h,l,2}$. We drop the indices h and l without causing confusion.

Lemma 4.8. *Let $\Theta = \{\theta_1, \ldots, \theta_{n+q+1}\} \subset \overline{\hat{\gamma}_l}$ be an open knot sequence for splines of degree $q \in \mathbb{N}$ and $h_j := \frac{\theta_{j+q+1} - \theta_j}{q+1} > 0$ for every $1 \le j \le n$. Furthermore, let*

$$\hat{e}_1 = \frac{d^q}{d\xi^q} \hat{B}^{2q}_1 = \sum_{j=1}^{q+1} \alpha_j \hat{B}^q_j, \qquad \hat{e}_2 = \frac{d^q}{d\xi^q} \hat{B}^{2q}_{n-q} = \sum_{j=n-q}^{n} \beta_j \hat{B}^q_j. \tag{38}$$

For every

$$v = \frac{c_1}{\alpha_1 \sqrt{h_1}} \, \hat{e}_1 + \frac{c_2}{\beta_n \sqrt{h_n}} \, \hat{e}_2 \tag{39}$$

we have

$$\kappa_q^{-1}(c_1^2 + c_2^2) \le \|v\|^2_{L^2(\hat{\gamma}_l)} \le 2 \binom{2q}{q} (c_1^2 + c_2^2),$$

where κ_q is the condition number of B-splines of degree q in (18).

Proof. We have $h_1 = \frac{\theta_{q+2}-\theta_1}{q+1}$ and $\theta_1 = \ldots = \theta_{q+1} = 0$. In order to find the precise coefficients α_j, the recurrence relation (19)

$$\frac{d}{d\xi}\hat{B}_j^m = \frac{m}{\theta_{j+m}-\theta_j}\hat{B}_j^{m-1} - \frac{m}{\theta_{j+m+1}-\theta_{j+1}}\hat{B}_{j+1}^{m-1}$$

is applied for B-splines of degree m, where $q+1 \le m \le 2q$ and $1 \le j \le 2q+1-m$. Within this range of indices, we have $\theta_j = \theta_{j+1} = 0$, and therefore

$$\min\{\theta_{j+m}-\theta_j, \theta_{j+m+1}-\theta_{j+1}\} \ge \theta_{1+m} \ge \theta_{q+2} = (q+1)h_1.$$

From here, we obtain that the coefficients α_j in (38) satisfy

$$0 < (-1)^{j-1}h_j\alpha_j \le \binom{q}{j-1}\prod_{m=q+2}^{2q}\frac{m}{\theta_{1+m}} = \binom{q}{j-1}h_1\alpha_1$$

for all $1 \le j \le 2q+1$. Since $h_j \ge h_1$, this also implies

$$\sum_{j=1}^{q+1}\frac{|\alpha_j|^2 h_j}{|\alpha_1|^2 h_1} \le \sum_{j=1}^{q+1}\binom{q}{j-1}^2 = \binom{2q}{q},$$

where the last identity is well-known in combinatorics. The stability result in (18) is applied to

$$\frac{\hat{e}_1}{\alpha_1\sqrt{h_1}} = h_1^{-1/2}\hat{B}_1^q + \sum_{j=2}^{n}\frac{\alpha_j\sqrt{h_j}}{\alpha_1\sqrt{h_1}}h_j^{-1/2}\hat{B}_j^q$$

and gives

$$\kappa_q^{-1} \le \left\|\frac{\hat{e}_1}{\alpha_1\sqrt{h_1}}\right\|_{L^2(\hat{\gamma}_l)}^2 \le 1 + \sum_{j=2}^{q+1}\frac{|\alpha_j|^2 h_j}{|\alpha_1|^2 h_1} \le \binom{2q}{q}.$$

The same upper bound is obtained for the norm of $\frac{\hat{e}_2}{\beta_n\sqrt{h_n}}$. Therefore, by Minkowski's inequality for v in (39), we obtain

$$\|v\|_{L^2(\hat{\gamma}_l)}^2 \le (|c_1|+|c_2|)^2\binom{2q}{q} \le 2\left(|c_1|^2+|c_2|^2\right)\binom{2q}{q},$$

and this provides the upper bound in the lemma. Furthermore, our assumption $n \ge q+2$ and Theorem 4.6(b) imply $\alpha_n = \beta_1 = 0$. Therefore, the first and last coefficients of the B-spline representation of v are $c_1 h_1^{-1/2}$ and $c_2 h_n^{-1/2}$, respectively. Another application of (18) provides the lower bound in the lemma. □

5. Mortar projection

In this section, we consider the space $M^1_{h,l}$ of Lagrange multipliers for the interface γ_l. An important operator for the error analysis of the discretization is the mortar projection. Its L^2-boundedness will be essential for the proof of the infsup-condition in the next section.

We define the mortar projection as in [5] with small modifications. For the interface γ_l, let $Q_{h,l} : L^2(\gamma_l) \to W_{h,l,0}$ be given by

$$\langle (f - Q_{h,l} f), \mu_l \rangle_{\rho_l} = 0 \quad \text{for all} \quad \mu_l \in M^1_{h,l}. \tag{40}$$

The associated operator on the parameter domain is defined by

$$\hat{Q}_{h,l} : L^2(\hat{\gamma}_l) \to \hat{S}^{q_l}_0(\Theta_{h,l}), \qquad \int_{\hat{\gamma}_l} (\hat{f} - \hat{Q}_{h,l} \hat{f})\, \hat{\mu}_l \, d\xi = 0 \quad \text{for all} \quad \hat{\mu}_l \in \hat{M}^1_{h,l}. \tag{41}$$

More precisely, we have by (7) and (27)

$$Q_{h,l} f = \left(\frac{1}{\hat{w}_l}\, \hat{Q}_{h,l}(\hat{w}_l\, (f \circ F_l)) \right) \circ F_l^{-1}. \tag{42}$$

An important observation about $M^1_{h,l}$ was the decoupling of the endpoints of γ_l in (32). By using this fact, the following simple connection between $\hat{Q}_{h,l}$ and the orthogonal projection $\hat{P}_{h,l} : L^2(\hat{\gamma}_l) \to \hat{S}^{q_l}(\Theta_{h,l})$ can be established. We use the basis functions $\hat{e}_{h,l,1}, \hat{e}_{h,l,2}$ of $\hat{E}^1_{h,l}$ and their coefficients α_j in (30) and β_j in (31).

Lemma 5.1. *Let $n = n_{h,l}$. For $\hat{f} \in L^2(\hat{\gamma}_l)$ we let $\hat{g}_f = \hat{P}_{h,l} \hat{f} \in \hat{S}^{q_l}(\Theta_{h,l})$. Then we have*

$$\hat{Q}_{h,l} \hat{f} = \hat{g}_f - \frac{\hat{g}_f(\xi_{l,1}) \hat{e}_{h,l,1}}{\alpha_1} - \frac{\hat{g}_f(\xi_{l,2}) \hat{e}_{h,l,2}}{\beta_n}. \tag{43}$$

Proof. Since $\hat{M}^1_{h,l} \subset \hat{S}^{q_l}(\Theta_{h,l})$, the spline function $\hat{g}_f = \hat{P}_{h,l} \hat{f}$ satisfies

$$\int_{\hat{\gamma}_l} \left(\hat{f} - \hat{g}_f \right) \hat{\mu}_l \, d\xi = 0 \quad \text{for all} \quad \hat{\mu}_l \in \hat{M}^1_{h,l}.$$

The orthogonality remains valid if any combination of $\hat{e}_{h,l,1}$ and $\hat{e}_{h,l,2}$ is added to $\hat{g}_f$. By (32) the function $\widetilde{g}_f$ on the right-hand side of (43) satisfies homogeneous boundary conditions and

$$\int_{\hat{\gamma}_l} \left(\hat{f} - \widetilde{g}_f \right) \hat{\mu}_l \, d\xi = 0 \quad \text{for all} \quad \hat{\mu}_l \in \hat{M}^1_{h,l}.$$

Clearly, it is the unique element of $\hat{S}^{q_l}(\Theta_{h,l})$ which combines both properties. □

We can now show the L^2-boundedness of the mortar projection $Q_{h,l}$.

Theorem 5.2. *There is $C > 0$, which depends on q_l, τ_l, and $\hat{w}_l$, but not on the knot sequence $\Theta_{h,l}$, such that*

$$\|Q_{h,l} f\|_{L^2(\gamma_l)} \le C \|f\|_{L^2(\gamma_l)} \quad \textit{for all} \quad f \in L^2(\gamma_l). \tag{44}$$

Proof. Let $q = q_l$ and $n = n_{h,l}$. By the equivalence of the standard and the weighted L^2-norms on $L^2(\gamma_l)$, it is sufficient to prove the boundedness of $\hat{Q}_{h,l}$ on $L^2(\hat{\gamma}_l)$. Let $\hat{f} \in L^2(\hat{\gamma}_l)$ and

$$\hat{g}_f = \hat{P}_{h,l}\hat{f} = \sum_{j=1}^{n} c_j h_j^{-1/2} \hat{B}^q_{h,l,j}.$$

By Lemma 5.1 and the endpoint conditions of the B-splines, we have

$$\hat{Q}_{h,l}\hat{f} = \hat{g}_f - \frac{\hat{g}_f(\xi_{l,1})\hat{e}_{h,l,1}}{\alpha_1} - \frac{\hat{g}_f(\xi_{l,2})\hat{e}_{h,l,2}}{\beta_n} = \hat{g}_f - \frac{c_1\hat{e}_{h,l,1}}{h_1^{1/2}\alpha_1} - \frac{c_n\hat{e}_{h,l,2}}{h_n^{1/2}\beta_n}.$$

The orthogonal projection gives

$$\|\hat{g}_f\|_{L^2(\hat{\gamma}_l)} \le \|\hat{f}\|_{L^2(\hat{\gamma}_l)},$$

and Lemma 4.8 shows that

$$\left\| \frac{c_1\hat{e}_{h,l,1}}{h_1^{1/2}\alpha_1} + \frac{c_n\hat{e}_{h,l,2}}{h_n^{1/2}\beta_n} \right\|_{L^2(\hat{\gamma}_l)} \le \left(2\binom{2q}{q}\right)^{1/2} \sqrt{c_1^2 + c_n^2}.$$

The stability result of (18) gives

$$\sqrt{c_1^2 + c_n^2} \le \kappa_q^{1/2} \|\hat{g}_f\|_{L^2(\hat{\gamma}_l)} \le \kappa_q^{1/2} \|\hat{f}\|_{L^2(\hat{\gamma}_l)}.$$

By combining these estimates, we obtain

$$\|\hat{Q}_{h,l}\hat{f}\|_{L^2(\hat{\gamma}_l)} \le C_q \|\hat{f}\|_{L^2(\hat{\gamma}_l)}, \qquad C_q := 1 + \left(2\kappa_q\binom{2q}{q}\right)^{1/2}, \tag{45}$$

so the constant C in (44) only depends on $q = q_l$ and, by the norm equivalence, on $\hat{\omega}_l$ and τ_l. □

Remark 5.3. The estimate of Theorem 5.2 immediately extends to the mesh-dependent norm (14)

$$\sum_{l=1}^{L} h_{s(l)}^{-2\sigma} \|Q_{h,l} f\|_{L^2(\gamma_l)} \le C \sum_{l=1}^{L} h_{s(l)}^{-2\sigma} \|f\|^2_{L^2(\gamma_l)} = C|f|^2_{\sigma,h} \quad \text{for all} \quad f \in L^2(S).$$

Moreover, if the knot sequence $\Theta_{h,l}$ is quasi-uniform of order $p_{s(l)}$, we also obtain the H_0^1-stability of $Q_{h,l}$ by a similar argument as given in Lemma 1.3 in [24]. Indeed, for a function $\hat{f} \in H_0^1(\hat{\gamma}_l)$ we can find an approximant $\hat{v} \in \hat{S}_0^{q_l}(\Theta_{h,l})$ with homogeneous boundary conditions such that

$$\|\hat{f} - \hat{v}\|_{L^2(\hat{\gamma}_l)} \le C h_{s(l)} |\hat{f}|_{H^1(\hat{\gamma}_l)}, \qquad |\hat{v}|_{H^1(\hat{\gamma}_l)} \le C|\hat{f}|_{H^1(\hat{\gamma}_l)},$$

where the last expression denotes the Sobolev semi-norm of $\hat{f}$ and C does not depend on $\hat{f}$. (This is property (Sc) in [24, p.12].) By the projection property $\hat{Q}_{h,l}\hat{v} = \hat{v}$ and an inverse inequality (here quasi-uniformity of order $p_{s(l)}$ of the knots is needed), we obtain

$$|\hat{Q}_{h,l}\hat{f}|_{H^1(\hat{\gamma}_l)} \le |\hat{Q}_{h,l}(\hat{f} - \hat{v})|_{H^1(\hat{\gamma}_l)} + |\hat{v}|_{H^1(\hat{\gamma}_l)} \le C h_{s(l)}^{-1} \|\hat{Q}_{h,l}(\hat{f} - \hat{v})\|_{L_2(\hat{\gamma}_l)} + |\hat{v}|_{H^1(\hat{\gamma}_l)} \le C|\hat{f}|_{H^1(\hat{\gamma}_l)}.$$

Furthermore, by a typical interpolation argument, we obtain that

$$\|\hat{Q}_{h,l}\hat{f}\|_{H_{00}^{1/2}(\hat{\gamma}_l)} \le C\|\hat{f}\|_{H_{00}^{1/2}(\hat{\gamma}_l)}, \qquad \hat{f} \in H_{00}^{1/2}(\hat{\gamma}_l).$$

A further generalization of this result to locally quasi-uniform knot sequences is not known to us.

6. Discrete infsup-condition

In this section, we prove the uniform infsup-inequality for the discrete spaces X_h and M_h^1. The method of proof is well known, see e.g. [9], and mainly based on Theorem 5.2. We include some details as far as explicit constants are concerned. Let us first consider the corresponding spaces on the parameter domain.

Theorem 6.1. *Let $1 \le l \le L$, $q = q_l$ and $C_q = \left(1 + \left(2\kappa_q \binom{2q}{q}\right)^{1/2}\right)$ as in* (45)*. Then*

$$\inf_{\hat{\mu}\in\hat{M}_{h,l}^1} \sup_{\hat{v}\in\hat{S}_0^q(\Theta_{h,l})} \frac{\int_{\hat{\gamma}_l} \hat{\mu}\hat{v}\, d\xi}{\|\hat{\mu}\|_{L^2(\hat{\gamma}_l)}\|\hat{v}\|_{L^2(\hat{\gamma}_l)}} \ge C_q^{-1}. \tag{46}$$

Proof. A duality argument, the definition of $\hat{Q}_{h,l}$ and (45) allow us to write

$$\|\hat{\mu}\|_{L^2(\hat{\gamma}_l)} = \sup_{f\in L^2(\hat{\gamma}_l)} \frac{\int_{\hat{\gamma}_l} f\hat{\mu}\, d\xi}{\|f\|_{L^2(\hat{\gamma}_l)}} = C_q \sup_{f\in L^2(\hat{\gamma}_l)} \frac{\int_{\hat{\gamma}_l} \hat{Q}_{h,l}f\ \hat{\mu}\, d\xi}{C_q\|f\|_{L^2(\hat{\gamma}_l)}} \le C_q \sup_{f\in L^2(\hat{\gamma}_l)} \frac{\int_{\hat{\gamma}_l} \hat{Q}_{h,l}f\ \hat{\mu}\, d\xi}{\|\hat{Q}_{h,l}f\|_{L^2(\hat{\gamma}_l)}}$$

for all $\hat{\mu} \in \hat{M}_{h,l}^1$. By letting $\hat{v} = \hat{Q}_{h,l}f$ we obtain (46). □

Remark 6.2. (i) The result of Theorem 6.1 holds for arbitrary open knot sequences $\Theta_{h,l}$. As mentioned before, an analogous result for the Lagrange multiplier space $\hat{M}_{h,l}^0$ in [12] is not known.

(ii) Since the dimensions of $\hat{M}_{h,l}^1$ and $\hat{S}_0^{q_l}(\Theta_{h,l})$ agree, the order of the spaces in the infsup-estimate can be switched, i.e.

$$\inf_{\hat{v}\in\hat{S}_0^{q_l}(\Theta_{h,l})} \sup_{\hat{\mu}\in\hat{M}_{h,l}^1} \frac{\int_{\hat{\gamma}_l} \hat{\mu}\hat{v}\, d\xi}{\|\hat{\mu}\|_{L^2(\hat{\gamma}_l)}\|\hat{v}\|_{L^2(\hat{\gamma}_l)}} \ge C_{q_l}^{-1}. \tag{47}$$

In fact, the best possible lower bound on the right-hand side of (46) and (47) is the smallest singular value of the "mixed Gramian" $(\langle\phi_j, \psi_k\rangle)_{j,k=1,\dots,n-2}$ with respect to L^2-orthonormal bases of both spaces. For more details see [14].

The observation in (47) is also useful in order to prove the following stability result for the local basis

$$\hat{\mu}_{h,l,j}^1 = (I - P_{\hat{E}_{h,l}^1})\hat{B}_{h,l,j}^q, \qquad 2 \le j \le n_{h,l} - 1,$$

in (35).

Theorem 6.3. *Let $q = q_l$ and $n = n_{h,l}$. Let κ_q, C_q be the constants in* (18) *and* (45)*. For an arbitrary open knot sequence $\Theta_{h,l} \subset \overline{\hat{\gamma}_l}$, with $h_j = \frac{\theta_{j+q+1}-\theta_j}{q+1} > 0$ for all j, and for arbitrary coefficients $c_j \in \mathbb{R}$ the following inequality holds:*

$$\kappa_q^{-1}C_q^{-2}\sum_{j=2}^{n-1}|c_j|^2 \le \left\|\sum_{j=2}^{n-1} c_j h_j^{-1/2}\hat{\mu}_{h,l,j}^1\right\|_{L^2(\hat{\gamma}_l)}^2 \le \sum_{j=2}^{n-1}|c_j|^2.$$

Proof. First note that for every $\hat{v} \in \hat{S}^q(\Theta_{h,l})$, the function $(I - P_{\hat{E}^1_{h,l}})\hat{v}$ is the orthogonal projection of $\hat{v}$ onto $\hat{M}^1_{h,l}$. By (47) and a duality argument, it follows that for all $\hat{v} \in \hat{S}^q_0(\Theta_{h,l})$

$$C_q^{-1}\|\hat{v}\| \le \sup_{\hat{\mu}\in\hat{M}^1_{h,l}} \frac{\int_{\hat{\gamma}_l} \hat{\mu}\hat{v}\, d\xi}{\|\hat{\mu}\|} = \sup_{\hat{\mu}\in\hat{M}^1_{h,l}} \frac{\int_{\hat{\gamma}_l} \hat{\mu}\,(I - P_{\hat{E}^1_{h,l}})\hat{v}\, d\xi}{\|\hat{\mu}\|} = \|(I - P_{\hat{E}^1_{h,l}})\hat{v}\|,$$

where norms are taken in $L^2(\hat{\gamma}_l)$. We let $\hat{v} = \sum_{j=2}^{n-1} c_j h_j^{-1/2} \hat{B}^q_{h,l,j}$ with arbitrary coefficients $c_j \in \mathbb{R}$ and obtain

$$C_q^{-1}\,\|\hat{v}\| \le \left\|(I - P_{\hat{E}^1_{h,l}})\hat{v}\right\| = \left\|\sum_{j=2}^{n-1} c_j h_j^{-1/2} \hat{\mu}^1_{h,l,j}\right\| \le \|\hat{v}\|\,.$$

Combined with (18), this gives the claim. □

The last result, in combination with the infsup-condition, shows that the block $\mathcal{M}_{h,l}$ of the mass matrix with entries

$$m_{i,j} = \langle \mu^1_{h,l,i}, N^{q_l}_{h,l,j}\rangle_{\rho_l} = \int_{\hat{\gamma}_l} \hat{\mu}^1_{h,l,i}\, \hat{B}^{q_l}_{h,l,j}\, d\xi, \qquad 2 \le i,j \le n_{h,l} - 1,$$

has a uniformly bounded condition number for arbitrary knot sequences. This property is the same as the "spectral equivalence" in [24, p.13]. Note that this block is banded due to the local support of the basis. In Section 8 we will present an even sparser block by choosing a different basis of $\hat{M}^1_{h,l}$. Although the new basis will have global support $\overline{\hat{\gamma}_l}$, the mass matrix has more zeros due to biorthogonality.

Next we consider the infsup-condition on the physical interfaces. It is obtained from the boundedness of the mortar projections $Q_{h,l}$ exactly in the same way as in [24, Lemma 1.9]. The use of the weight function ρ_l on the interface γ_l affects the lower bound only slightly. From this point on, the following assumption on the knot sequences of the discretization is required.

Assumption 2. *All refinement knot sequences $\Xi_{h,k}$ are quasi-uniform of order p_k and shape-regular with constants independent of h.*

Theorem 6.4. *Assume that Assumption 2 is satisfied. Then there is $c > 0$ depending only on all p_k and $\mathbf{F}_k$, such that*

$$\inf_{\mu\in M^1_h} \sup_{v\in X_h} \frac{b_\rho(v,\mu)}{\|v\|_X\ \|\mu\|_{-1/2,h}} \ge c. \tag{48}$$

Proof. We follow the proof in [24, Lemma 1.9] with minor changes caused by the parameterization. Let $\mu = (\mu_l : 1 \le l \le L) \in M^1_h$. By duality and by writing the weighted inner product $\langle \phi, \mu_l\rangle_{\rho_l}$ as a standard product $\langle \rho_l\phi, \mu_l\rangle$ in $L^2(\gamma_l)$, we have

$$h_l^{1/2}\|\mu_l\|_{L^2(\gamma_l)} = \sup_{\phi\in L^2(\gamma_l)} \frac{\langle \phi, \mu_l\rangle_{\rho_l}}{h_l^{-1/2}\|\rho_l\phi\|_{L^2(\gamma_l)}} \le C_1 \sup_{\phi\in L^2(\gamma_l)} \frac{\langle \phi, \mu_l\rangle_{\rho_l}}{h_l^{-1/2}\|\phi\|_{L^2(\gamma_l)}}$$

where $C_1 = \max_{1\le l\le L} \|1/\rho_l\|_\infty$ depends only on the parameterizations $\mathbf{F}_k$. The definition of the mortar projection in (40) and Theorem 5.2 give

$$\frac{|\langle \phi, \mu_l\rangle_{\rho_l}|}{\|\phi\|_{L^2(\gamma_l)}} = \frac{|\langle Q_{h,l}\phi, \mu_l\rangle_{\rho_l}|}{\|\phi\|_{L^2(\gamma_l)}} \le C\frac{|\langle Q_{h,l}\phi, \mu_l\rangle_{\rho_l}|}{\|Q_{h,l}\phi\|_{L^2(\gamma_l)}}$$

with the constant C in (44). Hence, we have

$$h_l^{1/2}\|\mu_l\|_{L^2(\gamma_l)} \le C_1 C \max_{\phi\in W_{h,l,0}} \frac{\langle \phi, \mu_l\rangle_{\rho_l}}{h_l^{-1/2}\|\phi\|_{L^2(\gamma_l)}}.$$

With the maximizing element $\phi_l \in W_{h,l,0}$, which is normalized by $h_l^{-1/2}\|\phi_l\|_{L^2(\gamma_l)} = 1$, we obtain

$$\|\mu\|^2_{-1/2,h} = \sum_{l=1}^{L} h_l\|\mu_l\|^2_{L^2(\gamma_l)} \le (C_1C)^2 \sum_{l=1}^{L}\langle \phi_l, \mu_l\rangle^2_{\rho_l}. \tag{49}$$

Next we let $\widetilde{\phi_l}$ be the extension by zero to all of $\partial\Omega_{s(l)}$. Lemma 5.1 in [8] provides us with a function $v_l \in X_h$, which is zero on all patches Ω_k with $k \ne s(l)$ and which is an extension of $\widetilde{\phi_l}$ to $\Omega_{s(l)}$, such that

$$\|v_l\|^2_{1,\Omega_{s(l)}} \le C_2\|\widetilde{\phi_l}\|^2_{H^{1/2}(\partial\Omega_{s(l)})} = C_2\|\phi_l\|^2_{H^{1/2}_{00}(\gamma_l)}. \tag{50}$$

The constant C_2 depends only on the geometry of the patches Ω_k, not on their discretization. By Assumption 2 and an inverse inequality for ϕ_l, there is a constant $C_3 > 0$ depending only on $p_{s(l)}$ such that

$$\|v_l\|^2_{1,\Omega_{s(l)}} \le C_2C_3h_l^{-1}\|\phi_l\|^2_{L^2(\gamma_l)} = C_2C_3. \tag{51}$$

Since v_l satisfies

$$v_l|_{\Omega_k} = 0 \ \text{ for } \ k \ne s(l), \qquad v_l|_{\gamma_m} = 0 \ \text{ for } \ l \ne m, \tag{52}$$

the linear combination

$$v_\mu = \sum_l \langle \phi_l, \mu_l\rangle_{\rho_l}\, v_l \in X_h$$

has jumps $[v_\mu]_l = \langle \phi_l, \mu_l\rangle_{\rho_l}\phi_l$ for $1 \le l \le L$. Therefore, we obtain

$$b_\rho(v_\mu, \mu) = \sum_l \langle \phi_l, \mu_l\rangle^2_{\rho_l}. \tag{53}$$

Let r_l denote the number of times the patch $\Omega_{s(l)}$ is counted as a slave domain. Then the Cauchy-Schwarz inequality and (51) and (52) imply

$$\begin{aligned}\|v_\mu\|^2_X &= \sum_{k=1}^{K}\|v_\mu\|^2_{1,\Omega_k} = \sum_{l=1}^{L}\frac{1}{r_l}\|v_\mu\|^2_{1,\Omega_{s(l)}} \\ &\le \sum_{l=1}^{L}\langle \phi_l, \mu_l\rangle^2_{\rho_l}\|v_l\|^2_{1,\Omega_{s(l)}} \le C_2C_3\sum_{l=1}^{L}\langle \phi_l, \mu_l\rangle^2_{\rho_l}.\end{aligned}$$

Combined with (49) and (53), this gives

$$\|v_\mu\|_X\ \|\mu\|_{-1/2,h} \le (C_2C_3)^{1/2}C_1C\ b_\rho(v_\mu, \mu).$$

This allows us to choose $c = (C_2C_3)^{-1/2}(C_1C)^{-1}$ in (48). □

7. A priori error estimate

We let $(u, \lambda) \in X \times M$ be the solution of (9) and $(u_h, \lambda_h) \in X_h \times M_h^1$ be the solution of (11). Recall from (10) that

$$\lambda|_{\gamma_l} = \frac{\alpha}{\rho_l} \frac{\partial u}{\partial \nu_l}.$$

The restrictions to Ω_k and γ_l will be denoted by u_k, $u_{h,k}$, and λ_l, $\lambda_{h,l}$, respectively. The standard approach to estimates of the a-priori error uses the coercivity of $a(v, v)$ on X_h and the identities (9), (11), in order to arrive at

$$\begin{aligned} c_1 \|u - u_h\|_X^2 &\leq a(u - u_h, u - u_h) \\ &= \inf_{v_h \in V_h} \big(a(u - u_h, u - v_h) + a(u - u_h, v_h - u_h) \big) \\ &= \inf_{v_h \in V_h} \big(a(u - u_h, u - v_h) + b_\rho(u_h - v_h, \lambda) \big). \end{aligned}$$

Note that $b_\rho(u_h - v_h, \lambda_h) = 0$ was used here, which follows from the definition of V_h in (12). Then the approximation error

$$E_a := \inf_{v_h \in V_h} \|u - v_h\|_X$$

and the consistency error

$$E_b := \sup_{v_h \in V_h} \frac{b_\rho(v_h, \lambda)}{\|v_h\|_X} \tag{54}$$

lead to the estimate (cf. [10])

$$\|u - u_h\|_X \leq C(E_a + E_b). \tag{55}$$

Because our setting differs from [24, Section 1.2], we include a step-by-step description, although some of the arguments are similar. We believe that the results presented in [12] are incomplete in the sense that additional requirements on the discretization are needed in order to obtain the optimal approximation rate.

7.1. Spline approximation on interfaces

The main cause of the defect is the lack of a "standard" trace theorem for Sobolev spaces on domains with non-smooth boundary. Note that non-smooth interfaces γ_l are typical for the IGA mortar method, as soon as splines with interior knots in $\hat{\gamma}_l$ are used for the parameterizations F_l. More precisely, $\gamma_l \subset \partial\Omega_k$ is a $C^{\kappa,1}$-curve, with $\kappa \leq p_k - 1$ depending on the maximal mulitplicity of the interior knots of Θ_l. Suppose that the component $u_k = u|_{\Omega_k}$ of the solution (u, λ) is an element of $H^{p_k+1}(\Omega_k)$, where p_k denotes the degree of the B-splines in the definition (3) of $\mathbf{F}_k$. Then $u_k|_{\gamma_l}$ is an element of $H^{\kappa+1}(\gamma_l)$ by [19, Remark 4.3, p. 85]. However, a Sobolev space $H^{p_k+1/2}(\gamma_l)$, as in a standard trace theorem for smooth boundaries, is not even defined.

One step towards the resolution of this defect was already described by Bazilevs et al. [3], and used in [12]. They introduce the notion of bent Sobolev spaces on the parameter domain $\hat{\gamma}_l \subset \mathbb{R}$. In short, by the result in [4, Lemma 4.1], the bent Sobolev space

$$\mathcal{H}^s(\hat{\gamma}_l; \Theta_l) = H^s(\hat{\gamma}_l) + \hat{S}^{p_k}(\Theta_l) \tag{56}$$

of integer order $0 \le s \le p_k + 1$ is defined. The norm is the broken Sobolev norm with respect to the knot intervals of Θ_l. One part of our additional work is an extension of [4, Propositions 4.3 and 4.25] to non-integer $s = p_k + 1/2$ in Theorem 7.6. This will provide the optimal order for the approximation error E_a in Subsection 7.2.

The resolution of the defect in the upper bound for the consistency error E_b is more subtle, as it requires an additional condition of the knot sequence $\Theta_{h,l}$ which was not mentioned in [12]. Interestingly, this extra condition is only needed, if the original parameterization $\mathbf{F}_k$ of Ω_k uses knot sequences with multiple knots. The defect could not be observed in the numerical examples of [12], where knot sequences with simple knots were used throughout. Nevertheless, knot sequences with multiple knots occur in practical examples as the output of standard CAD surface models. In Section 9 we provide numerical examples to demonstrate this defect. We show in Theorem 7.6 that the following assumptions will be sufficient in order to resolve this defect. Both Assumptions 3 and 4 are very easy to realize in numerical implementations.

Assumption 3. All interfaces γ_l are $C^{1,1}$-curves. In more detail, let $1 \le l \le L$ and $k = s(l)$. The interface $\gamma_l = F_l(\hat{\gamma}_l)$ is parameterized as a NURBS curve of degree p_k and with open knot sequence $\Theta_l \subset \overline{\hat{\gamma}_l}$. The distinct knots of Θ_l are denoted by ζ_i, with $\zeta_1 = \xi_{l,1}$ and $\zeta_{N_l} = \xi_{l,2}$ at the endpoints of $\hat{\gamma}_l$. We assume that the multiplicities of the interior knots ζ_i, $2 \le i \le N_l - 1$, are $1 \le \kappa_i \le p_k - 1$; i.e., γ_l is $p_k - \kappa_i$-times continuously differentiable in a neighbourhood of ζ_i. Consequently, γ_l is differentiable on $(0, 1)$, its tangent τ_l and its unit normal ν_l are Lipschitz-continuous.

Remark 7.1. Note that Assumption 3 does not allow to consider interfaces γ_l which are only C^0-continuous, but not smooth at some knot ζ_i. This complies with the practical experience, that vertices on an interface γ_l should be treated by splitting the adjacent domains accordingly, thus introducing an additional interface. In fact, this is incorporated in all standard CAD programs. However, modifications by hand could possibly result in a non-smooth interface or such points may already exist in industrial CAD files. Therefore, they should be properly treated by a patch coupling method. If no additional interface is desired, we can keep the patch geometry, but split γ_l at the relevant location into two parts $\gamma_{l,1}, \gamma_{l,2}$ and then follow the same method described in Remark 2.1 for T-intersections of type NC2. Thus our results in this section can be extended to geometries with interfaces containing C^0-points. A numerical example with this feature is presented in Section 9.1.3.

We next discuss the case when Θ_l contains multiple knots except for both endpoints. We define the "augmented" knot sequence

$$\Theta_l^+ = \Theta_l \dot{\cup} \{\zeta_j : \kappa_j \ge 2 \text{ with } 2 \le j \le N_l - 1\}. \tag{57}$$

(By definition, $\Theta_l^+ = \Theta_l$ if all ζ_i, $2 \le i \le N_l - 1$, are simple knots.) Here, taking the union is understood in the sense of ordered sets; i.e., the multiplicity of every interior knot ζ_j is increased by one, if ζ_j is a multiple knot of Θ_l. By Assumption 3, every spline in $\hat{S}^{p_k}(\Theta_l^+)$ is continuous.

Assumption 4. With the same notations as in Assumption 3, we assume that $\Theta_{h,l}$ is a refinement of Θ_l^+.

The following observations provide more insight concerning Assumption 3 and the definition of Θ_l^+.

Proposition 7.2. *let* $1 \le l \le L$, $k = s(l)$ *and* $\hat{w}_l$ *be the denominator of* F_l *in* (6). *Assume that* $u_k \in H^{p_k+1}(\Omega_k)$. *Then*

$$\hat{w}_l \, (u_k \circ F_l) \in H^1(\hat{\gamma}_l) \cap \mathcal{H}^{p_k}(\hat{\gamma}_l, \Theta_l) = H^{p_k}(\hat{\gamma}_l) + \hat{S}^{p_k}(\Theta_l). \tag{58}$$

If Θ_l *satisfies Assumption 3 and the factor* α *in* (1) *is in* $C^{p_k-1,1}(\overline{\Omega_k})$, *then*

$$\hat{w}_l \, (\lambda_l \circ F_l) = \frac{\tau_l}{\hat{w}_l} \, (\alpha \circ F_l) \, ((\nabla u \cdot \nu_l) \circ F_l) \in \mathcal{H}^{p_k-1}(\hat{\gamma}_l; \Theta_l^+) = H^{p_k-1}(\hat{\gamma}_l) + \hat{S}^{p_k}(\Theta_l^+). \tag{59}$$

Proof. Let $t = \hat{w}_l \, (u_k \circ F_l)$ and $y = \hat{w}_l \, (\lambda_l \circ F_l)$. The standard trace theorem gives $t \in H^{p_k+1/2}(I_i)$ for all $I_i = (\zeta_i, \zeta_{i+1})$, because $\hat{w}_l$ and F_l are smooth (and even analytic) functions on I_i. At each interior knot ζ_i of Θ_l, the left-sided and right-sided derivatives $D_-^j t(\zeta_i)$ and $D_+^j t(\zeta_i)$ agree for all $0 \le j \le p_k - \kappa_i$, where $\kappa_i \ge 1$ is the multiplicity of ζ_i in Θ_l. (This is the precise smoothness property of the parameterization F_l at ζ_i.) Hence, the condition $t \in \mathcal{H}^{p_k}(\hat{\gamma}_l, \Theta_l)$, written in terms of the definition of bent Sobolev spaces in [4, Eq. (4.1)] as

$$D_-^j t(\zeta_i) = D_+^j t(\zeta_i) \quad \text{for all} \quad 0 \le j \le \min\{p_k - \kappa_i, p_k - 1\},$$

is satisfied.

In a similar way, because $\nabla u \in (H^{p_k}(\Omega_k))^2$ and all other constituents of λ_l are in $C^{p_k-1,1}(I_i)$, we have $y \in H^{p_k-1/2}(I_i)$ for all i. Moreover, since the tangent and normal vectors of γ_l are included in the definition of y, the smoothness across ζ_i is reduced by 1 and satisfies

$$D_-^j y(\zeta_i) = D_+^j y(\zeta_i) \quad \text{for all} \quad 0 \le j \le p_k - \kappa_i - 1. \tag{60}$$

If $\kappa_i \ge 2$, then the multiplicity of ζ_i in Θ_l^+ is $\kappa_i^+ = \kappa_i + 1$, otherwise $\kappa_i^+ = \kappa_i = 1$. The smoothness condition for $f \in \mathcal{H}^{p_k-1}(\hat{\gamma}_l, \Theta_l^+)$ in [4, Eq. (4.1)] reads as

$$D_-^j f(\zeta_i) = D_+^j f(\zeta_i) \quad \text{for all} \quad 0 \le j \le \min\{p_k - \kappa_i^+, p_k - 2\}.$$

Hence, by (60) we have $y \in \mathcal{H}^{p_k-1}(\hat{\gamma}_l, \Theta_l^+)$. □

Remark 7.3. The result of [4, Lemma 4.1] provides linear projectors

$$\Gamma_1 : \mathcal{H}^{p_k}(\hat{\gamma}_l; \Theta_l) \to \hat{S}^{p_k}(\Theta_l), \qquad \Gamma_2 : \mathcal{H}^{p_k-1}(\hat{\gamma}_l; \Theta_l^+) \to \hat{S}^{p_k}(\Theta_l^+), \tag{61}$$

such that

$$f - \Gamma_1 f \in H^{p_k}(\hat{\gamma}_l), \quad D^{p_k}(\Gamma_1 f|_{I_i}) = 0 \ \text{ for all } \ 1 \le i \le N_l - 1,$$

and

$$f - \Gamma_2 f \in H^{p_k-1}(\hat{\gamma}_l), \quad D^{p_k-1}(\Gamma_2 f|_{I_i}) = 0 \ \text{ for all } \ 1 \le i \le N_l - 1.$$

The splines $\Gamma_1 f$ and $\Gamma_2 f$ are defined in order to "swallow up" all jumps of derivatives of f at the knots ζ_i.

Remark 7.4. For further clarification of Assumption 4, we mention that $\lambda_l \circ F_l$ falls short of the smoothness requirements for the bent Sobolev space $\mathcal{H}^{p_k-1}(\hat{\gamma}_l, \Theta_l)$, if Θ_l contains multiple knots ζ_i, $2 \le i \le N_l - 1$. Therefore, the order of approximation by splines in $\hat{S}^{p_k}(\Theta_{h,l})$ may be deficient if $\Theta_{h,l}$ does not satisfy Assumption 4. This defect will carry over to the consistency error E_b.

The method in [3, 4] provides the following error estimates. We use the notations $I_{h,i} = (\theta_{h,l,i}, \theta_{h,l,i+1})$ for non-empty knot intervals associated with $\Theta_{h,l}$, and $\widetilde{I}_{h,i} = (\theta_{h,l,i-p_k}, \theta_{h,l,i+p_k+1})$ for the support extensions. Here we use the convention that $i - p_k \le 0$ is substituted by 1 and $i + p_k + 1 \ge n_{h,l} + p_k + 2$ is substituted by $n_{h,l} + p_k + 1$. The following result combines Proposition 7.2 with [4, Propositions 4.3 and 4.25].

Proposition 7.5. *Let $1 \le l \le L$, $k = s(l)$ and $\hat{w}_l$ be the denominator of F_l. Assume that $u|_{\Omega_k} \in H^{p_k+1}(\Omega_k)$, $\alpha \in C^{p_k-1,1}(\overline{\Omega_k})$, Θ_l satisfies Assumption 3 and $\Theta_{h,l}$ satisfies Assumption 2.*

(a) There exists a constant $C > 0$ depending only on p_k and $\mathbf{F}_k$ such that the local spline projector $\hat{\Pi}_{h,l} : L^2(0,1) \to \hat{S}^{p_k}(\Theta_{h,l})$ satisfies

$$\|D^j(\mathrm{id} - \hat{\Pi}_{h,l})(\hat{w}_l\, u_k \circ F_l)\|_{L_2(I_{h,i})} \le C|\widetilde{I}_{h,i}|^{p_k-j}\, |\hat{w}_l\, u_k \circ F_l|_{\mathcal{H}^{p_k}(\widetilde{I}_{h,i})}, \qquad j = 0, 1. \tag{62}$$

(b) If, in addition, $\Theta_{h,l}$ satisfies Assumption 4, there exists a constant $C > 0$ depending only on p_k, α and $\mathbf{F}_k$ such that

$$\|(\mathrm{id} - \hat{\Pi}_{h,l})(\hat{w}_l\, \lambda_l \circ F_l)\|_{L_2(I_{h,i})} \le C|\widetilde{I}_{h,i}|^{p_k-1}\, |\hat{w}_l\, \lambda_l \circ F_l|_{\mathcal{H}^{p_k-1}(\widetilde{I}_{h,i})}. \tag{63}$$

Here we use the semi-norm defined by

$$|f|_{\mathcal{H}^s(\widetilde{I}_{h,i})} = \left(\sum_{j=i-p_k}^{i+p_k} \|f^{(s)}\|^2_{L_2(\theta_{h,l,j}, \theta_{h,l,j+1})} \right)^{1/2}.$$

Without change, we can replace the local spline projector in (62) *by the projector $\widetilde{\Pi}_{h,l}$ in [4, Eq. (2.29)] to match the boundary values of $\hat{w}_l\, u_k \circ F_l$ at $\xi = \xi_{l,1}$ and $\xi = \xi_{l,2}$.*

The results in Proposition 7.5 are valid under milder conditions than Assumption 2. Instead of quasi-uniform knot sequences $\Theta_{h,l}$, we can also allow locally quasi-uniform sequences, see [4, Assumption 2.1] for more details.

Based on Assumption 2, we can replace $|\widetilde{I}_{h,i}|$ in (62) and (63) by Ch_k with C depending on p_k. Optimal estimates of the approximation error and the consistency error require an extra factor $h_k^{1/2}$ in both relations (62) and (63). This will be obtained by performing an analysis of super-convergence similar to the techniques in [23].

Theorem 7.6. *Let the assumptions of Proposition 7.5 be satisfied.*

(a) There exists a constant $C > 0$ depending only on p_k and $\mathbf{F}_k$, such that the local spline projector $\hat{\Pi}_{h,l} : L^2(\hat{\gamma}_l) \to \hat{S}^{p_k}(\Theta_{h,l})$ satisfies

$$\|D^j(\mathrm{id} - \hat{\Pi}_{h,l})(\hat{w}_l\, u_k \circ F_l)\|_{L_2(\hat{\gamma}_l)} \le Ch_k^{p_k+1/2-j}\, \|u\|_{H^{p_k+1}(\Omega_k)}, \qquad j = 0, 1. \tag{64}$$

(b) If, in addition, $\Theta_{h,l}$ satisfies Assumption 4, there exists a constant $C > 0$ depending only on p_k, α and $\mathbf{F}_k$ such that

$$\|(\mathrm{id} - \hat{\Pi}_{h,l})(\hat{w}_l\, \lambda_l \circ F_l)\|_{L_2(\hat{\gamma}_l)} \le Ch_k^{p_k-1/2}\, \|u\|_{H^{p_k+1}(\Omega_k)}. \tag{65}$$

The same estimates are valid for the projector $\widetilde{\Pi}_{h,l}$ matching the boundary values at $\xi = \xi_{l,1}$ and $\xi = \xi_{l,2}$.

Proof. (a) Let $t = \hat{w}_l(u_k \circ F_l)$. We explained in the proof of Proposition 7.2 that $t \in H^{p_k+1/2}(I_i)$, where $I_i = (\zeta_i, \zeta_{i+1})$ is a knot-interval of the initial knot sequence Θ_l. Let $\Gamma_1 t \in \hat{S}^{p_k}(\Theta_l) \subset \hat{S}^{p_k}(\Theta_{h,l})$ be the spline in Remark 7.3 such that

$$t - \Gamma_1 t \in H^{p_k}(\hat{\gamma}_l) \quad \text{and} \quad D^{p_k}(\Gamma_1 t|_{I_i}) = 0. \tag{66}$$

In the main part of the proof, we split

$$t - \Gamma_1 t = t_1 + t_2$$

into two parts, where

- $t_1 \in H^{p_k+1/2}(\hat{\gamma}_l)$,
- $t_2 \in \hat{S}^{p_k}(\Theta_l)$ is a spline of degree p_k with simple knots ζ_i, so

$$t_2(\xi) = \sum_{i=2}^{N_l-1} d_i \frac{(\xi - \zeta_i)_+^{p_k}}{p_k!}. \tag{67}$$

Let $F_l = (F_{l,1}, F_{l,2}) : \hat{\gamma}_l \to \mathbb{R}^2$ be the parameterization of γ_l inherited from $\mathbf{F}_k$. In order to define t_1 and t_2, we start from $t - \Gamma_1 t \in H^{p_k}(\hat{\gamma}_l)$ and consider the expansion of $D^{p_k}(t - \Gamma_1 t)$ by means of Leibniz' and Faa di Bruno's formulas. By collecting all terms with partial derivatives of u_k of order p_k, we obtain

$$t_3 := \hat{w}_l \sum_{r_1+r_2=p_k} (F'_{l,1})^{r_1} (F'_{l,2})^{r_2} \, (D^{(r_1,r_2)} u_k) \circ F_l. \tag{68}$$

By Assumption 3, all factors $\hat{w}_l (F'_{l,1})^{r_1} (F'_{l,2})^{r_2}$ are in $C^{0,1}(\overline{\hat{\gamma}_l})$. Combined with $D^{(r_1,r_2)} u_k \in H^1(\Omega_k)$, the trace theorem in [19, Theorem 5.5, p. 95] gives

$$t_3 \in H^{1/2}(\hat{\gamma}_l), \quad |t_3|_{H^{1/2}(\hat{\gamma}_l)} \le C \sum_{r_1+r_2=p_k} |(D^{(r_1,r_2)} u_k) \circ F_l|_{H^{1/2}(\hat{\gamma}_l)} \le C \|u\|_{H^{p_k+1}(\Omega_k)}. \tag{69}$$

The constant C depends only on p_k, $\hat{w}_l$, F_l and Ω_k, so on $\mathbf{F}_k$ after all.

All other terms of $D^{p_k}(t - \Gamma_1 t)$ contain partial derivatives of u_k of order less than or equal to $p_k - 1$ and derivatives of $\hat{w}_l, F_{l,1}, F_{l,2}$ up to order p_k. Therefore, by $u_k \in H^{p_k+1}(\Omega_k)$ and the trace theorem on smooth parts of γ_l, we have

$$D^{p_k}(t - \Gamma_1 t) - t_3 \in H^1(I_i) \quad \text{for every} \quad I_i = (\zeta_i, \zeta_{i+1}), \tag{70}$$

with

$$\|D^{p_k}(t - \Gamma_1 t) - t_3\|_{H^1(I_i)} \le C \|u\|_{H^{p_k+1}(\Omega_k)}. \tag{71}$$

The constant C depends only on p_k, $\hat{w}_l$, F_l and Ω_k, as before. Since $H^1(I_i)$ is imbedded in $C(\overline{I_i})$, the difference of one-sided limits

$$d_i = (D^{p_k}(t - \Gamma_1 t) - t_3)(\zeta_i+) - (D^{p_k}(t - \Gamma_1 t) - t_3)(\zeta_i-) \tag{72}$$

is bounded by

$$|d_i| \le C(\|D^{p_k}(t - \Gamma_1 t) - t_3\|_{H^1(I_i)} + \|D^{p_k}(t - \Gamma_1 t) - t_3\|_{H^1(I_{i-1})}) \le C\|u\|_{H^{p_k+1}(\Omega_k)}. \tag{73}$$

The new constant C depends further on $|I_{i-1}|$ and $|I_i|$, caused by the imbedding $H^1 \to C$, but not on h_k. The numbers d_i define the spline t_2 in (67), which is an element of $H^{p_k}(\hat{\gamma}_l)$. Therefore, we have

$$t_1 = t - \Gamma_1 t - t_2 \in H^{p_k}(\hat{\gamma}_l).$$

In order to show that $t_1 \in H^{p_k+1/2}(\hat{\gamma}_l)$ holds, we write $D^{p_k} t_1$ as

$$D^{p_k} t_1 = t_3 + D^{p_k}(t - \Gamma_1 t) - t_3 - D^{p_k} t_2.$$

The first term t_3 is in $H^{1/2}(\hat{\gamma}_l)$ by (69). By (70), the second part $t_4 := D^{p_k}(t - \Gamma_1 t) - t_3 - D^{p_k} t_2$ has pieces in $H^1(I_i)$ and satisfies

$$t_4(\zeta_i+) - t_4(\zeta_i-) = d_i - d_i = 0.$$

The continuity across all intervals implies $t_4 \in H^{1/2}(\hat{\gamma}_l)$ (even $t_4 \in H^1(\hat{\gamma}_l)$ is true), and

$$|t_4|_{H^{1/2}(\hat{\gamma}_l)} \le C \sum_{i=1}^{N_l-1} |t_4|_{H^{1/2}(I_i)} \le C \sum_{i=1}^{N_l-1} \left(|D^{p_k}(t - \Gamma_1 t) - t_3|_{H^{1/2}(I_i)} + |D^{p_k} t_2|_{H^{1/2}(I_i)} \right).$$

Because $D^{p_k}(t_2|_{I_i})$ is constant, the last semi-norm vanishes. By (71) and the imbedding $H^1(I_i) \to H^{1/2}(I_i)$ we obtain

$$|t_4|_{H^{1/2}(\hat{\gamma}_l)} \le C \sum_{i=1}^{N_l-1} \|D^{p_k}(t - \Gamma_1 t) - t_3\|_{H^1(I_i)} \le C\|u\|_{H^{p_k+1}(\Omega_k)}.$$

(The constant C from (71) has grown by a factor N_l which is independent of h_k.) Therefore, we have shown that $D^{p_k} t_1 = t_3 + t_4 \in H^{1/2}(\hat{\gamma}_l)$, and consequently $t_1 \in H^{p_k+1/2}(\hat{\gamma}_l)$ with

$$|t_1|_{H^{p_k+1/2}(\hat{\gamma}_l)} \le |t_3|_{H^{1/2}(\hat{\gamma}_l)} + |t_4|_{H^{1/2}(\hat{\gamma}_l)} \le C\|u\|_{H^{p_k+1}(\Omega_k)}.$$

Now we can prove (64). Since $\Gamma_1 t, t_2 \in \hat{S}^{p_k}(\Theta_l) \subset \hat{S}^{p_k}(\Theta_{h,l})$, the local spline projector in Proposition 4.3 provides the approximation

$$\|D^j(t - \hat{\Pi}_{h,l} t)\|_{L_2(\hat{\gamma}_l)} = \|D^j(t_1 - \hat{\Pi}_{h,l} t_1)\|_{L_2(\hat{\gamma}_l)} \le C h_k^{p_k+1/2-j} |t_1|_{H^{p_k+1/2}(\hat{\gamma}_l)} \le C h_k^{p_k+1/2-j} \|u\|_{H^{p_k+1}(\Omega_k)}$$

for $j = 0$ and $j = 1$.

(b) A similar proof is given for

$$y := \hat{w}_l \, \lambda_l \circ F_l = \frac{\tau_l}{\hat{w}_l} \, (\alpha \circ F_l) \, ((\nabla u \cdot \nu_l) \circ F_l)$$

in (65). We include the proof although many arguments are adaptations of the first part. Assumption 4 guarantees that the spline $\Gamma_2 y \in \hat{S}^{p_k}(\Theta_l^+)$ in Remark 7.3 is an element of $\hat{S}^{p_k}(\Theta_{h,l})$. The splitting of

$$y - \Gamma_2 y = y_1 + y_2$$

will be constructed in a similar way as before, but the spline y_2 is not in $\hat{S}^{p_k}(\Theta_{h,l})$. Therefore, the last step of the proof is extended and includes the consideration of the approximation of y_2 by splines in $\hat{S}^{p_k}(\Theta_{h,l})$.

We explained in the proof of Proposition 7.2 that y is a piecewise $H^{p_k-1/2}$-function on the parameter interval $\hat{\gamma}_l$. For the splitting, we construct $y_1 \in H^{p_k-1/2}(\hat{\gamma}_l)$ and a spline y_2 of degree $p_k - 1$ with simple knots ζ_i,

$$y_2(\xi) = \sum_{i=2}^{N_l-1} \tilde{d}_i \frac{(\xi - \zeta_i)_+^{p_k-1}}{(p_k-1)!}. \tag{74}$$

For the construction of y_2, and in analogy to the first part, we collect all terms of $D^{p_k-1}(y - \Gamma_2 y)$ with highest order partial derivatives of u_k into

$$y_3 = \frac{\tau_l}{\hat{w}_l} \, (\alpha \circ F_l) \sum_{r_1+r_2=p_k-1} (F_{l,1}')^{r_1} (F_{l,2}')^{r_2} \left((D^{(r_1,r_2)} \nabla u_k) \circ F_l \right) \cdot (\nu_l \circ F_l). \tag{75}$$

By Assumption 3, all factors $\tau_l, \hat{w}_l, \nu_l \circ F_l$ and $(F_{l,1}')^{r_1}(F_{l,2}')^{r_2}$ are in $C^{0,1}(\overline{\hat{\gamma}_l})$. Combined with the smoothness of α and $D^{(r_1,r_2)} \nabla u_k \in H^1(\Omega_k)$, the trace theorem gives

$$y_3 \in H^{1/2}(\hat{\gamma}_l), \quad |y_3|_{H^{1/2}(\hat{\gamma}_l)} \le C \sum_{r_1+r_2=p_k-1} |(D^{(r_1,r_2)} \nabla u_k) \circ F_l|_{H^{1/2}(\hat{\gamma}_l)} \le C \|u\|_{H^{p_k+1}(\Omega_k)}. \tag{76}$$

All other terms of $D^{p_k-1}(y - \Gamma_2 y)$ contain partial derivatives of u_k of order less than or equal to $p_k - 1$ and derivatives of $\alpha, \tau_l, \hat{w}_l, \nu_l$ and F_l up to order $p_k - 1$ as well. Therefore, by $u_k \in H^{p_k+1}(\Omega_k)$ we obtain the local properties

$$D^{p_k-1}(y - \Gamma_2 y) - y_3 \in H^1(I_i) \quad \text{for every} \quad I_i = (\zeta_i, \zeta_{i+1}), \tag{77}$$

with

$$\|D^{p_k-1}(y - \Gamma_2 y) - y_3\|_{H^1(I_i)} \le C \|u\|_{H^{p_k+1}(\Omega_k)}. \tag{78}$$

The constant C depends on $\alpha|_{\gamma_l} \in C^{p_k-1,1}$, F_l and Ω_k. With

$$\tilde{d}_i = (D^{p_k-1}(y - \Gamma_2 y) - y_3)(\zeta_i+) - (D^{p_k-1}(y - \Gamma_2 y) - y_3)(\zeta_i-) \tag{79}$$

we define y_2 in (74). The imbedding $H^1 \to C$ gives

$$|\tilde{d}_i| \le C(\|D^{p_k-1}(y - \Gamma_2 y) - y_3\|_{H^1(I_{i-1})} + \|D^{p_k-1}(y - \Gamma_2 y) - y_3\|_{H^1(I_i)}) \le C \|u\|_{H^{p_k+1}(\Omega_k)}. \tag{80}$$

As a spline of degree $p_k - 1$ with simple knots, y_2 is an element of $W^{p_k-1,\infty}(\hat{\gamma}_l) \subset H^{p_k-1}(\hat{\gamma}_l)$. In exactly the same way as in the first part, we can show that $y_1 = y - \Gamma_2 y - y_2 \in H^{p_k-1/2}(\hat{\gamma}_l)$ with

$$|y_1|_{H^{p_k-1/2}(\hat{\gamma}_l)} \leq C\|u\|_{H^{p_k+1}(\Omega_k)}.$$

Hence, the local spline projector provides the approximation

$$\|y_1 - \hat{\Pi}_{h,l} y_1\|_{L_2(\hat{\gamma}_l)} \leq Ch^{p_k-1/2}|y_1|_{H^{p_k-1/2}()}\hat{\gamma}_l \leq Ch^{p_k-1/2}\|u\|_{H^{p_k+1}(\Omega_k)}. \tag{81}$$

Finally, we consider the approximation order of y_2, a spline of degree $p_k - 1$ with simple knots ζ_i, $2 \leq i \leq N_l - 1$. The local spline projector $\hat{\Pi}_{h,l}$ reproduces the polynomial pieces of y_2 everywhere in $(0, 1)$, except for small intervals

$$J_{h,i} \subset (\zeta_i - ch_k, \zeta_i + ch_k), \qquad 2 \leq i \leq N_l - 1.$$

The constant c only depends on p_k and the constants c_1, c_2 of quasi-uniformity in Definition 4.1. We assume that h_k is small enough such that these intervals are disjoint. By $y_2 \in W^{p_k-1,\infty}(\hat{\gamma}_l)$ and (80) we have

$$\|D^{p_k-1} y_2\|_\infty \leq \sum_{i=2}^{N_l-1} |\tilde{d}_i| \leq CN_l\|u\|_{H^{p_k+1}(\Omega_k)}.$$

Combined with Assumption 2, the standard error estimate for the local spline projector gives

$$\|y_2 - \hat{\Pi}_{h,l} y_2\|_{L_2(J_{h,i})} \leq Ch_k^{p_k-1}|D^{p_k-1} y_2|_{L_2(\zeta_i - ch_k, \zeta_i + ch_k)} \leq Ch_k^{p_k-1/2}\|D^{p_k-1} y_2\|_\infty.$$

Note that the additional factor $h_k^{1/2}$ is obtained from the length of the interval $(\zeta_i - ch_k, \zeta_i + ch_k)$. By taking the union of all intervals $J_{h,i}$ we arrive at

$$\|y_2 - \hat{\Pi}_{h,l} y_2\|_{L_2(\hat{\gamma}_l)} \leq CN_l^2 h_k^{p_k-1/2}\|u\|_{H^{p_k+1}(\Omega_k)}. \tag{82}$$

By combining (81) and (82) we obtain the result in (65). □

Remark 7.7. (i) The result of Theorem 7.6(a) is also valid if $k = s(l)$ is replaced by $m(l)$, F_l is replaced by the restriction of $\mathbf{F}_{m(l)}$ to the parameter interval $\widetilde{\gamma}_l := \mathbf{F}_{m(l)}^{-1}(\gamma_l)$, and the spline space $\hat{S}^{p_k}(\Theta_l)$ is replaced by $\hat{S}^{p_{m(l)}}(\Theta_{h,m(l)})$, where $\Theta_{h,m(l)}$ is the part of the knot sequence of the NURBS parameterization $\mathbf{F}_{m(l)}$ which is relevant for γ_l.

(ii) For smoother functions $u_k := u|_{\Omega_k} \in H^{p_k+3}(\Omega_k)$ and $\alpha \in C^{p_k,1}(\overline{\Omega_k})$ we obtain better error bounds

$$\|(\mathrm{id} - \hat{\Pi}_{h,l})(\hat{w}_l\, u_k \circ F_l)\|_{L_2(\hat{\gamma}_l)} \leq Ch_k^{p_k+1}\, \|u\|_{H^{p_k+2}(\Omega_k)} \tag{83}$$

and

$$\|(\mathrm{id} - \hat{\Pi}_{h,l})(\hat{w}_l\, \lambda_l \circ F_l)\|_{L_2(\hat{\gamma}_l)} \leq Ch_k^{p_k+1}\, \|u\|_{H^{p_k+3}(\Omega_k)}. \tag{84}$$

The proof is much simpler than the proof of Theorem 7.6. The additional smoothness yields that $t := \hat{w}_l\, u_k \circ F_l$ is in $H^{p_k+5/2}(I_i)$ and $y := \hat{w}_l\, \lambda_l \circ F_l$ is in $H^{p_k+3/2}(I_i)$. Then we obtain the projectors Γ_1 into $S^{p_k}(\Theta_l)$ and Γ_2 into $S^{p_k}(\Theta_l^+)$ from [4, Lemma 4.1] such that

$$t - \Gamma_1 t \in H^{p_k+1}(\hat{\gamma}_l), \quad D^{p_k+1}(\Gamma_1 t|_{I_i}) = 0 \text{ for all } 1 \leq i \leq N_l - 1,$$

x	0.5	0.6	0.4	0.5
y	0	0.3	0.7	1
w	1	1	1	1

Table 1: Control points for the initial interface curve with an interior knot with C^1-smoothness

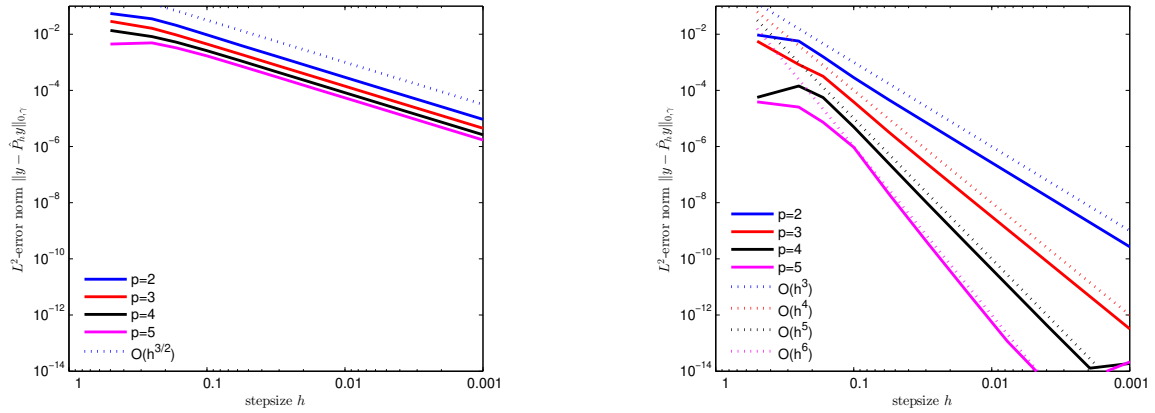

(a) L^2-error when the multiplicity $p-1$ of 0.5 is retained

(b) L^2-error when the multiplicity of 0.5 is raised to p.

Figure 2: L^2-error for spline approximation of degree $2 \le p \le 5$ of the normal derivative $y = \partial u/\partial \nu$ of $u(x,y) = \sin 3x \sin 2y$ on a spline curve γ with C^1-smoothness at knot $\zeta = 0.5$.

and

$$y - \Gamma_2 y \in H^{p_k+1}(\hat{\gamma}_l), \quad D^{p_k+1}(\Gamma_2 y|_{I_i}) = 0 \ \text{ for all } \ 1 \le i \le N_l - 1.$$

The results in (83) and (84) follow from the standard results on spline approximation. The complications by the split $t = t_1 + t_2$ in the proof of Theorem 7.6 are needed, because the term $D^{p_k} t(\zeta_i+) - D^{p_k} t(\zeta_i-)$ for the definition of $\Gamma_1 t$ is not always defined for $t \in H^{p_k+1/2}(I_i)$. The same difficulty occurs for derivatives of y of order $p_k - 1$ and p_k. The milder smoothness assumptions in Theorem 7.6 are used in accordance with the results for optimal error bounds in the non-IGA setting with Lagrange finite elements.

Example 7.8. We demonstrate the importance of Assumption 4, if an interface γ has limited smoothness. The function $u(x,y) = \sin(3x)\sin(2y)$ is analytic on the unit square $0 \le x, y \le 1$. We define a curved interface with initial degree $p_{\text{ini}} = 2$, knot sequence $\Xi = \{0,0,0,0.5,1,1,1\}$ and control points as listed in Table 1. The point $(x,y) = (0.5, 0.5)$ corresponds to the parameter $\xi = 0.5$ on the interface, where the curve has only C^1-smoothness. We let $y = \nabla u \cdot \nu$ be the normal derivative along γ and compute the error of the L^2-projector onto $S^{p_k}(\Theta_h)$, where Θ_h is a knot sequence of uniform stepsize h on both intervals $[0, 0.5]$ and $[0.5, 1]$. Note that y is only C^0-continuous at $\xi = 0.5$, as a consequence of the same property of the unit normal on γ. After reparameterization of γ using degree $p \ge 2$, the knot $\zeta = 1/2$ has multiplicity $p-1$ in accordance with the C^1-smoothness of γ. The left part of Figure 2 depicts the L^2-error $\|y - \hat{P}_{h,l} y\|_{0,\gamma}$, if Assumption 4 is not satisfied, i.e. the multiplicity $p-1$ of the knot $\zeta = 1/2$ in Θ_h is retained. The approximation rate $O(h^{3/2})$ is obtained for all degrees $2 \le p \le 5$. No improvement occurs

for higher degrees, because $O(h^{3/2})$ is the optimal approximation order of functions with isolated points of C^0-continuity by C^1-splines. After raising the multiplicity of the knot $\zeta = 1/2$ to p, we see in the right part of Figure 2 that the optimal approximation order $O(h^{p+1})$ is achieved for all $2 \le p \le 5$.

7.2. Approximation error

The method in [24, Section 1.2] shows how to find an optimal bound for the approximation error E_a. We consider the geometrically conforming case in Theorem 7.9 and provide the extension to the non-conforming case without proof in Remark 7.10.

Theorem 7.9. *Assume that every interface γ_l is a full edge of $\Omega_{s(l)}$ and $\Omega_{m(l)}$. Further assume that the weak solution u of (2) satisfies $u \in H^1(\Omega)$ and $u_k = u|_{\Omega_k} \in H^{p_k+1}(\Omega_k)$ for all $1 \le k \le K$ where p_k is the degree of the NURBS parameterization of Ω_k. If Assumptions 1–3 are satisfied, there is a constant C depending only on the parameterizations $\mathbf{F}_k$ and the degrees p_k such that*

$$\inf_{v_h \in V_h} \|u - v_h\|_X^2 \le C \sum_{k=1}^{K} h_k^{2p_k} \|u\|_{H^{p_k+1}(\Omega_k)}^2. \tag{85}$$

Proof. We follow the method described in [24, Lemma 1.4]. Instead of writing inequalities with explicit constants, we use the symbol $\lesssim$ and note that the implicit constants do not depend on h. First, we choose $w_h = (w_{h,k})_{1 \le k \le K} \in X_h$ such that the functions $\hat{w}_{h,k} = w_{h,k} \circ \mathbf{F}_k \in \hat{X}_{h,k}$ are tensorized local NURBS approximants of $u_k \circ \mathbf{F}_k$ with boundary conditions, see e.g. [4, Proposition 4.26]. By Assumption 3 the parameterization satisfies $\mathbf{F}_k \in C^{1,1}([0,1]^2)$, and by continuity and local smoothness of the NURBS function $\hat{w}_{h,k}$ we have $\hat{w}_{h,k} \in C^{0,1}([0,1]^2)$. The error analysis in [4, Corollary 4.21] can be adapted to the spline projector with boundary conditions, see [4, Remark 4.22]. It provides the estimate

$$\|u_k - w_{h,k}\|_{0,\Omega_k} + h_k |u_k - w_{h,k}|_{1,\Omega_k} \lesssim h_k^{p_k+1} \|u_k\|_{H^{p_k+1}(\Omega_k)}.$$

Moreover, for each interface γ_l, $1 \le l \le L$, and $k = s(l)$, the tensor-product approach implies that $w_{h,k}|_{\gamma_l}$ is a local approximant of $u_k|_{\gamma_l}$ and interpolates u_k at both endpoints of γ_l, so $(u_k - w_{h,k})|_{\gamma_l} \in H_0^1(\gamma_l)$. We can omit the factor $\hat{w}_l \in C^{1,1}([0,1])$ in Theorem 7.6(a), replace the derivative in the parameter domain by a tangential derivative on γ_l, and obtain

$$\|u_k - w_{h,k}\|_{0,\gamma_l} + h_k |u_k - w_{h,k}|_{1,\gamma_l} \lesssim h_k^{p_k+1/2} \|u_k\|_{H^{p_k+1}(\Omega_k)}.$$

Standard interpolation theory of Banach spaces provides the error estimate in the $H_{00}^{1/2}$-norm

$$\|u_k - w_{h,k}\|_{H_{00}^{1/2}(\gamma_l)} \lesssim h_k^{p_k} \|u_k\|_{H^{p_k+1}(\Omega_k)}.$$

In the same way, since we restrict ourselves to the geometrically conforming case, we obtain

$$\|u_{m(l)} - w_{h,m(l)}\|_{H_{00}^{1/2}(\gamma_l)} \lesssim h_{m(l)}^{p_{m(l)}} \|u_{m(l)}\|_{H^{p_{m(l)}+1}(\Omega_{m(l)})}.$$

Note that $u_k \in H^{p_k+1}(\Omega_k) \subset C(\overline{\Omega_k})$, so we can identify $u_k|\gamma_l = u|_{\gamma_l} = u_{m(l)}|_{\gamma_l}$. The jump

$$[w_h]_l = w_{h,k}|_{\gamma_l} - w_{h,m(l)}|_{\gamma_l} = (u - w_{h,m(l)})|_{\gamma_l} - (u - w_{h,k})|_{\gamma_l} \tag{86}$$

can be non-zero, due to different refinements of the initial NURBS parameterizations $\mathbf{F}_k$ and $\mathbf{F}_{m(l)}$. By the interpolation conditions at the endpoints of γ_l, we have $[w_h]_l \in H^1_0(\gamma_l)$ in the geometrically conforming case and

$$\begin{aligned} \|[w_h]_l\|_{H^{1/2}_{00}(\gamma_l)} &\leq \|u - w_{h,k}\|_{H^{1/2}_{00}(\gamma_l)} + \|u - w_{h,m(l)}\|_{H^{1/2}_{00}(\gamma_l)} \\ &\lesssim h_k^{p_k} \|u\|_{H^{p_k+1}(\Omega_k)} + h_{m(l)}^{p_{m(l)}} \|u\|_{H^{p_{m(l)}+1}(\Omega_{m(l)})}. \end{aligned} \tag{87}$$

Next we describe the construction of the approximant $v_h \in V_h$. We use the mortar projection $Q_{h,l}$ and define $\phi_l = Q_{h,l}([w_h]_l) \in W_{h,l,0}$. Let $\widetilde{\phi}_l$ be the extension of ϕ_l to $\partial\Omega_k$ by zero. Then we choose $v_l \in X_h$, which is zero in all patches $\Omega_j \neq \Omega_k$ and satisfies

$$v_l|_{\partial\Omega_k} = \widetilde{\phi}_l, \qquad \|v_l\|_{1,\Omega_k} \lesssim \|\phi_l\|_{H^{1/2}_{00}(\gamma_l)}. \tag{88}$$

We obtain from the quasi-uniformity, the $H^{1/2}_{00}$-stability of $Q_{h,l}$ in Remark 5.3 and (87) that

$$\|v_l\|_{1,\Omega_k} \lesssim \|[w_h]_l\|_{H^{1/2}_{00}(\gamma_l)} \lesssim h_k^{p_k} \|u\|_{H^{p_k+1}(\Omega_k)} + h_{m(l)}^{p_{m(l)}} \|u\|_{H^{p_{m(l)}+1}(\Omega_{m(l)})}.$$

Finally, we define the function

$$v_h = w_h - \sum_{l=1}^{L} v_l \in X_h.$$

It is an element of V_h, because

$$[v_h]_l = [w_h]_l - \sum_{j=1}^{L} [v_j]_l = [w_h]_l - \phi_l = (I - Q_{h,l})[w_h]_l$$

for every $1 \leq l \leq L$, so that the definitions (8) and (40) give $b_\rho(v_h, \mu) = 0$ for every $\mu \in M^1_h$. For each k let L_k be the set of indices $1 \leq l \leq L$ with $\Omega_{s(l)} = \Omega_k$. Then we obtain the error bound

$$\begin{aligned} \|u - v_h\|_{1,\Omega_k} &\leq \|u - w_h\|_{1,\Omega_k} + \sum_{l \in L_k} \|v_l\|_{1,\Omega_k} \\ &\lesssim h_k^{p_k} \|u\|_{H^{p_k+1}(\Omega_k)} + \sum_{l \in L_k} \left(h_k^{p_k} \|u\|_{H^{p_k+1}(\Omega_k)} + h_{m(l)}^{p_{m(l)}} \|u\|_{H^{p_{m(l)}+1}(\Omega_{m(l)})} \right). \end{aligned}$$

Note that the cardinality of L_k is bounded by a constant which depends only on the global geometry; in our case of 2-D tensor-product patches we have $L_k \leq 4$. Therefore, summing the squared norms leads to the result. □

Remark 7.10. The geometrically non-conforming scenario NC1 of Remark 2.1 is treated as follows. Let $L_0 \subset \{1,\dots,L\}$ be the subset of indices such that γ_l is a proper subset of an edge of $\Omega_{m(l)}$. Then we cannot assume, as done in the proof of Theorem 7.9, that $w_{h,m(l)}$ interpolates u at both endpoints of γ_l. Hence, the jump $[w_h]_l$ in (86) is not in $H^1_0(\gamma_l)$. However, the method in [24, p.18] describes a way how we obtain the upper bound

$$\inf_{v_h\in V_h} \|u - v_h\|_X^2 \le C\left(\sum_{k=1}^{K} h_k^{2p_k}\|u\|^2_{H^{p_k+1}(\Omega_k)} + \sum_{l\in L_0} \frac{h_{m(l)}^{2p_{m(l)}+1}}{h_{s(l)}}\|u\|^2_{H^{p_{m(l)+1}}(\Omega_{m(l)})}\right). \tag{89}$$

The norm of the last term can be reduced by considering the restriction of u to a strip $\widetilde{\Omega}_l \subset \Omega_{m(l)}$ adjacent to γ_l and of width $h_{m(l)}$. For more details we refer to [24].

Things are much easier in the geometrically non-conforming scenario NC2. Recall from Remark 2.1 that the elements of $X_{h,k}$ need only be continuous across the prolongations of T-intersections from adjacent patches. Therefore, in the first step of the proof of Theorem 7.9, both components $w_{h,s(l)}$ and $w_{h,m(l)}$ can be chosen to interpolate u at both endpoints of γ_l. Then we obtain the same result as for the geometrically conforming case.

7.3. Consistency error

We follow the method in [24, Section 1.2] to find an upper bound for the consistency error E_b. Recall the definition of $\hat{M}^1_{h,l} \subset \hat{S}^{p_k}(\Theta_{h,l})$ in Proposition 4.6 as the orthogonal complement of $\hat{E}^1_{h,l}$ in (34). The basis functions $\hat{e}_{h,l,1}$ and $\hat{e}_{h,l,2}$ of $\hat{E}^1_{h,l}$ have supports

$$J_{h,l,1} = [\xi_{l,1}, \theta_{h,l,2p_k+2}], \qquad J_{h,l,2} = [\theta_{h,l,n_{h,l}-p_k}, \xi_{l,2}]. \tag{90}$$

If h_k is sufficiently small, these intervals are disjoint and, more importantly, contained in the first/last knot interval of the initial knot sequence Θ_l. Therefore, γ_l is a C^∞-curve in both intervals.

Proposition 7.11. *Let $1 \le l \le L$ and $k = s(l)$. Assume that $u|_{\Omega_k} \in H^{p_k+1}(\Omega_k)$, $\alpha \in C^{p_k-1,1}(\overline{\Omega_k})$, Θ_l satisfies Assumption 3, and $\Theta_{h,l}$ satisfies Assumptions 2 and 4. Let $h_0 > 0$ be given, such that for all $h \le h_0$ the intervals $J_1 := J_{h,l,1}$, $J_2 := J_{h,l,2}$ in* (90) *are contained in the first/last knot interval of the initial knot sequence Θ_l. There exists a constant $C > 0$ depending only on p_k, $\mathbf{F}_k$, and $\alpha|_{\Omega_k}$ such that*

$$\inf_{\hat{\mu}\in\hat{M}^1_{h,l}} \|\hat{w}_l\lambda_l \circ F_l - \hat{\mu}\|_{L_2(\hat{\gamma}_l)} \le C h_k^{p_k-1/2}\, \|u\|_{H^{p_k+1}(\Omega_k)}. \tag{91}$$

Proof. By Theorem 7.6(b), the orthogonal projection into the spline space

$$\hat{v} = \hat{P}_{h,l}(\hat{w}_l\,\lambda_l \circ F_l)$$

has the desired approximation order. Because the supports of both basis functions $\hat{e}_{h,l,1}$ and $\hat{e}_{h,l,2}$ are disjoint, the orthogonal projection

$$P_{\hat{E}^1_{h,l}}\hat{v} = P_{\hat{E}^1_{h,l}}(\hat{w}_l\,\lambda_l \circ F_l) = d_1\frac{\hat{e}_{h,l,1}}{\|\hat{e}_{h,l,1}\|_{L_2(J_1)}} + d_2\frac{\hat{e}_{h,l,2}}{\|\hat{e}_{h,l,2}\|_{L_2(J_2)}}$$

has the coefficients

$$d_i = \frac{1}{\|\hat{e}_{h,l,i}\|_{L_2(J_i)}} \int_{J_i} \hat{w}_l \, \lambda_l \circ F_l \, \hat{e}_{h,l,i} \, d\xi, \qquad i = 1, 2.$$

Orthogonality of $\hat{e}_{h,l,i}$ to all polynomials of degree $p_k - 1$ and the Cauchy-Schwarz inequality give

$$|d_i| \leq \inf_r \|\hat{w}_l \, \lambda_l \circ F_l - r\|_{L_2(J_i)},$$

where the infimum is taken over all polynomials r of degree $p_k - 1$. Moreover, the parameterization F_l is smooth in both intervals J_i, $i = 1, 2$, so $\lambda_l \circ F_l \in H^{p_k - 1/2}(J_i)$ by the trace theorem. This gives

$$|d_i| \leq C|J_i|^{p_k - 1/2} |\hat{w}_l \, \lambda_l \circ F_l|_{H^{p_k - 1/2}(J_i)} \leq C|J_i|^{p_k - 1/2} \|u\|_{H^{p_k+1}(\Omega_k)}.$$

By Assumption 2, we have $|J_k| \leq c_2(p_k + 1)h_k$, and Minkowski's inequality gives

$$\|P_{\hat{E}^1_{h,l}} \hat{v}\|_{L_2(\hat{\gamma}_l)} \leq |d_1| + |d_2| \leq C h_k^{p_k - 1/2} \|u\|_{H^{p_k+1}(\Omega_k)}.$$

The result follows with the definition of $\hat{\mu} = \hat{v} - P_{\hat{E}^1_{h,l}} \hat{v} \in \hat{M}^1_{h,l}$. □

Remark 7.12. It seems that the property $\frac{\partial u}{\partial \nu_l} \circ F_l \in \mathcal{H}^{p_k - 1/2}(\hat{\gamma}_l; \Theta_{h,l})$ was assumed, without further notice, in the proof of [12, Theorem 5.5]. Our discussion at the beginning of this section makes clear that this property is not justified by $u \in H^{p_k+1}(\Omega_k)$ and Assumption 4 should be added. We demonstrate this effect in the examples given in Secs. 9.1.2 and 9.1.3.

The upper bound for the consistency error E_b is now obtained as in [24, Lemma 1.8].

Theorem 7.13. *Let the assumptions of Proposition 7.11 be satisfied for all* $1 \leq l \leq L$*; in particular, Assumptions 1–4 are satisfied and the weak solution* $u \in H^1(\Omega)$ *of* (2) *satisfies* $u|_{\Omega_k} \in H^{p_k+1}(\Omega_k)$ *for all* $k = s(l)$, $1 \leq l \leq L$. *Let* $h_0 > 0$ *be given, such that for every* $h \leq h_0$ *and every interface* γ_l *the intervals* $J_{h,l,1}, J_{h,l,2}$ *in* (90) *are contained in the first/last knot interval of the initial knot sequence* Θ_l. *Then there is a constant* $C > 0$ *which only depends on all* p_k *and* $\mathbf{F}_k$*, such that*

$$E_b = \sup_{v_h \in V_h} \frac{b_\rho(v_h, \lambda)}{\|v_h\|_X} \leq C \left(\sum_{l=1}^{L} h_{s(l)}^{2p_{s(l)}} \, \|u\|^2_{H^{p_{s(l)}+1}(\Omega_{s(l)})} \right)^{1/2}. \tag{92}$$

Proof. For each interface γ_l, we use the same notations as before and let

$$y_l = \hat{w}_l \, \lambda_l \circ F_l = \frac{\tau_l}{\hat{w}_l} \left(\alpha \frac{\partial u}{\partial \nu_l} \right) \circ F_l. \tag{93}$$

Let $v_h = (v_{h,k})_{1 \leq k \leq K} \in V_h$. The standard computations as in (7) and the definition (12) of V_h give

$$b_\rho(v_h, \lambda) = \sum_{l=1}^{L} \int_{\hat{\gamma}_l} (y_l - \hat{\mu}_l)(\xi) \hat{w}_l(\xi) \, [v_h]_l \circ F_l(\xi) \, d\xi$$

with arbitrary elements $\hat{\mu}_l \in \hat{M}^1_{h,l}$. The Cauchy-Schwarz inequality gives

$$|b_\rho(v_h,\lambda)|^2 \le \sum_{l=1}^{L} \inf_{\hat{\mu}_l\in\hat{M}^1_{h,l}} h_{s(l)}\|y_l-\hat{\mu}_l\|^2_{L_2(\hat{\gamma}_l)} \sum_{l=1}^{L} h^{-1}_{s(l)}\|\hat{w}_l\,[v_h]_l\circ F_l\|^2_{L_2(\hat{\gamma}_l)}. \tag{94}$$

For the first sum in (94), we apply the result of Proposition 7.11 and obtain

$$\sum_{l=1}^{L} \inf_{\hat{\mu}_l\in\hat{M}^1_{h,l}} h_{s(l)}\|y_l-\hat{\mu}_l\|^2_{L_2(\hat{\gamma}_l)} \le C\sum_{l=1}^{L} h^{2p_{s(l)}}_{s(l)}\|u\|^2_{H^{p_{s(l)}+1}(\Omega_{s(l)})}.$$

A bound for the second sum in (94) is obtained in analogy to [11, Lemma 3.5] as

$$\sum_{l=1}^{L} h^{-1}_{s(l)}\|\hat{w}_l\,[v_h]_l\circ F_l\|^2_{L_2(\hat{\gamma}_l)} \le C\sum_{l=1}^{L}\left(\|v_{h,s(l)}\|^2_{H^1(\Omega_{s(l)})}+\|v_{h,m(l)}\|^2_{H^1(\Omega_{m(l)})}\right) \le C\|v_h\|^2_X.$$

So we have obtained the upper bound in (92). □

By combining the approximation error (85) and the consistency error (92), the inequality (55) becomes

$$\|u-u_h\|^2_X \le C\sum_{k=1}^{K} h^{2p_k}_k\|u\|^2_{H^{p_k+1}(\Omega_k)} \tag{95}$$

in the geometrically conforming case. If the decomposition is geometrically non-conforming (i.e., with T-intersections), the same result is valid for the type NC2 in Remark 2.1. For the type NC1, instead, the bounds (89) and (92) give

$$\|u-u_h\|^2_X \le C_1\sum_{k=1}^{K} h^{2p_k}_k\|u\|^2_{H^{p_k+1}(\Omega_k)} + C_2\sum_{l\in L_0}\frac{h^{2p_{m(l)}+1}_{m(l)}}{h_{s(l)}}\|u\|^2_{H^{p_{m(l)}+1}(\Omega_{m(l)})}. \tag{96}$$

7.4. Error bound for the Lagrange multiplier

The error bound for the Lagrange multiplier in (10) is given for the mesh-dependent norm $\|\lambda-\lambda_h\|_{-1/2,h}$. It is derived from the infsup-condition and the approximation error in the standard way as shown in [24, p. 26]. We only describe the geometrically conforming case. For the non-conforming situation, the same adaptation as in (89) is needed.

Theorem 7.14. *With the assumptions of Theorem 7.9 we have*

$$\|\lambda-\lambda_h\|^2_{-1/2,h} \le C\sum_{k=1}^{K} h^{2p_k}_k\|u\|^2_{H^{p_k+1}(\Omega_k)}, \tag{97}$$

where C only depends on α and all p_k and $\mathbf{F}_k$.

Proof. The same method as in [24, p.25] leads to

$$\begin{aligned}\|\lambda-\lambda_h\|_{-1/2,h} &\le \inf_{\mu_h\in M^1_h}\left(\|\lambda-\mu_h\|_{-1/2,h}+\|\lambda_h-\mu_h\|_{-1/2,h}\right)\\ &\le C\left(\|u-u_h\|_X+\inf_{\mu_h\in M^1_h}\|\lambda-\mu_h\|_{-1/2,h}\right).\end{aligned}$$

The result follows from (55), Theorems 7.9 and 7.13 and Proposition 7.11. □

8. Implementation

In our implementation of the mortar finite element method, we use the mass matrix $\mathcal{M}_h$ for the substitution of all nodal coefficients of $\Omega_{s(l)}$ associated with the interior of γ_l by a linear transform, as described in [5, p. 194]. We show how to choose a basis for M_h^1, different from the one in Proposition 4.6, in order to obtain simple relations for this substitution.

Let $1 \le l \le L$ and $k = s(l)$. First, we develop the expressions for the entries of the mass matrix which are associated with the interface γ_l and with the basis elements of $\hat{M}_{h,l}^1$ in Proposition 4.6. The rows of the mass matrix are indexed by $2 \le i \le n_{h,l} - 1$ according to the enumeration of the basis elements of $\hat{M}_{h,l}^1$.

There are two blocks of columns for each row. The first block is associated with finite elements on Ω_k which are non-zero on γ_l,

$$m_{l,i,j} = \langle N_{h,l,j}, \mu_{h,l,i}^1 \rangle_{\rho_l} = w_{h,l,j} \int_{\hat{\gamma}_l} \hat{\mu}_{h,l,i}^1 \, \hat{B}_{h,l,j}^{p_k} \, d\xi, \qquad 2 \le i \le n_{h,l} - 1, \quad 1 \le j \le n_{h,l}. \tag{98}$$

Here, $w_{h,l,j}$ is the weight factor in the numerator of the NURBS function $\hat{N}_{h,l,j}$. Both functions $\hat{\mu}_{h,l,i}^1$, $\hat{B}_{h,l,j}^{p_k}$ are splines in $\hat{S}^{p_k}(\Theta_{h,l})$, so there are fast methods for the computation of these integrals. The analysis in Section 6 shows that the square submatrix

$$\mathcal{M}_{h,l} = (m_{l,i,j})_{2 \le i,j \le n_{h,l}-1} \tag{99}$$

has a uniformly bounded condition number for arbitrary knot sequences. This property is the same as the "spectral equivalence" in [24, p.13]. Note that this block is banded due to the local support of the basis.

The second block is associated with finite elements on $\Omega_{m(l)}$ which are non-zero on γ_l. We denote the corresponding NURBS basis functions on $\mathbf{F}_{m(l)}^{-1}(\gamma_l)$ by $\hat{N}_{h,l,j}^m$, $1 \le j \le \tilde{n}_{h,l}$. Note that a sign factor is introduced by the jump operation. In both geometrically conforming and non-conforming cases, we have

$$\tilde{m}_{l,i,j} = -\int_{\hat{\gamma}_l} \hat{\mu}_{h,l,i}^1 \, \hat{w}_l \, \hat{N}_{h,l,j}^m \circ \mathbf{F}_{m(l)}^{-1} \circ F_l \, d\xi, \qquad 2 \le i \le n_{h,l} - 1, \quad 1 \le j \le \tilde{n}_{h,l}. \tag{100}$$

In a conforming geometry, we often have $\mathbf{F}_{m(l)}^{-1} \circ F_l = \mathrm{id}$, so this term can be omitted. It must be included in the integral for a non-conforming geometry, because γ_l is only a portion of the edge parameterized by $\mathbf{F}_{m(l)}$.

Next we define another basis $(\hat{\eta}_{h,l,i}^1 : 2 \le i \le n_{h,l} - 1)$ of $\hat{M}_{h,l}^1$ such that the corresponding entries are

$$m_{l,i,j}^\eta = w_{h,l,j} \int_{\hat{\gamma}_l} \hat{\eta}_{h,l,i}^1 \, \hat{B}_{h,l,j}^{p_k} \, d\xi, \qquad 2 \le i \le n_{h,l} - 1, \quad 1 \le j \le n_{h,l} \tag{101}$$

and

$$\tilde{m}_{l,i,j}^\eta = -\int_{\hat{\gamma}_l} \hat{\eta}_{h,l,i}^1 \, \hat{w}_l \, \hat{N}_{h,l,j}^m \circ \mathbf{F}_{m(l)}^{-1} \circ F_l \, d\xi, \qquad 2 \le i \le n_{h,l} - 1, \quad 1 \le j \le \tilde{n}_{h,l}. \tag{102}$$

The basis will be chosen such that the square submatrix

$$\mathcal{M}_{h,l}^{\eta} = (m_{l,i,j}^{\eta})_{2\le i,j\le n_{h,l}-1} \tag{103}$$

is a diagonal matrix. For this definition, we use the dual B-splines

$$\widetilde{B}_{h,l,j}^{q_l} \in \hat{S}^{q_l}(\Theta_{h,l}), \qquad 1 \le j \le n_{h,l},$$

which satisfy the biorthogonality relation

$$\int_{\hat{\gamma}_l} \widetilde{B}_{h,l,j}^{q_l} \hat{B}_{h,l,k}^{q_l}\, d\xi = \delta_{j,k} \quad \text{for all} \quad 1 \le j,k \le n_{h,l}.$$

Here $\delta_{j,k}$ denotes the Kronecker delta. The support of the dual B-splines is the whole interval $\overline{\hat{\gamma}_l}$. Although the new basis will have global support γ_l, the mass matrix is sparse due to the biorthogonality.

We recall the definition of the two functions

$$\hat{e}_{h,l,1} = \frac{d^{q_l}}{d\xi^{q_l}}\, \hat{B}_{h,l,1}^{2q_l} = \sum_{j=1}^{n_{h,l}} \alpha_j \hat{B}_{h,l,j}^{q_l}$$

in (30) and

$$\hat{e}_{h,l,2} = \frac{d^{q_l}}{d\xi^{q_l}}\, \hat{B}_{h,l,n-q_l}^{2q_l} = \sum_{j=1}^{n_{h,l}} \beta_j \hat{B}_{h,l,j}^{q_l}$$

in (31), which span the orthogonal complement $\hat{E}_{h,l}^1$ of $\hat{M}_{h,l}^1$. Note that all coefficients α_j with $j > q_l + 1$ and β_j with $j < n - q_l$ are zero.

Proposition 8.1. *Let $q = q_l$, $n = n_{h,l}$ and assume $n \ge q + 2$.*

(a) The functions

$$\hat{\eta}_{h,l,i}^1 = \widetilde{B}_{h,l,i}^q - \frac{\alpha_i}{\alpha_1}\widetilde{B}_{h,l,1}^q - \frac{\beta_i}{\beta_n}\widetilde{B}_{h,l,n}^q, \qquad i = 2,\dots,n-1, \tag{104}$$

are a basis of $\hat{M}_{h,l}^1$. In particular, if $n \ge 2q+3$, then $\hat{\eta}_{h,l,i}^1 = \widetilde{B}_{h,l,i}^q$ for $j = q+2,\dots,n-q-1$.

(b) The entries of the mass matrix in (103) *are*

$$m_{l,i,j}^{\eta} = w_{h,l,j} \int_{\hat{\gamma}_l} \hat{B}_{h,l,j}^q \hat{\eta}_{h,l,i}^1\, d\xi = w_{h,l,j}\left(\delta_{i,j} - \frac{\alpha_i}{\alpha_1}\delta_{j,1} - \frac{\beta_i}{\beta_n}\delta_{j,n}\right), \quad 1 \le j \le n,\ \ 2 \le i \le n-1. \tag{105}$$

In particular, the block $\mathcal{M}_{h,l}^{\eta}$ in (103) *is diagonal.*

Proof. Part (a) follows from two simple observations. First, the specified splines $\hat{\eta}_{h,l,i}^1$, $2 \le i \le n-1$, are linearly independent, because $\widetilde{B}_{h,l,i}^q$ only appears in the representation of $\hat{\eta}_{h,l,i}^1$. Secondly, their orthogonality to $\hat{e}_{h,l,1}$ and $\hat{e}_{h,l,2}$ is easily verified. Part (b) follows directly from the biorthogonality of B-splines and dual B-splines. □

Based on this result, the substitution method can be easily implemented as follows. We let $u_h = (u_{h,k})_{1\le k\le K}$ be an element of X_h.

- Let $n = n_{h,l}$ and $\tilde{n} = \tilde{n}_{h,l}$. The restriction of $u_{h,s(l)}$ to γ_l has the NURBS representation

$$u_{h,s(l)}\,|_{\gamma_l} = \sum_{j=1}^{n} \mathbf{U}_{h,l,j}\hat{N}_{h,l,j} \circ \mathbf{F}_{s(l)}^{-1} \tag{106}$$

  and the restriction of $u_{h,m(l)}$ to γ_l has the representation

$$u_{h,m(l)}|_{\,\gamma_l} = \sum_{j=1}^{\tilde{n}} \mathbf{U}^m_{h,l,j}\hat{N}^m_{h,l,j} \circ \mathbf{F}_{m(l)}^{-1}. \tag{107}$$

  The superscript m is used in order to denote coefficients $\mathbf{U}^m_{h,l,j}$ and basis functions $\hat{N}^m_{h,l,j}$ on the master side of γ_l.

- Since $\mathcal{M}^\eta_{h,l}$ is a diagonal matrix, we have $m^\eta_{l,i,j} = 0$ for all $2 \le j \le n-1$, $j \ne i$. The weak continuity condition $b_\rho(u_h, \mu) = 0$ is used, where $\mu = (\mu_l)_{1\le l\le L}$ is chosen with a fixed basis element $\mu_l = \eta_{h,l,i} \in M^1_{h,l}$, $2 \le i \le n-1$, and $\mu_r = 0$ for $r \ne l$. This gives

$$0 = b_\rho(u_h, \mu) = \langle [u_h]_l, \eta_{h,l,i}\rangle_{\rho_l} = w_{h,l,i}\mathbf{U}_{h,l,i} - \frac{w_{h,l,1}\alpha_i}{\alpha_1}\mathbf{U}_{h,l,1} - \frac{w_{h,l,n}\beta_i}{\beta_n}\mathbf{U}_{h,l,n} - \sum_{j=1}^{\tilde{n}} \tilde{m}^\eta_{l,i,j}\mathbf{U}^m_{h,l,j}.$$

  Hence, the substitution

$$\mathbf{U}_{h,l,i} = \frac{1}{w_{h,l,i}}\left(\frac{w_{h,l,1}\alpha_i}{\alpha_1}\mathbf{U}_{h,l,1} + \frac{w_{h,l,n}\beta_i}{\beta_n}\mathbf{U}_{h,l,n} + \sum_{j=1}^{\tilde{n}} \tilde{m}^\eta_{l,i,j}\mathbf{U}^m_{h,l,j}\right) \tag{108}$$

  can be used for all coefficients $\mathbf{U}_{h,l,i}$, $2 \le i \le n-1$, on the slave side of γ_l.

Remark 8.2. (i) Note that the nodal coefficients $\mathbf{U}_{h,l,1}$ and $\mathbf{U}_{h,l,n_{h,l}}$ associated with the two endpoints of γ_l in the slave-cell are treated as free parameters. Indeed, as in [5] and for the geometrically conforming case, we define separate control points for each cell Ω_k meeting at a vertex of the decomposition. Hence, different interfaces are completely decoupled and there is no interference of the control points on γ_l with other cells than $\Omega_{s(l)}$ and $\Omega_{m(l)}$. The same decoupling remains valid for the geometrically non-conforming types NC1 and NC2 in Remark 2.1. This is clear for NC1, because both endpoints of γ_l are vertices of $\Omega_{s(l)}$ and can be treated in the same way as in the geometrically conforming case. For the type NC2, the control points $\mathbf{U}_{h,l,1}$ and $\mathbf{U}_{h,l,n}$ in (106) can be non-vertex points of $\Omega_{s(l)}$. This occurs if one (or both) of them are endpoints of the prolongation of a T-intersection at a vertex of the master patch $\Omega_{m(l)}$. If this is the case, the same control point is used as an endpoint of another interface γ_m, $m \ne l$, and can either belong to the slave patch or the master patch of γ_m. Since it is treated as a free parameter in both cases (slave or master control point for γ_m), there is no complication as compared to the geometrically conforming case.

(ii) The computation of $\tilde{m}^{\eta}_{l,i,j}$ in (102) requires explicit expressions for the dual B-splines $\widetilde{B}^{q}_{h,l,j}$, $1 \leq j \leq n$, with knot sequence $\Theta_{h,l}$. In our implementation, these are computed via the inversion of the Gram matrix $(\langle \hat{B}^{q}_{h,l,i}, \hat{B}^{q}_{h,l,j} \rangle)_{1 \leq i,j \leq n}$ of the B-spline basis on $\hat{\gamma}_l$. In [16] we described a modification of the mortar method which avoids matrix inversion by the use of approximate dual B-splines. It introduces another consistency error for the error analysis in Section 7. The error analysis will be presented in our forthcoming work.

9. Numerical Examples

We present our numerical results for two examples. In Section 9.1 we consider the Poisson equation on the unit square, and Section 9.2 considers a benchmark problem of linear elasticity, namely an elastic plate with hole. In both cases, the numerical results can be compared to an analytical solution. Thus, the convergence behavior of the proposed mortar formulation can be assessed properly. Several discretizations are tested for each example. All computations are performed using an in-house isogeometric analysis code within Matlab.

9.1. Poisson equation solved on the unit square

In this example the Poisson equation $-\Delta u = f$ is solved on the unit square $\Omega = (0,1)^2$. The manufactured analytical solution for the body load $f(x,y) = 13\sin(3x)\sin(2y)$ is $u(x,y) = \sin(3x)\sin(2y)$. The associated boundary conditions are $g = \nabla u \cdot \nu$ on Neumann boundaries Γ_N with the outer normal vector ν, and $u = 0$ on the Dirichlet boundary Γ_D. Within this work the lower edge ($x \in (0,1)$, $y = 0$) is chosen as Dirichlet boundary, whereas all other edges are Neumann boundaries. Other choices are possible, but do not yield significantly different results, see the work of Zou et al. [25] where different combinations of boundary conditions are compared. In the following, we study several different possibilities to discretize the domain with NURBS patches. The accuracy of the computations is assessed with the help of the L_2-error $\|u - u^h\|_{0,\Omega}$ which is plotted over the maximal element diagonal h. Since f is infinitely smooth, optimal error bounds for discretizations of degree p have the order $O(h^{p+1})$ according to the general theory of finite elements [10].

9.1.1. Two conforming patches with straight interface

The first discretization scheme serves as a reference and uses a decomposition into two rectangular patches which intersect at $x = 0.5$. The discrete spaces $X_{h,k}$, $k = 1,2$, are tensor-product splines relative to conforming, equally spaced knot sequences and equal degrees $2 \leq p \leq 5$ in both patches. The canonical parameterizations $\mathbf{F}_1(\xi_1,\xi_2) = (\xi_1/2, \xi_2)$ and $\mathbf{F}_2(\xi_1,\xi_2) = ((1+\xi_1)/2, \xi_2)$ and the constant NURBS denominator $\hat{w}_k = 1$, $k = 1,2$, lead to a constant weight function $\rho = 1/2$ for the bilinear form b_ρ. Figure 3a shows the resulting error, if strong continuitiy conditions across the interface γ are used; here the two patches are coupled by shared degrees of freedom along γ and no consistency error occurs. Equivalently, the space V_h consists of all tensor-product splines of coordinate degree p on the full unit square with Dirichlet boundary conditions for $y = 0$, whose knot vector $\Xi^{(1)} \subset [0,1]$ has a knot $\xi = 0.5$ of multiplicity p and simple knots with uniform stepsize h in both intervals $[0, 0.5]$, $[0.5, 1]$. The results for degrees $2 \leq p \leq 5$ are shown as the solid lines in the double logarithmic diagram of Figure 3a and labeled by 'conf'. The expected rates $O(h^{p+1})$

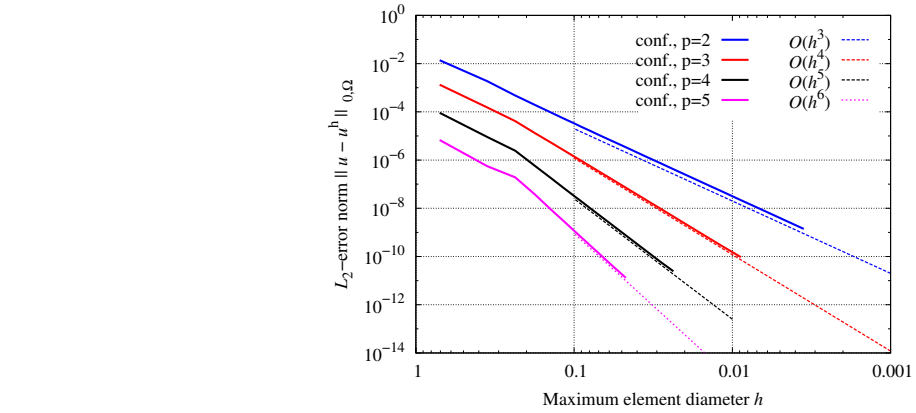

(a) Coupling by shared degrees of freedom

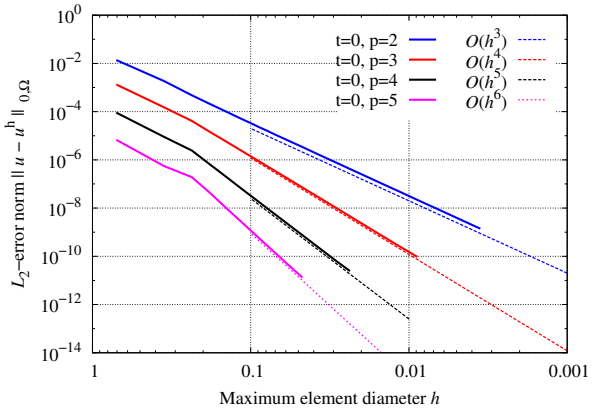

(b) Mortar coupling using $t = 0$ approach

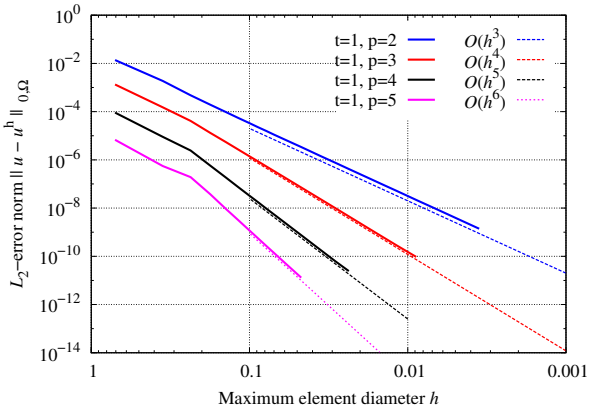

(c) Mortar coupling using $t = 1$ approach

Figure 3: Poisson Equation: Comparison of error level and convergence rates for the discretization scheme with straight interface and conforming knot sequences.

are obtained, as can be seen by direct comparison with the dashed lines of slope $p + 1$. We use the same ordinates in all figures in order to facilitate the comparison of the mortar method with this reference case. The results for the mortar coupling using Lagrange multiplier spaces M_h^t, $t = 0, 1$, for weak continuity conditions across the interface are given in Figures 3b and 3c. Both proposed methods yield the same accuracy level and the same expected convergence rates as the conforming reference computations (Figure 3a). Thus, the global error of u_h is not affected by using the mortar method instead of a direct connection by shared degrees of freedom.

9.1.2. Two non-conforming patches with curved interface with internal C^1-continuity

Our next example demonstrates the importance of Assumption 4, if an interface has limited smoothness. We choose two NURBS patches with a curved interface with initial degree $p_{\text{ini}} = 2$, knot sequence $\boldsymbol{\Xi} = \{0, 0, 0, 0.5, 1, 1, 1\}$ and control points as listed in Table 1, see Example 7.8. The point $(x, y) = (0.5, 0.5)$ corresponds to the parameter $\xi = 0.5$ on the interface, where the curve has only C^1-smoothness. A non-conforming discretization with an element ratio of $2 : 3$ along the interface is obtained by choosing this ratio for the coarsest mesh and then performing uniform

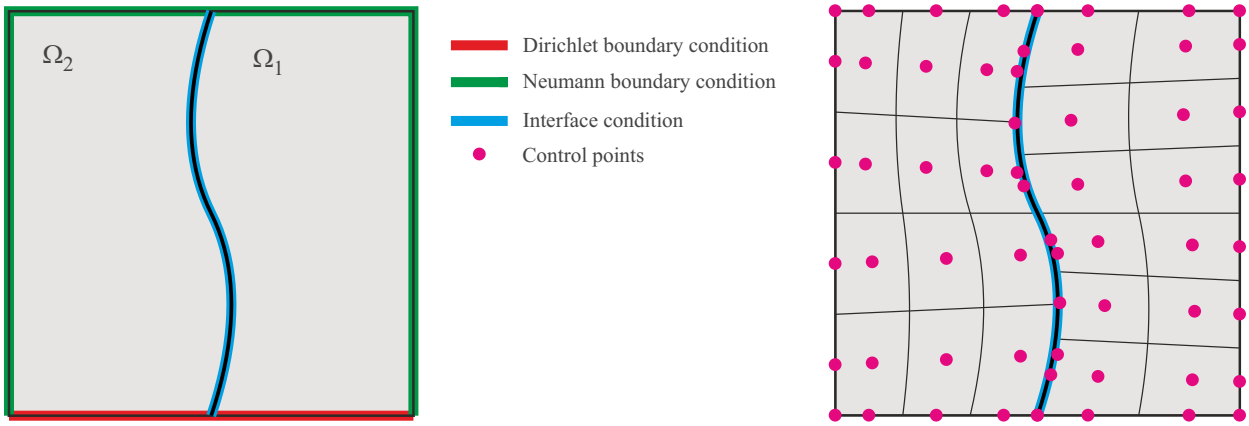

Figure 4: Poisson equation: Discretization scheme with curved interface and an interior knot with C^1-continuity (left). Coarsest non-conforming mesh for this scheme with control points for the parameterization of degree 2 (right).

subdivision in both patches. The same degrees are chosen in both patches. The maximal element diameter h is alike in both patches; see Fig. 4.

In order to demonstrate the effect of the limited smoothness of γ on the a priori error in Sec. 7, we first perform computations for degrees $2 \leq p \leq 5$ without reduced smoothness. The initial parameterization of γ is rewritten with B-splines of degree p by raising the multiplicity of the endpoints to $p+1$ and of $\zeta = 0.5$ to $p-1$. The uniform refinement uses an open knot sequence Θ_h with endpoints of multiplicity $p+1$, knot $\zeta = 0.5$ of multiplicity $p-1$, and additional simple knots of stepsize h in both intervals $(0, 0.5)$ and $(0.5, 1)$. We already observed in Example 7.8 that the orthogonal projection of $\nabla u \cdot \nu$ onto the spline space of degree p has an L^2-error of size $O(h^{3/2})$, regardless of the degree $2 \leq p \leq 5$. Therefore, the order of approximation in Proposition 7.11 is not achieved for $3 \leq p \leq 5$. This results in a defect of the consistency error E_b and, finally, in a degraded a-priori error as can be seen in Figure 5. On the other hand, when we increase the multiplicty of $\zeta = 0.5$ to p as described in Assumption 4 (at least for $p \geq 3$), then the optimal convergence rate $p+1$ for the a-priori error is recovered for all considered degrees and both cases $t = 0$ and 1, see Figure 6. This clearly shows that the reduction of smoothness at interior knots is needed in order to recover the optimal convergence rates.

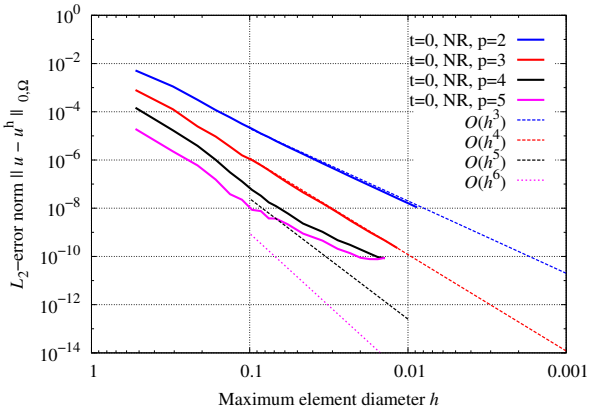

(a) Mortar coupling using $t = 0$ approach

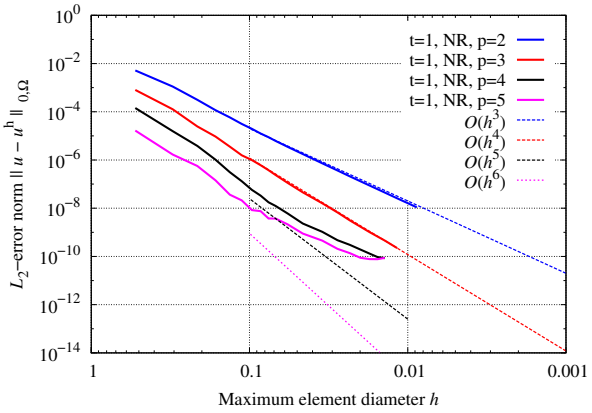

(b) Mortar coupling using $t = 1$ approach

Figure 5: Poisson Equation: Comparison of error level and convergence rates for the discretization scheme with curved interface and an interior knot with C^1-continuity. No reduction of continuity at internal knots.

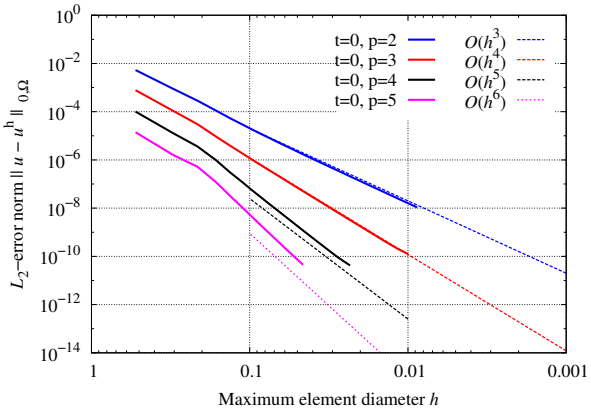

(a) Mortar coupling using $t = 0$ approach

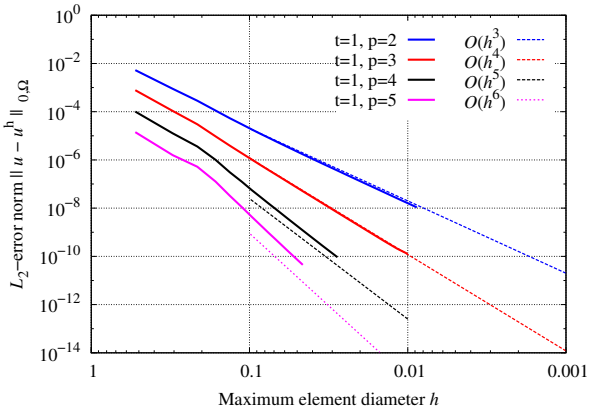

(b) Mortar coupling using $t = 1$ approach

Figure 6: Poisson Equation: Comparison of error level and convergence rates for the discretization scheme with curved interface and an interior knot with C^1-continuity. Reduction of continuity at internal knots according to Assumption 4.

x	0.5	0.55	0.52	0.5	0.4	0.42	0.56	0.55	0.5	0.5
y	0	0.1	0.2	0.32	0.45	0.55	0.69	0.8	0.95	1
w	1	1.2	1.4	0.8	1	1.3	1.1	1.5	0.9	1

Table 2: Poisson equation: Control points for the initial interface curve with $p = 3$ and different internal continuities

9.1.3. Two non-conforming patches with higher order curved interface with different continuities

Our next discretization scheme defines two NURBS patches with a curved interface γ with initial degree $p = 3$, knot sequence $\Xi = \{0,0,0,0,0.3,0.3,0.5,0.5,0.5,0.7,1,1,1,1\}$ and control points as listed in Tab. 2. At the points $\xi = 0.3$ and $\xi = 0.7$, the interface curve is only C^1 and C^2-continuous, respectively. At the point $\xi = 0.5$, the curve is C^0-continuous, and has a kink as can be seen in Figure 7. The points on the interface with reduced internal continuity are marked on the right side of Figure 7. With this example we demonstrate the importance of Assumption 4 for different orders of smoothness and also include the treatment of points with C^0-continuity, which was explained in Remark 7.1.

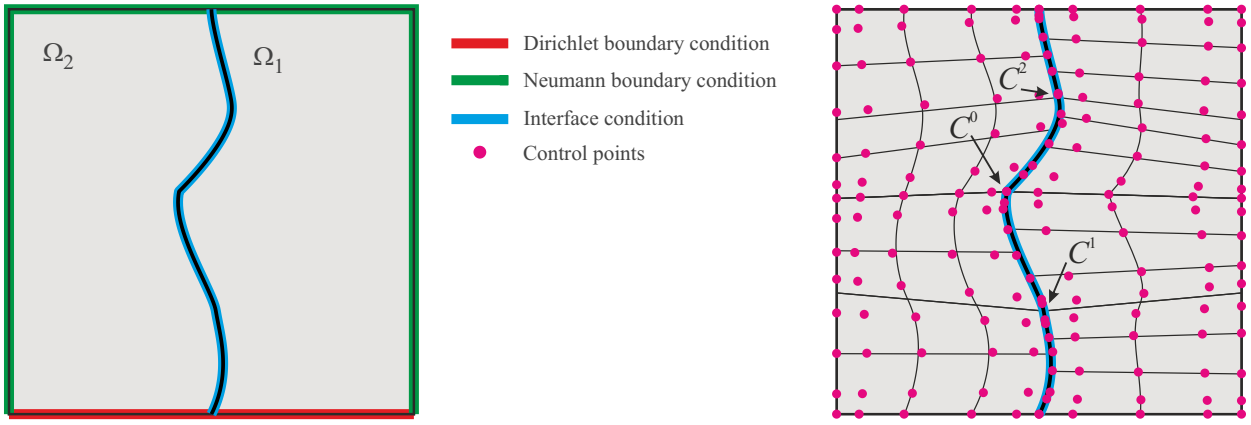

Figure 7: Poisson equation: Discretization scheme with curved interface with initial order $p = 3$ and different internal continuities (left). Coarsest non-conforming mesh for this scheme with (right). The points at the interface with limited internal continuity are labeled by C^2, C^1 and C^0.

A non-conforming discretization with an element ratio of $2:3$ along the interface is obtained by choosing a coarse decomposition with this ratio and subsequent uniform subdivision, see Figure 7. The same degree $3 \leq p \leq 5$ is chosen for both patches. The error of $\|u - u_h\|_{0,\Omega}$ is shown in Figures 8(a) and 8(b)for both spaces of Lagrange multipliers ($t = 0$ or 1) and for different choices of the reduction of smoothness at interior knots of Ξ. The mortar method which employs reduced smoothness in the definition of the discrete spaces $X_{h,k}$ according to Remark 7.1 and Assumption 4 shows optimal convergence (solid lines in 8(a) and (b)). For comparison, in computations labeled by NR we perform no reduction of smoothness; i.e. the knot vectors Θ_h related to the interface have knots $0.3, 0.5, 0.7$ with multiplicities $p-1, p, p-2$, respectively. The convergence rate is not optimal for all considered degrees $3 \leq p \leq 5$. It seems to be limited to $O(h^{1.5})$, which follows the mathematical reasoning in Example 7.8. Furthermore, the label N1 indicates that the C^0-point at

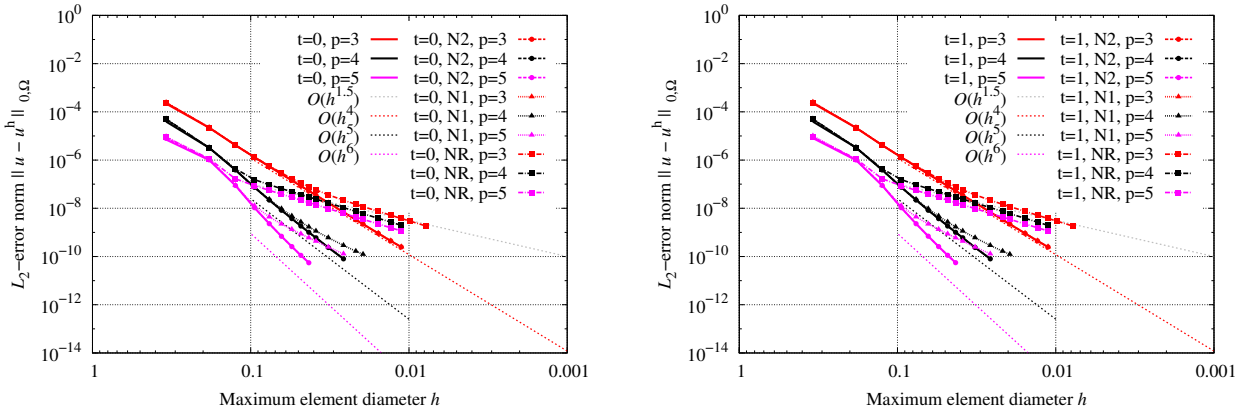

(a) Mortar coupling using $t = 0$ approach

(b) Mortar coupling using $t = 1$ approach

Figure 8: Poisson Equation: Comparison of error level and convergence rates for the discretization scheme with curved interface with initial order $p = 3$ and different internal continuities. Different cases of reduction of continuity at internal knots are shown. In computations labeled by N2, no reduction is performed at C^2-points. In computations labeled by N1, no reduction is performed at C^2 and C^1-points. In computations labeled by NR, no reduction at all is performed.

$\xi = 0.5$ is treated by the method which was sketched in Remark 7.1, but no reduction of smoothness is performed at $0.3, 0.7$. The convergence rate is optimal only for $p = 3$, but deficient for higher degrees. Finally, the computations with reduced smoothness only at $\xi = 0.3$ and proper treatment of the C^0-point $\xi = 0.5$ are labeled by N2. The optimal convergence rate is obtained and the results cannot be distinguished by the eye from the solid lines. It seems that the defect of the consistency error shown in Figure 9 is damped, but we have no analytical explanation yet. These results give further numerical evidence for the a priori error estimate in Sec. 7 and at the same time indicate that it might be sufficient to reduce the continuity in C^0 and C^1-points. However, a reduction at all initial internal knots is not counterproductive.

For a better understanding of the size of the consistency error E_b in (54), Figure 9 shows the L^2-error of the orthogonal projection of $\nabla u \cdot \nu$ onto the full spline space $\hat{S}^p(\Theta_h)$ for $3 \leq p \leq 5$. The labels NR, N1, and N2 inidcate the partial reduction of smoothness as explained before. No label is used for the solid line in Fig. 9(b), which shows the results where the reduction of smoothness at both knots 0.3 and 0.7 is performed according to Assumption 4 and the point $\xi = 0.5$ is treated as in Remark 7.1.

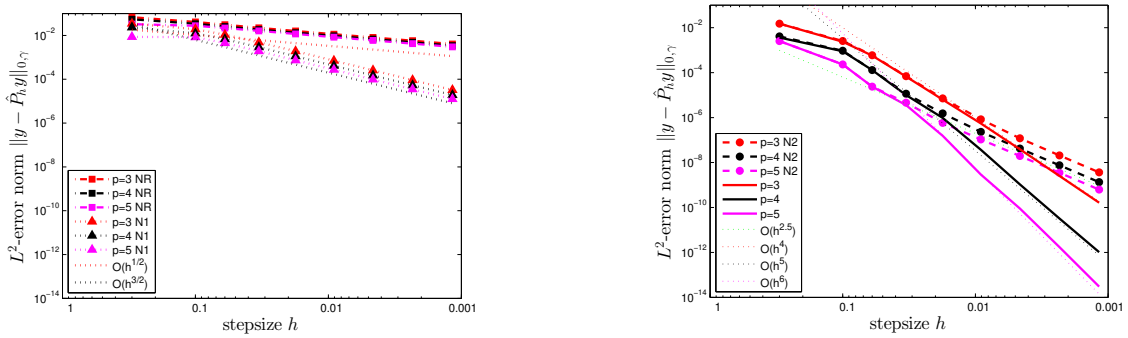

(a) No reduction of smoothness and N1

(b) Full reduction of smoothness and N2

Figure 9: L^2-error for spline approximation of degree $3 \leq p \leq 5$ of the normal derivative $y = \partial u/\partial \nu$ of $u(x, y) = \sin 3x \sin 2y$ on a spline curve γ with a C^0-point $\zeta = 0.5$, a C^1-point $\zeta = 0.3$ and a C^2-point $\zeta = 0.7$.

9.1.4. Discretization with ten patches and different kinds of intersections

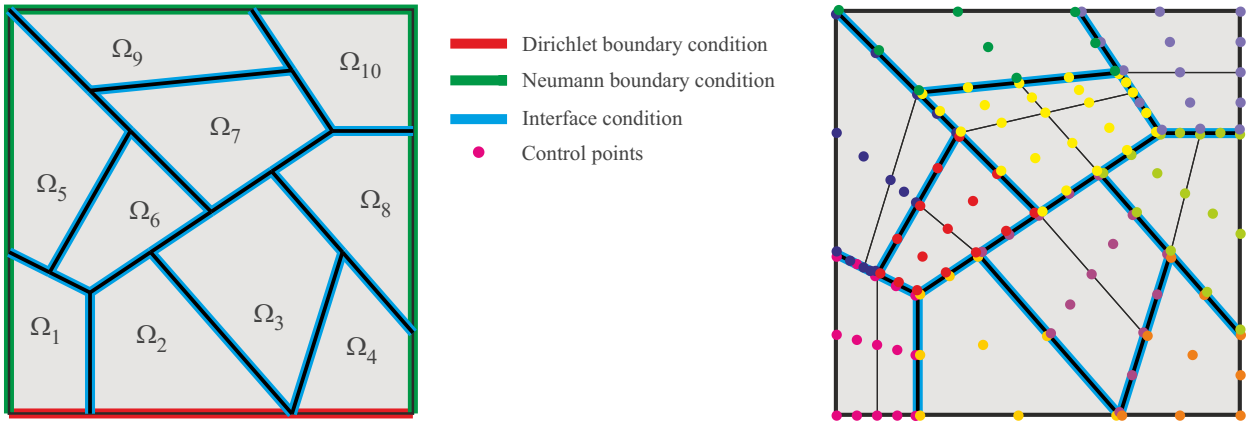

Figure 10: Poisson equation: Discretization scheme with ten non-conforming patches and different kinds of intersections (left). Coarsest non-conforming mesh for this scheme (right).

Our final discretization scheme is with ten non-conforming patches, where seven T-intersections and two star-intersections are present. A sketch of the patch layout is given on the left side in Fig. 10. The interfaces are straight lines and the geometry is waterproof, i.e., the parametrizations match along the interfaces. In the convergence studies, every patch is uniformly subdivided by the same refinement factor and equal degrees are used. The presence of T-intersections, where one patch boundary borders two other patches, together with the additional knots in the patches with T-intersections yields non-conforming meshes at most interfaces. In the initial mesh given on the right of Figure 10, no interior knots are present besides the additional knots at T-intersections, which are resolved by the method described as NC2 in Remark 2.1. Three sample meshes are given in Figure 11 for a better depiction of the obtained non-conformity.

From a mathematical point of view there is no criterion for an optimal choice of patches to be master or slave. However, experience in numerical simulations in [12, 16] suggests to use the patch with more elements as slave patch. The numerical results for this case are given in Fig. 12.

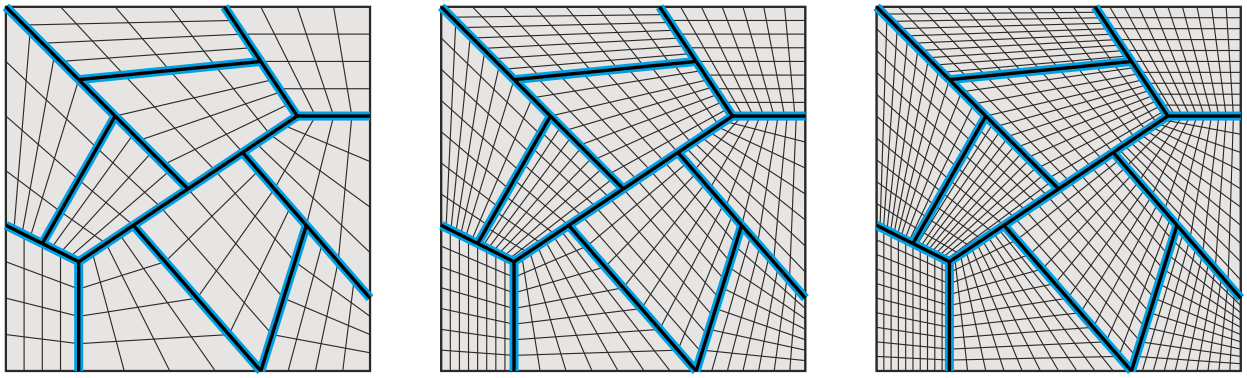

(a) Refinement factor of 4 (b) Refinement factor of 7 (c) Refinement factor of 10

Figure 11: Poisson Equation: Sample meshes for the discretization scheme with with ten non-conforming patches and different kinds of intersections.

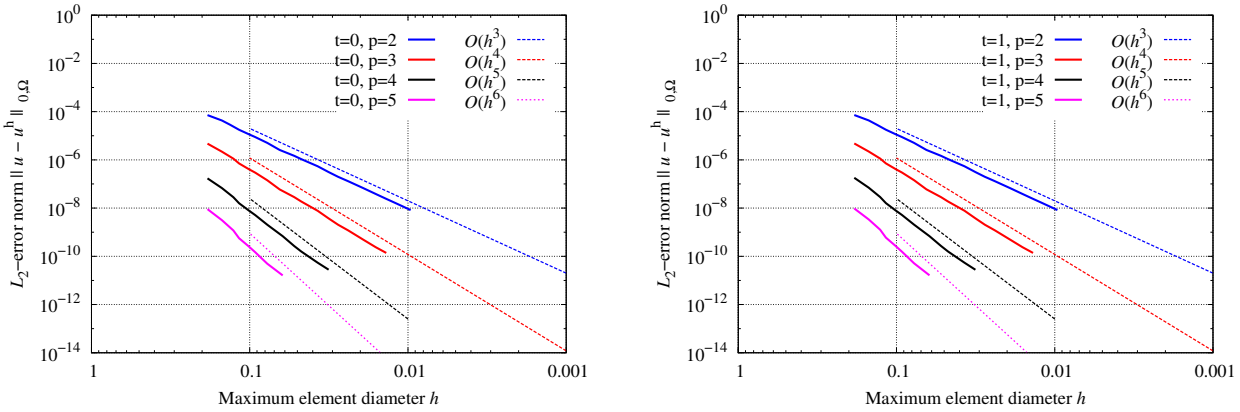

(a) Mortar coupling using $t = 0$ approach (b) Mortar coupling using $t = 1$ approach

Figure 12: Poisson Equation: Comparison of error level and convergence rates for the discretization scheme with ten patches and different kinds of intersections.

We obtain optimal convergence rates for all degrees $2 \leq p \leq 5$ and for both choices of Lagrange multipliers $M^t_{h,l}$, $t = 0$ or 1, see Figures 12a and 12b. This shows that the proposed formulation is able to handle multiple interfaces with different kinds of intersections properly. We also performed the same computation for an inverted master/slave classification with essentially no changes.

9.2. Linear elasticity solved on an elastic plate with hole

In this example the differential equations for linear elasticity are solved for an infinite plate with hole, where uniaxial tension is applied in $x \longrightarrow \pm\infty$. The mechanical equilibrium on a domain $\Omega \subset \mathbb{R}^2$ is given by

$$\operatorname{div} \boldsymbol{\sigma} + \boldsymbol{f} = \mathbf{0}$$

with the boundary conditions $\boldsymbol{u}|_{\Gamma_D} = \mathbf{0}$ and $\boldsymbol{\sigma} \cdot \boldsymbol{n}|_{\Gamma_N} = \boldsymbol{g}$, where $\boldsymbol{n}$ is the outer normal vector with respect to Γ_N. In the chosen planar linear elastic context with isotropic constitutive law, the

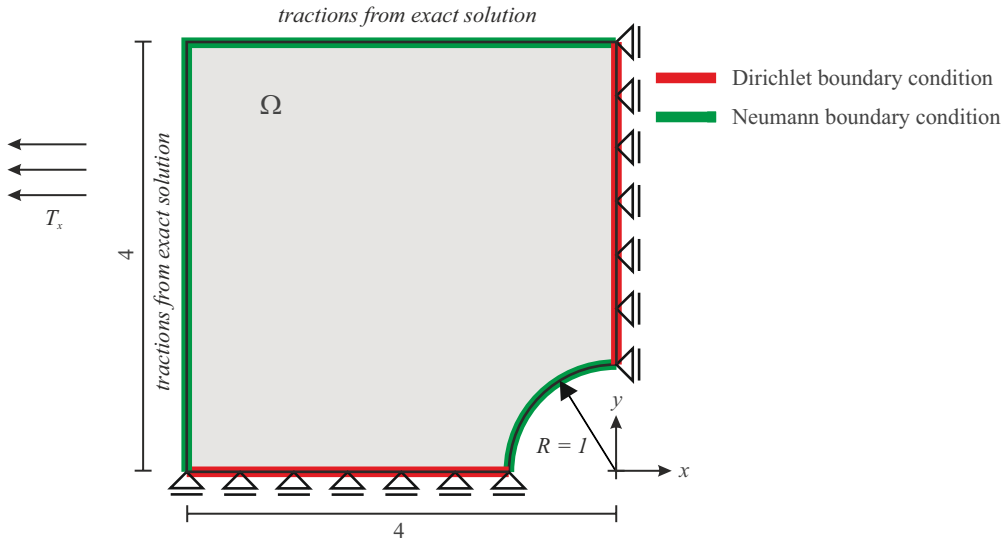

Figure 13: Elastic plate with hole: Sketch of geometry and boundary conditions.

relations between stresses $\boldsymbol{\sigma}$, strains $\boldsymbol{\varepsilon}$ and displacements $\boldsymbol{u}$ are given by

$$\boldsymbol{\sigma} = \lambda \operatorname{tr}(\boldsymbol{\varepsilon})\boldsymbol{I} + 2\mu\boldsymbol{\varepsilon} \qquad \text{and} \qquad \boldsymbol{\varepsilon} = \tfrac{1}{2}\left(\nabla\boldsymbol{u} + \nabla^{\mathrm{T}}\boldsymbol{u}\right),$$

where λ and μ are the Lamé parameters, $\boldsymbol{I}$ is the identity matrix and ∇ is the gradient operator. Accordingly, the saddle point problem (9) changes to: *Find* $(\boldsymbol{u}, \boldsymbol{\lambda}) \in X \times M$ *such that*

$$\begin{aligned} a(\boldsymbol{u},\boldsymbol{v}) + b_\rho(\boldsymbol{v},\boldsymbol{\lambda}) &= \int_\Omega \boldsymbol{v}^{\mathrm{T}}\boldsymbol{f}\, dx + \int_{\Gamma_N} \boldsymbol{v}^{\mathrm{T}}\boldsymbol{g}\, ds, & \boldsymbol{v} &\in X, \\ b_\rho(\boldsymbol{u},\boldsymbol{\mu}) &= 0, & \boldsymbol{\mu} &\in M, \end{aligned} \tag{109}$$

where X and M are bivariate extensions of the spaces used in Eq.(9). The bilinear forms $a(\boldsymbol{u},\boldsymbol{v})$ and $b_\rho(\boldsymbol{u},\boldsymbol{\mu})$ are given by

$$a(\boldsymbol{u},\boldsymbol{v}) = \sum_{k=1}^{K} \int_{\Omega_k} (\nabla\boldsymbol{v})^{\mathrm{T}}\boldsymbol{\sigma}\, dx \qquad \text{and} \qquad b_\rho(\boldsymbol{u},\boldsymbol{\mu}) = \sum_{l=1}^{L} \langle [\boldsymbol{u}]_l, \boldsymbol{\mu}_l \rangle_{\rho_l},$$

respectively.

For our computations, we limit the domain to finite size and apply the tractions of the exact solution, which can be found e.g. in [2], as Neumann boundary conditions on the relevant edges. Furthermore, we consider only one quarter due to symmetry and apply the associated symmetry boundary conditions. Thus, we consider a domain $\Omega = \left\{(x,y) \in (-4,0)\times(0,4) \;:\; x^2 + y^2 \geq 1\right\}$, see Fig. 13. The known analytical solution of this problem allows performing convergence studies for a complex stress distribution and is thus commonly used for numerical studies, especially in the framework of isogeometric analysis.

In the following, we study three different possibilities to discretize the domain with NURBS patches. In all cases the geometry is modeled exactly. The accuracy of the computations is assessed with the help of the L_2-error norm $\|\boldsymbol{\sigma} - \boldsymbol{\sigma}^h\|_{0,\Omega}$ which is plotted over the maximal element diagonal

h. According to the theory of finite elements [10], the slope in the double logarithmic diagram should be p, which is indicated by the dashed lines in the same diagram. In order to allow a straightforward comparison of the mortar results to the reference case, we use the same axes in all figures for this example. The reference example for a conforming method of degrees $2 \leq p \leq 5$ is provided in Fig. 15a.

9.2.1. Two patches with curved interface with internal C^1-continuity with conforming meshes

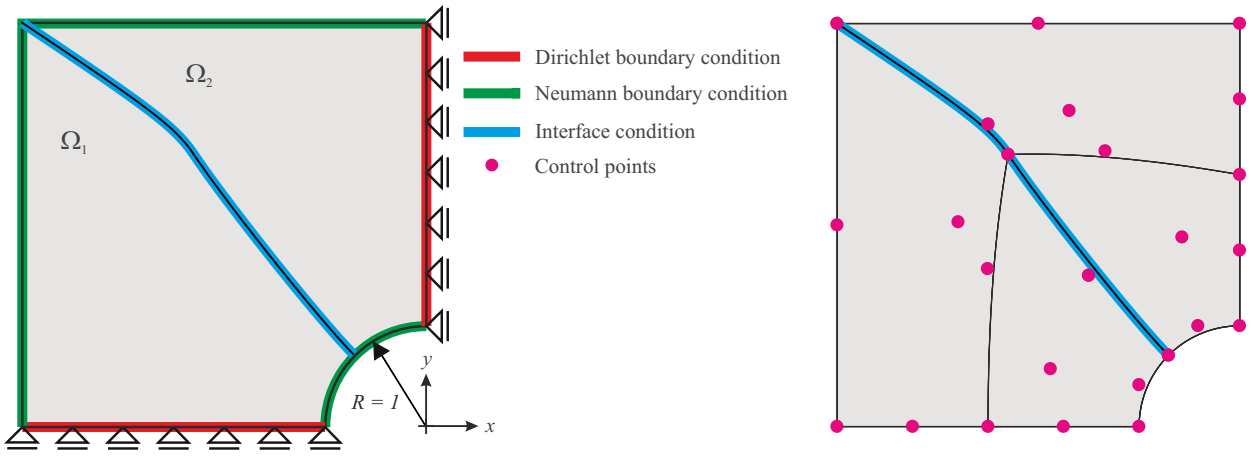

Figure 14: Elastic plate with hole: Discretization scheme with curved interface (left). Coarsest mesh with conforming discretization for this scheme (right)

The first decomposition is with two NURBS patches with a curved interface with initial order $p_{\text{ini}} = 2$, knot sequence $\boldsymbol{\Xi} = \{0,0,0,0.5,1,1,1\}$ and control points as listed in Table 3. At the point $\xi = 0.5$, the interface γ is only C^1-continuous. The mesh is chosen conforming in both patches. A sketch of this discretization scheme along with the coarsest computed mesh is given in Figure 14. Finer meshes for the convergence analysis are obtained by uniform subdivision. This discretization is used to assess the ability of the mortar method to capture the same approximation rate as conforming finite element methods. A computation where the two patches are coupled by shared degrees of freedom along the interface, is used as reference. These results are labeled by *conf.* in Figure 15a. The numerical results for the mortar method with Lagrange multiplier space $M^t_{h,l}$, $t = 0$ or 1, are given in Figures 15b and 15c. While both methods yield a lower accuracy level for coarse discretizations than the conforming method, they seem to *catch up* in terms of accuracy for fine meshes as almost the same error level as in the reference computations is obtained for small stepsizes h. Thus, the expected convergence rates are obtained, even though the error level is higher for coarse meshes. The mortar method does not improve the error as compared to

x	$-\sqrt{2}/2$	-1.5	-2.5	-4
y	$\sqrt{2}/2$	1.5	3	4
w	1	0.5	2	1

Table 3: Elastic plate with hole: Control points for the initial interface curve with an interior knot with C^1-continuity

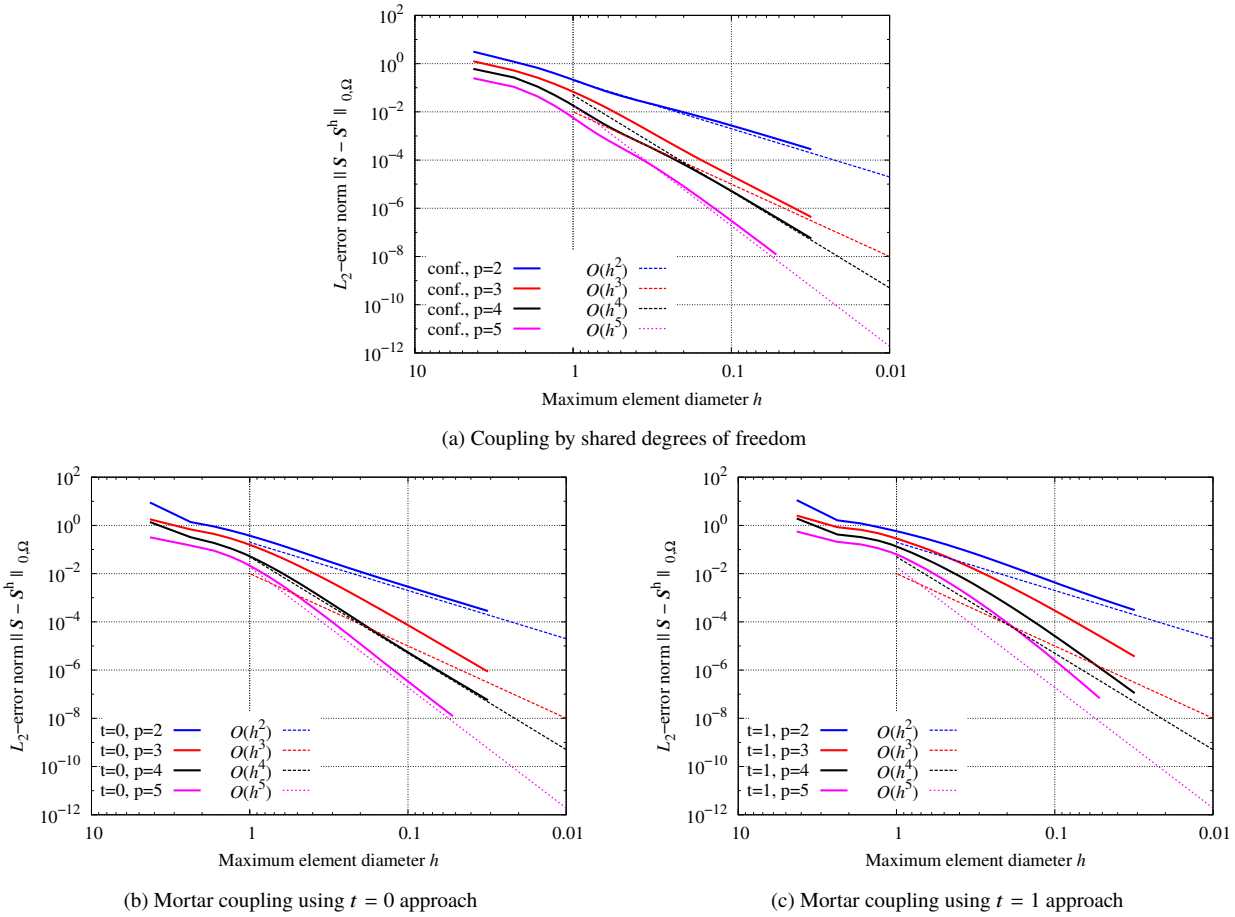

(a) Coupling by shared degrees of freedom

(b) Mortar coupling using $t = 0$ approach

(c) Mortar coupling using $t = 1$ approach

Figure 15: Elastic plate with hole: Comparison of error level and convergence rates for the discretization scheme with curved interface and conforming discretization.

conforming FEM, but it is clearly competitive. We mention that the use of the mortar method does not primarily lie in computations with conforming meshes, after all.

Another way of comparing the conforming FEM and the proposed mortar methods is obtained by plotting the logarithmic error $\log(\|\sigma_{vM} - \sigma_{vM}^h\|/\|\sigma_{vM}\|)$ of the von Mises stresses $\sigma_{vM} = \sqrt{\sigma_{11}^2 + \sigma_{22}^2 - \sigma_{11}\sigma_{22} + 3\sigma_{12}^2}$ for a fixed discretization. We use a subdivision factor of 20 and degree $p = 5$ in Figure 16. In the stress error plot of the reference computations (Figure 16(a)) the largest error is inside the domain, while for both proposed methods (Figures 16(b) and 16(c)) the largest errors are at the end points of the interface. This peculiarity can be explained as follows: In the conforming case, the number of control points along the interface is equal on both sides of the interface, i.e. $n_{h,l} = \tilde{n}_{h,l}$. By using the endpoint modification for $M_{h,l}^t$, the control points at both endpoints of the slave patch become free parameters. This leads to a situation, where the number $n_{h,l} - 2$ of slave control points is smaller than the number of master control points, which can result in a substantial increase of the consistency error near both endpoints. As a simple work-around, we subdivide the first and last two rows of elements in patch Ω_2. By doing so, the mesh turns

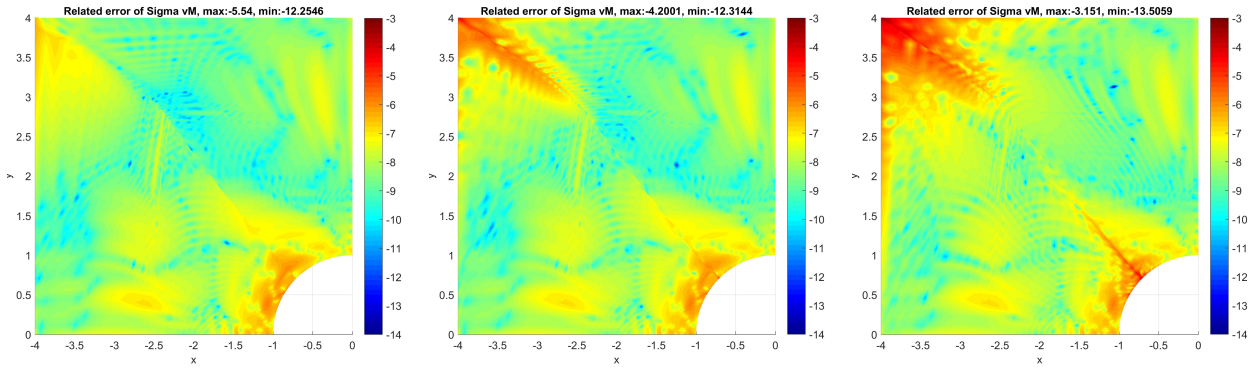

(a) Coupling by shared degrees of freedom (b) Mortar coupling using $t = 0$ approach (c) Mortar coupling using $t = 1$ approach

Figure 16: Elastic plate with hole: Logarithmic error of the von Mises stress for a subdivision factor of 20 and order $p = 5$.

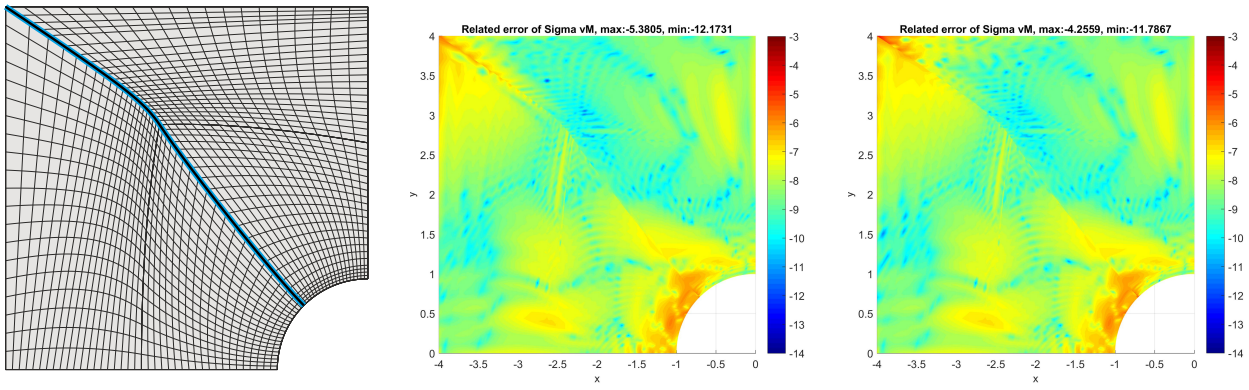

(a) Mesh for one-sided interface end refinement (b) Mortar coupling using $t = 0$ approach (c) Mortar coupling using $t = 1$ approach

Figure 17: Elastic plate with hole: Mesh for one-sided interface end refinement and logarithmic error of the von Mises stress for a subdivision factor of 20 and order $p = 5$.

into a non-conforming mesh, where the number of interface slave control points is larger than the number of interface master control points. This reduces the concentrated error at the endpoints of the interface significantly. A sample mesh is given in Fig. 17(a). The corresponding stress error plots are given in Figs. 17(b) and 17(c).

9.2.2. Two patches with curved interface with internal C^1-continuity and non-conforming mesh

The second discretization scheme uses the same initial discretization as in Sec. 9.2.1, but now non-conforming meshes are chosen. This is obtained by using a subdivision factor of $2j + 1$ along the interface in patch Ω_2 and j in patch Ω_1. This yields a ratio of $2j + 1 : j$ elements along the interface. In the second parametric direction, the subdivision factor is chosen in a complementary way in order to obtain a similar number of elements in both patches. The patch Ω_2 with the smaller stepsize along the interface is chosen as the slave patch. The obtained meshes for a subdivision factor of $j = 5$ and $j = 10$ of this discretization scheme are given in Fig. 18.

This discretization is used to assess the ability of the proposed methods to use discretizations

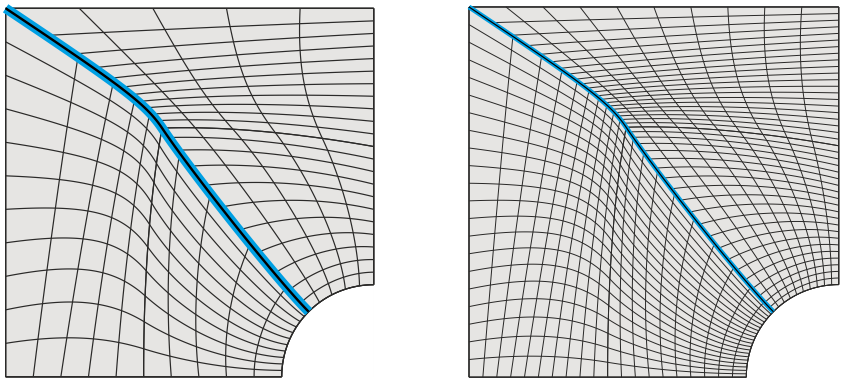

(a) Refinement factor of $j = 5$ (b) Refinement factor of $j = 10$

Figure 18: Elastic plate with hole: Sample meshes for the discretization with curved interface with internal C^1-continuity and non-conforming mesh.

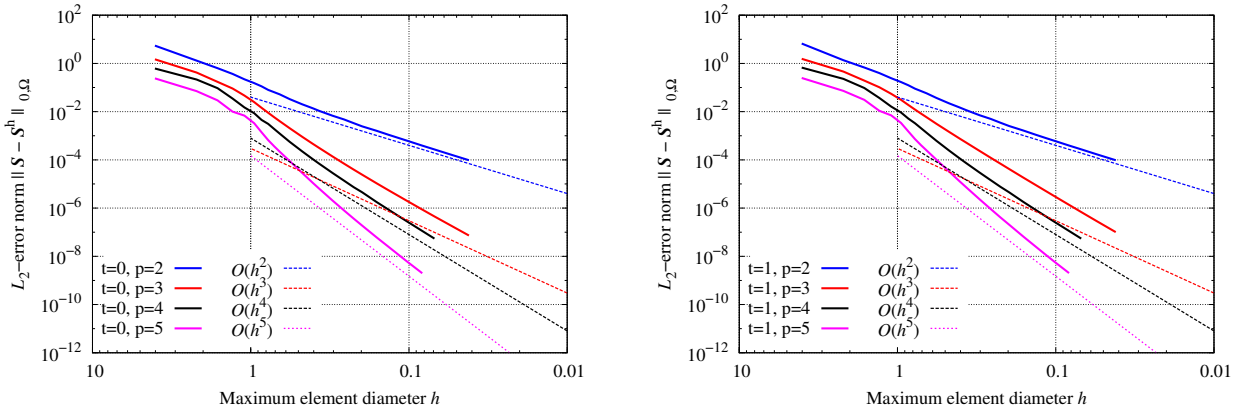

(a) Mortar coupling using $t = 0$ approach (b) Mortar coupling using $t = 1$ approach

Figure 19: Elastic plate with hole: Comparison of error level and convergence rates for the discretization scheme with curved interface and non-conforming discretization.

with curved NURBS interfaces with limited internal smoothness and strongly non-conforming knot sequences. The error norms of the global stress distribution computed using the Lagrange multiplier spaces $M^t_{h,l}$, $t = 0, 1$, are given in Figures 19a and 19b). Both methods yield optimal convergence rates and the error levels are comparable to the conforming case using shared degrees of freedom given in Fig. 15a.

Besides accuracy, also efficiency of the methods is studied. This is done by comparing computational costs for the individual stages of the computations. Furthermore, the stability of the methods is assessed by means of the condition number of the global stiffness matrix. The results of Sec. 9.2.1 for the coupling by shared degrees of freedom are used as reference. These results are labeled by *conf*.

The computational cost for the formation of the global stiffness matrix is compared in Figure 20, where the results are shown in CPU seconds on a contemporary dual core notebook with 8 GB of RAM. The peaks in the diagrams are due to background activity of the operating system. The

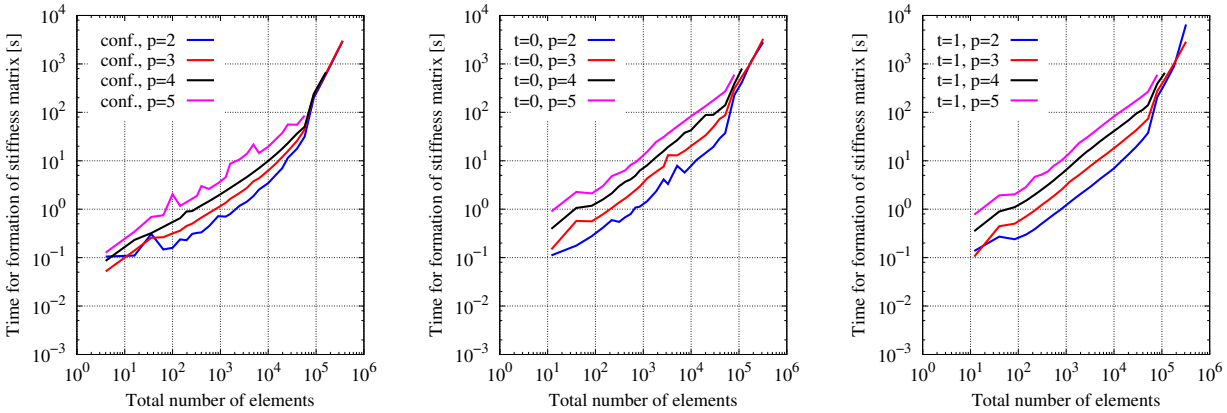

(a) Conforming mesh, coupling by shared degrees of freedom

(b) Non-conforming mesh, mortar coupling using $t = 0$ approach

(c) Non-conforming mesh, mortar coupling using $t = 1$ approach

Figure 20: Elastic plate with hole discretized by two patches: Comparison of the CPU time in seconds for the formation of the global stiffness matrix.

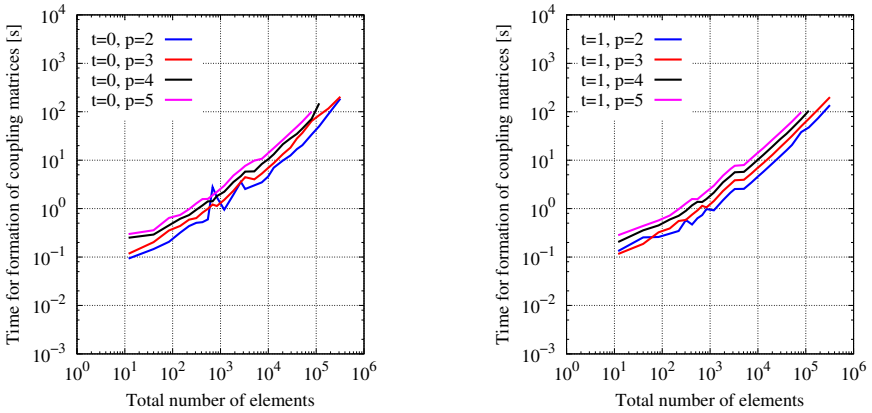

(a) Non-conforming mesh, mortar coupling using $t = 0$ approach

(b) Non-conforming mesh, mortar coupling using $t = 1$ approach

Figure 21: Elastic plate with hole discretized by two patches: Comparison of the CPU time in seconds for the formation of the coupling matrices.

entries are computed by optimal integration as proposed in [18] and directly assembled into the sparse matrix format of Matlab, whereby vectorized assembly is used. The computational cost for conforming meshes given in Fig. 20a is lower than for the mortar methods (Figures 20b and 20c), but they range in the same order of magnitude. The difference occurs in the assembly process, when the entries of the slave interface control points are assembled to master interface degrees of freedom according to Eq. 108. The excessive growth of computational costs in the fine limit is attributed to limitations of RAM, which was restricted to 8 GB for this study.

The computational cost for the formation of the mass matrices as explained in Sec. 8 are given in Figure 21 for both proposed mortar methods with $M^t_{h,l}, t = 0, 1$. There is no significant difference between both methods. In the conforming case, this cost is saved since a direct connection by

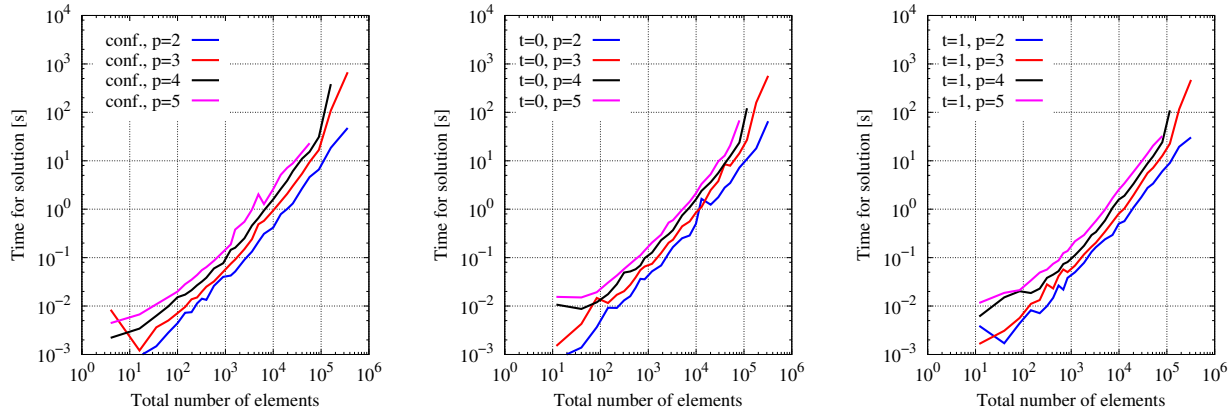

(a) Conforming mesh, coupling by shared degrees of freedom

(b) Non-conforming mesh, mortar coupling using $t = 0$ approach

(c) Non-conforming mesh, mortar coupling using $t = 1$ approach

Figure 22: Elastic plate with hole discretized by two patches: Comparison of the CPU time in seconds for the solution of the global system of equations.

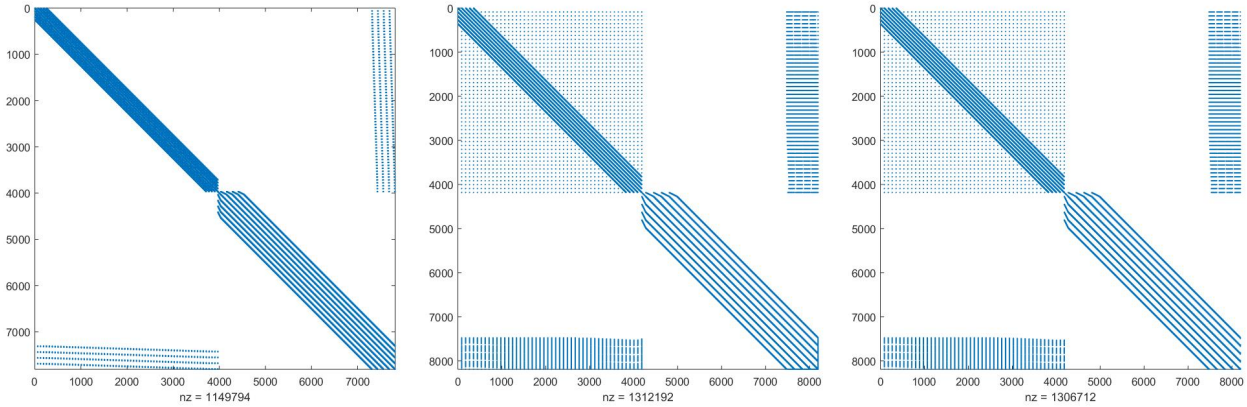

(a) Conforming mesh, coupling by shared degrees of freedom

(b) Non-conforming mesh, mortar coupling using $t = 0$ approach

(c) Non-conforming mesh, mortar coupling using $t = 1$ approach

Figure 23: Elastic plate with hole discretized by two patches: Sparsity pattern of the global stiffness matrix. For the conforming mesh a subdivision factor of 28 and $p = 4$ is used (total number of elements is 3136). For the non-conforming meshes a subdivision factor of 20 and order $p = 4$ is used (total number of elements is 3280).

shared degrees of freedom is used. Note that the cost is in the same order of magnitude as the cost for the formation of the global stiffness matrix, besides the fact that the coupling matrices require the computation of a line integral only, whereas the global stiffness matrix requires computations of a global surface integral. However, there is some potential for a speed-up of the computation of the entries $\tilde{m}^{\eta}_{l,i,j}$ of the mass matrices in (102). First, the computation of the line integrals in (102) uses the time-consuming iterative point inversion algorithm for the mapping from the slave to the master patch, which is required in every integration point. This routine could be written as an external routine in C or Fortran. Secondly, we did not yet implement a fast method for the inversion of the Gram matrix of the B-splines on the slave patch in order to compute the dual B-splines in

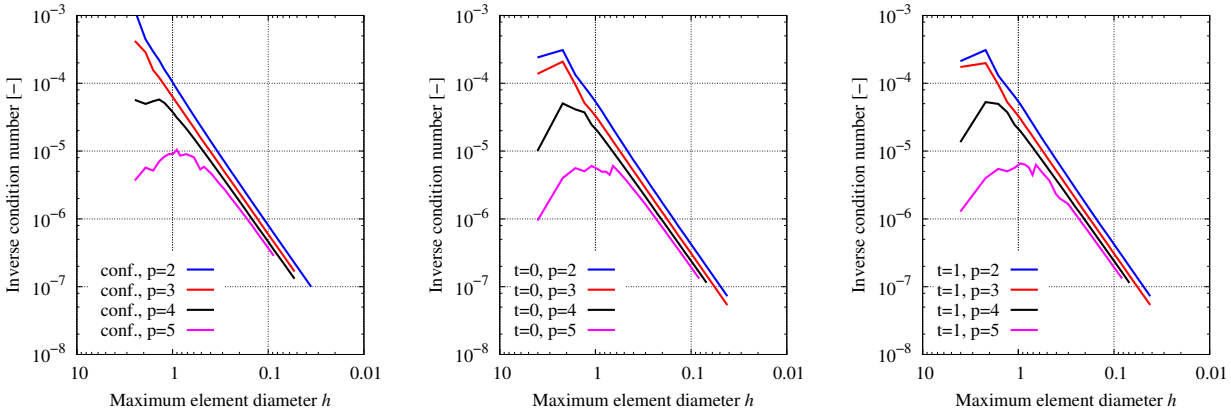

(a) Conforming mesh, coupling by shared degrees of freedom

(b) Non-conforming mesh, mortar coupling using $t = 0$ approach

(c) Non-conforming mesh, mortar coupling using $t = 1$ approach

Figure 24: Elastic plate with hole discretized by two patches: Comparison of the inverse condition number of the global system of equations.

(104), see also Remark 8.2.

The computational cost for the solution of the global system of equations is given in Figure 22. There are no significant differences between the computations using shared degrees of freedom (Figure 22a) and both proposed mortar methods (Figures 22b and 22c). The computational cost for the solution grows almost linearly, as can be expected for the used sparse matrix format. It is roughly two orders of magnitude smaller than the cost for the formation of the stiffness matrix.

The influence of the proposed mortar methods on the sparsity of the global stiffness matrix is depicted in Figure 23, whereby the number of non-zero entries (nz) of the stiffness matrix is given below the diagrams. The sparsity pattern of computations using about 3200 elements are compared between coupling by shared degrees of freedom and the mortar method. The upper left block represents the stiffness matrix for the master patch Ω_1, the lower right block is for the slave patch Ω_2. The sparsest pattern is clearly generated by using shared degrees of freedom, see Figure 23a. The global support along the interface of the dual B-splines used in the proposed implementation in Section 8 generates a coupling between all interface degrees in the master patch. This explains the quadratic structure of the upper left block, whereas the lower right block of the slave patch has a banded structure. The nonzero entries in the upper right and lower left corners appear by the substitution (108). The difference between both choices of Lagrange multiplier spaces $M^t_{h,l}$ is quite small in this case: The number of non-zero entries for $t = 1$ in Figure 23c is about 0.5 % smaller than for $t = 0$ in Figure 23b). It can be observed in the very last rows and columns of the stiffness matrix. The nonzero entries for $t = 0$ result from the interrelation between all interface control points $\mathbf{U}_{h,l,i}$ in the slave patch with both control points $\mathbf{U}_{h,l,1}$ and $\mathbf{U}_{h,l,n}$ at the endpoints of the interface, see (108). This interrelation is reduced to only few interface control points near the endpoints for $t = 1$, because most coefficients α_i and β_i in (108) are zero. This advantage is only small for 2D-problems, but will be more pronounced for 3D-problems. Moreover, in our planned extension of the mortar method by the use of an h-dependent bilinear form $b_{h,rho}$ in our future work, we reduce all blocks of the stiffness matrix to banded form by the

application of locally supported "approximate duals" instead of the dual B-splines.

The condition number of the global stiffness matrix is compared in Fig. 24 between computations using shared degrees of freedom and the proposed mortar methods. The results show that the condition number is not perceivably affected by using the proposed mortar methods, which is an important requirement for robust and accurate computations.

9.2.3. Discretization with ten patches and different kinds of intersections

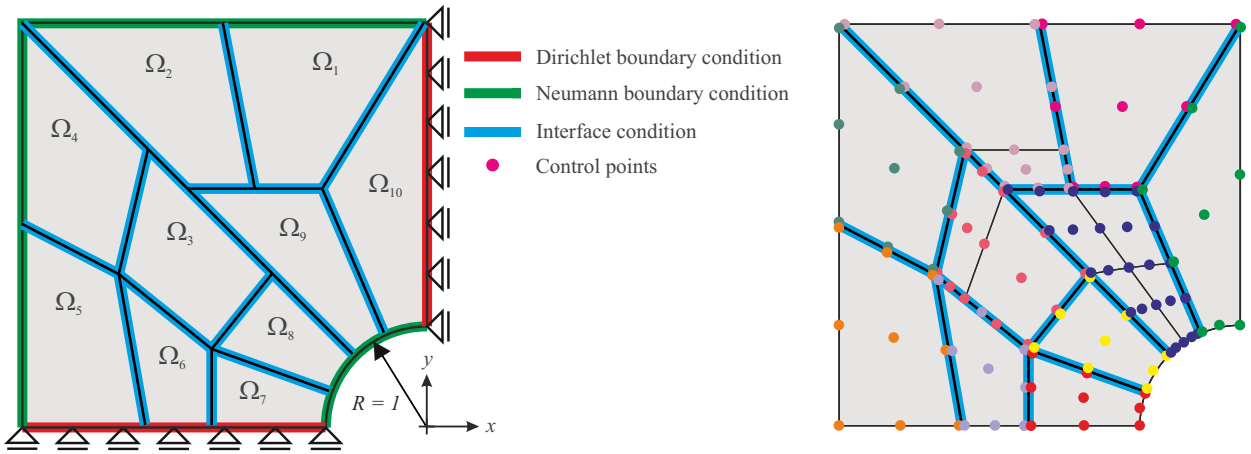

Figure 25: Elastic plate with hole: Discretization scheme with ten non-conforming patches and different kinds of intersections (left). Coarsest initial mesh with order $p = 2$ for this scheme, whereby the patches are not refined except for the prolongation of ending interfaces at T-intersections (right).

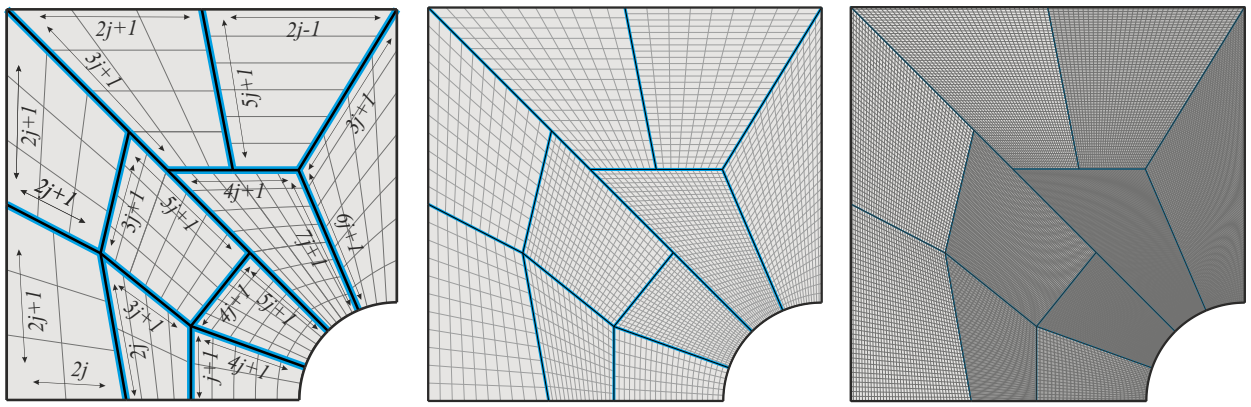

(a) Initial non-conforming mesh (b) Refinement factor $j = 5$ (c) Refinement factor $j = 20$

Figure 26: Elastic plate with hole: Sample meshes for the discretization scheme with ten non-conforming patches and different kinds of intersections. The applied refinement rule is given in a). All finer meshes are obtained by choosing a factor $j \in \mathbb{N}$.

In order to assess the ability of our method to deal with different types of geometry, we use a discretization scheme with ten non-conforming patches with four T-intersections and three star-intersections. A sketch of the patch layout is given on the left side in Figure 25. The interfaces

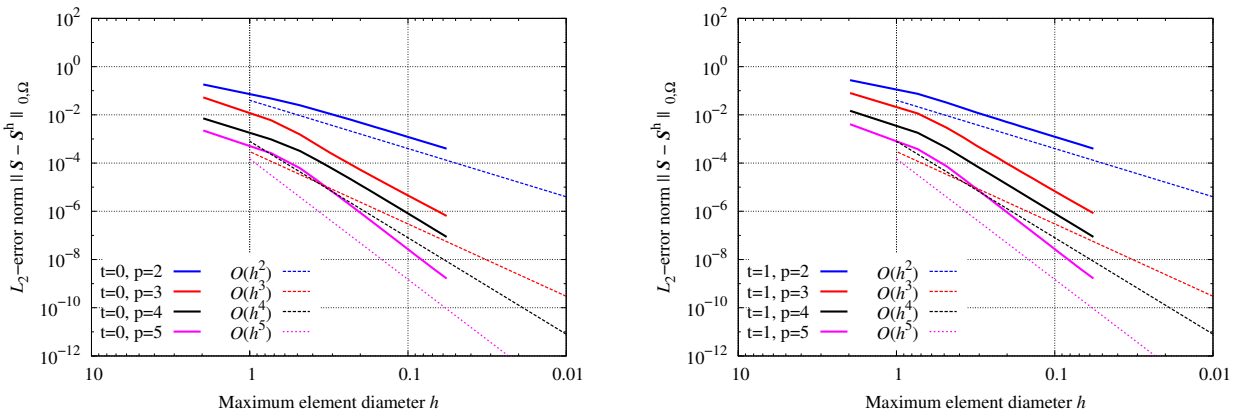

(a) Mortar coupling using $t = 0$ approach

(b) Mortar coupling using $t = 1$ approach

Figure 27: Elastic plate with hole: Comparison of error level and convergence rates for the discretization scheme with ten non-conforming patches and different kinds of intersections.

are straight and have infinite internal continuity, so Assumptions 3 and 4 can be neglected. The geometry is waterproof, as the parametrizations along the interfaces are matching. On the right side in Figure 25 the coarsest initial mesh is drawn, where the prolongation of all T-intersections as C^0-continuous lines is already included (type NC2 in Remark 2.1). In the convergence studies, every patch is refined using a number of $a \cdot j + b$ elements, where the values of a and b are given in Fig. 26a for each parametric direction within each patch. The refinement is performed in a way that the lengths of the element spans are as similar as possible in the knot vector under consideration of the prescribed element boundaries which arise due to the prolongation of ending interfaces at T-intersections. The order of the basis functions is chosen uniformly within the whole domain. Three sample meshes are given in Fig. 26 for a better depiction of the obtained non-conformity.

The error norm of the global stress distributions are given in Figure 27. Both proposed methods (Figures 27a and 27b) yield optimal convergence rates. The error levels are slightly higher than in the conforming case (Figure 15a), where shared degrees of freedom are used. It is to be noted that in the conforming case the difference between the individual element diameters h is smaller than in the case with ten patches, and thus naturally a lower error level is produced.

The computational costs for the formation of the global stiffness matrix ranges in the same order of magnitude as for the conforming case. The difference occurs in the assembly process and grows with the ratio of interface degrees of freedom to domain degrees of freedom, see Section 9.2.2. The same statements as in Section 9.2.2 can be made about the computational cost for the formation of the mass matrix and for the global solution.

The influence of the proposed mortar methods on the sparsity of the global stiffness matrix is studied in Figure 28. The sparsity pattern of computations using 3141 elements are compared between both proposed mortar methods. The number of non-zero entries for $t = 1$ is about 0.8 % smaller than for $t = 0$. It can be observed that the proposed approach for $t = 1$ creates less interrelations between patches than for $t = 0$. Furthermore, the interrelation within patches is less pronounced, see the banded structure of the block in the center of the diagrams: For $t = 0$, there is an interrelation between the control points at both ends of the interface (visualized by the square

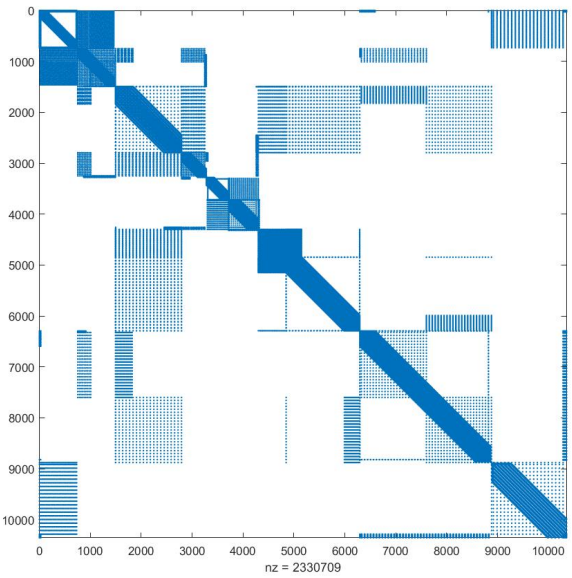

(a) Non-conforming mesh, mortar coupling using $t = 0$ approach

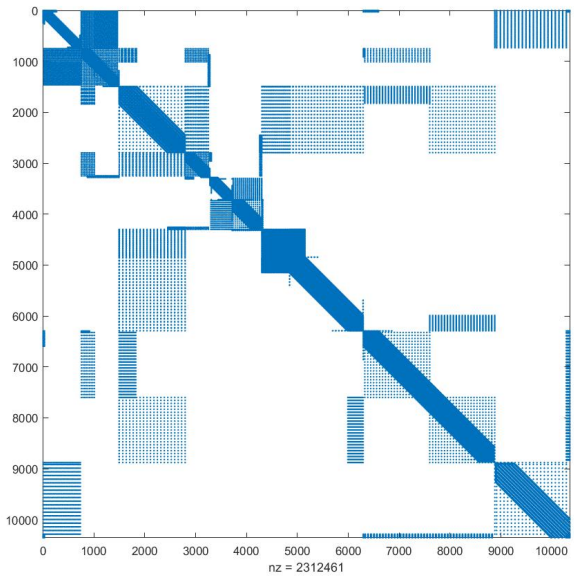

(b) Non-conforming mesh, mortar coupling using $t = 1$ approach

Figure 28: Elastic plate with hole discretized by ten non-conforming patches: Sparsity pattern of the global stiffness matrix. A subdivision factor $j = 5$ and order $p = 5$ is used (total number of elements is 3141).

around the banded structure). For $t = 1$, there is no such interrelation.

The condition number of the global stiffness matrix is compared in Fig. 29 between computations using shared degrees of freedom and the proposed mortar methods. Apart from very coarse meshes, the behavior of the condition number is very similar, both in magnitude and in slope. No negative impact of the proposed coupling method on the condition number can be detected. This shows that robust and accurate computations are possible with the proposed mortar method.

References

[1] P. Antolin, M. Fabre, and A. Buffa. A priori error for unilateral contact problems with Lagrange multipliers and isogeometric analysis. 07 2018.

[2] A. Apostolatos, R. Schmidt, R. Wüchner, and K.-U. Bletzinger. A Nitsche-type formulation and comparison of the most common domain decomposition methods in isogeometric analysis. *Int. J. Numer. Meth. Engng.*, 97(7):473–504, 2014.

[3] Y. Bazilevs, L. Beirão da Veiga, J. A. Cottrell, T. J. R. Hughes, and G. Sangalli. Isogeometric analysis: approximation, stability and error estimates for h-refined meshes. *Math. Models Methods Appl. Sci.*, 16(7):1031–1090, 2006.

[4] L. Beirão da Veiga, A. Buffa, G. Sangalli, and R. Vázquez. Mathematical analysis of variational isogeometric methods. *Acta Numerica*, 23:157–287, 2014.

[5] F. Ben Belgacem. The Mortar finite element method with Lagrange multipliers. *Numer. Math.*, 84(2):173–197, 1999.

[6] F. Ben Belgacem and Y. Maday. The mortar element method for three dimensional finite elements. *RAIRO Math. Model Anal. Numer.*, 31:289–302, 1997.

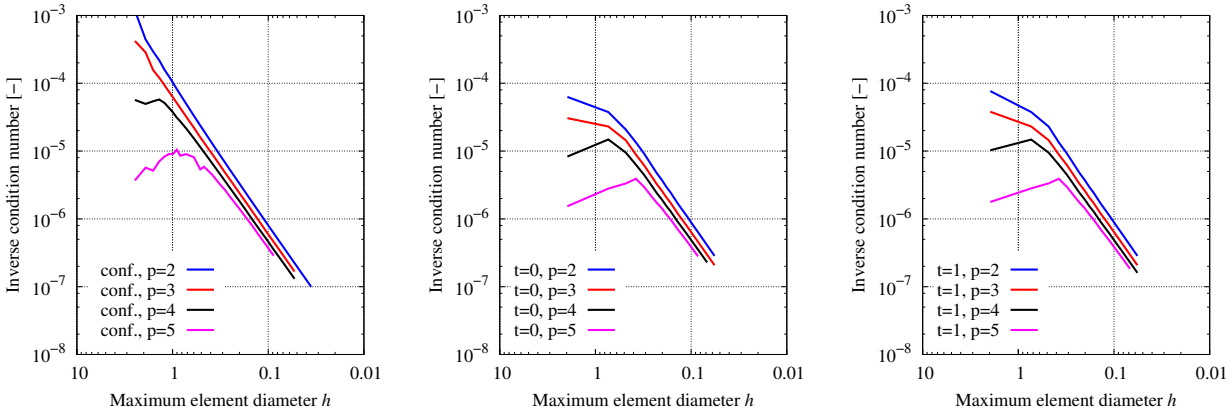

(a) Conforming mesh, coupling by shared degrees of freedom

(b) Non-conforming mesh, mortar coupling using $t = 0$ approach

(c) Non-conforming mesh, mortar coupling using $t = 1$ approach

Figure 29: Elastic plate with hole: Inverse condition number of the global system of equations. Comparison between the conforming discretization of Sec. 9.2.1 and the discretization scheme with ten patches of this section.

[7] C. Bernardi, Y. Maday, and A. T. Patera. Domain Decomposition by the Mortar Element Method. In H. G. Kaper, M. Garbey, and G. W. Pieper, editors, *Asymptotic and Numerical Methods for Partial Differential Equations with Critical Parameters*, pages 269–286. Springer Netherlands, Dordrecht, 1993.

[8] P. E. Bjørstad and O. B. Widlund. Iterative methods for the solution of elliptic problems on regions partitioned in substructures. *SIAM J. Numer. Anal.*, 23:1097–1120, 1986.

[9] D. Boffi, F. Brezzi, and M. Fortin. *Mixed Finite Element Methods and Applications*. Series in Computational Matheamtics 44. Springer, Berlin-Heidelberg, 2013.

[10] D. Braess. *Finite Elements. Theory, Fast Solvers, and Applications in Solid Mechanics.* Cambridge University Press, Cambridge, 1997.

[11] D. Braess, W. Dahmen, and C. Wieners. A multigrid algorithm for the mortar finite element method. *SIAM J. Numer. Anal.*, 37(1):48–69, 1999.

[12] E. Brivadis, A. Buffa, B. Wohlmuth, and L. Wunderlich. Isogeometric mortar methods. *Comput. Meth. Appl. Mech. Engrg.*, 284:292–319, 2015.

[13] C. de Boor. The quasi-interpolant as a tool in elementary polynomial spline theory. In *Approximation Theory*, 1973.

[14] L. Demkowicz. "Babuška ⇔ Brezzi ??". Technical Report 06-08, University of Texas, ICES, Austin, 2006.

[15] W. Dornisch and S. Klinkel. Boundary Conditions and Multi-Patch Connections in Isogeometric Analysis. *Proc. Appl. Math. Mech.*, 11(1):207–208, 2011.

[16] W. Dornisch, R. Müller, and J. Stöckler. Dual and approximate dual basis functions for B-splines and NURBS – Comparison and application for an efficient coupling of patches with the isogeometric mortar method. *Comput. Meth. Appl. Mech. Engrg.*, 316:449–496, 2017.

[17] W. Dornisch, G. Vitucci, and S. Klinkel. The weak substitution method – An application of the mortar method for patch coupling in NURBS-based isogeometric analysis. *Int. J. Numer. Meth. Engng.*, 103(3):205–234, 2015.

[18] K. A. Johannessen. Optimal quadrature for univariate and tensor product splines. *Comput. Meth. Appl. Mech. Engrg.*, 316:84–99, 2017.

[19] J. Nečas. *Direct Methods in the Theory of Elliptic Equations*. Springer, Berlin, 2012.

[20] A. Popp. State-of-the-art computational methods for finite deformation contact modeling of solids and structures. In P. A. and W. P., editors, *Contact Modeling for Solids and Particles*, volume 585 of *CISM International Centre for Mechanical Sciences (Courses and Lectures)*, pages 1–86. Springer, Cham, 2018.

[21] L. L. Schumaker. *Spline functions: Basic theory*. Cambridge mathematical library. Cambridge University Press, Cambridge and New York, 3rd ed. edition, 2007.

[22] A. Seitz, P. Faraha, J. Kremhellera, B. Wohlmuth, W. A. Wall, and A. Popp. Isogeometric dual mortar methods

for computational contact mechanics. *Comput. Methods Appl. Mech. Engrg.*, 301:259—280, 2016.

[23] L. B. Wahlbin. *Super Convergence in Galerkin Finite Element Methods*. Springer, Berlin, 1995.

[24] B. I. Wohlmuth. *Discretization methods and iterative solvers based on domain decomposition*, volume 17 of *Lecture notes in computational science and engineering*. Springer, Berlin, New York, 2001.

[25] Z. Zou, M. A. Scott, M. J. Borden, D. C. Thomas, W. Dornisch, and E. Brivadis. Isogeometric Bézier dual mortaring: Refineable higher-order spline dual bases and weakly continuous geometry. *Comput. Meth. Appl. Mech. Engrg.*, 333:497–534, 2018.